SPECIATION AND INTERCONVERSION MECHANISM OF MIXED HALO O,O'- AND N,O-BIDENTATE LIGAND COMPLEXES OF HAFNIUM

MASTER OF SCIENCE
in
CHEMISTRY

JOHANNES AUGUSTINUS VILJOEN

SPECIATION AND INTERCONVERSION MECHANISM OF MIXED HALO O,O'- AND N,O-BIDENTATE LIGAND COMPLEXES OF HAFNIUM

by

JOHANNES AUGUSTINUS VILJOEN

DISSERTATION

Submitted in the fulfilment
of the requirements for the degree

MASTER OF SCIENCE

in

CHEMISTRY

in the

FACULTY OF NATURAL AND AGRICULTURAL SCIENCES

at the

UNIVERSITY OF THE FREE STATE

SUPERVISOR: PROF. A. ROODT
CO-SUPERVISOR: DR. ALFRED. J. MULLER

April 2009

Acknowledgements

I wish to express my gratitude:

Firstly I would like to thank the Lord Almighty and Heavenly Father for the countless blessings that you bestowed on me. To You, God, I give this and I give my all.

Professor Andreas Roodt, thank you for guidance, support and motivation. It will always be a privilege to have had you as a promoter.

To Prof. Deon Visser, thank you for your help, guidance and input.

To Dr. Fanie Muller, thank you for your guidance throughout this project. All the advice, new ideas and the editing of all the quarterly reports is appreciated.

To my 'assistant', Miss. Maryke Steyn, thank you for always being there with me in the lab and bearing with me throughout this project.

The UFS inorganic group: thank you all for the continuous support and friendship.

Michelle Viljoen, my wife, thank you for being there for me every day with all your love and kindness.

Financial assistance from the Advanced Metals Initiative (AMI) and the Department of Science and Technology (DST) of South Africa as well as The New Metals Development Network (NMDN) and the South African Nuclear Energy Corporation Limited (Necsa) and the University of the Free State are gratefully acknowledged.

Table of Contents

5 Crystallographic Study of Hafnium Compounds

6 Kinetic Study of the Halide Substitution in $[HfCl_4]$ by Oxine as Entering Ligand

7 Study Evaluation

List of Abbreviations

Symbol / Abbreviation	Meaning
(L,L')	Bidentate ligand
acacH	Acetylacetone
tfaaH	1,1,1-trifluoroacetylacetone
hfaaH	1,1,1,5,5,5-hexafluoroacetylacetone
tropH	Tropolone
OxH	8-Hydroxyquinoline
bzbz	Dibenzoylmethanate
thd	Tetramethylheptanedione
tod	Trimethyloctanedione
bzac	1-Phenylbutane-1,3-dione
MOCVD	Metal-organic chemical vapour deposition
Z	Number of molecules in a unit cell
Å	Angstrong
NMR	Nuclear Magnetic Resonance spectroscopy
KMR	Kern Magnetiese Resonanse spektroskopie
ppm	(Unit of chemical shift) parts per million
IR	Infrared spectroscopy
υ	Stretching frequency on IR
π	Pi
σ	Sigma
α	Alpha
β	Beta
γ	Gamma
σ^*	Sigma anti-bonding
λ	Wavelength
θ	Sigma
^{o}	Degrees
^{o}C	Degrees Celsius
cm	Centimetre
g	Gram
M	(mol/L)
mg	Milligram
ΔH	Enthalpy of activation
ΔS	Entropy of activation
CO	Carbonyl
F_{hkl}	structure factor
k_{obs}	Observed pseudo-first-order rate constant
UV	Ultraviolet region in light spectrum
Vis	Visible region in light spectrum
DMF	N,N-dimethylformamide
Tol	Toluene

Abstract

Key words: *Hafnium; Zirconium; bidentate ligands; separation; synthesis; crystallographic characterisation; kinetics; mechanistic study.*

Hafnium and zirconium show extremely similar chemical properties and occur together in nature. Zirconium ore (commonly referred to as zircon) always contains 1 – 3% hafnium, and the separation of hafnium and zirconium is very difficult due to the similarities in chemical behaviour.

The aim of this study was to investigate the chelating behaviour of hafnium with different organic bidentate ligands e.g. trifluoroacetylacetone (tfaaH), hexafluoroacetylacetone (hfaaH) and 8-hydroxyquinoline (OxH) and characterizing new compounds obtained from this by means of single crystal X-ray crystallography, NMR- and UV/Vis spectroscopy. Any differences in solution behaviour, whether it being reaction mechanism, solubility, coordination modes, equilibrium behaviour, etc., could possibly be exploited in developing novel separation techniques for the two metals.

The structures of three new complexes, namely the $[Hf(tfaa)_4]$, $[Hf(OH)(hfaa)_3]_2$ and $[Hf(Ox)_4]$ were solved. This enabled the identification of products for kinetic studies and increased the available pool of these rare compounds in literature. The crystallographic characterization of these complexes are presented and compared with literature. Both $[Hf(tfaa)_4]$ and $[Hf(OH)(hfaa)_3]_2$ crystallized in a monoclinic space group, *C*2/*c* with Z = 4. $[Hf(Ox)_4]$ crystallized in a triclinic space group, $P\bar{1}$, with Z = 2. All three the structures include solvent molecules as part of the basic molecular unit. The co-crystallisation of the solvent molecules does not observably restrict or interfere with any significant physical properties of the solvated crystalline moieties. $[Hf(tfaa)_4]$ was coordinated to eight O atoms of the four tfaa ligands with an average Hf–O distance of 2.172(26) Å and O–Hf–O bite angle of 75.62(7)°. The hfaa ligands in $[Hf(OH)(hfaa)_3]_2$ formed three six-membered metallocycles with an average Hf—O bond distance of 2.190(21) Å and O—Hf—O bite angle of 75.3(5)°.

$[Hf(Ox)_4]$ was coordinated by four O and four N atoms which formed four five-membered metallocycles with average Hf—O and Hf—N bond distances of 2.095(13) Å and 2.399(15) Å, respectively and an O—Hf—N bite angle of 70.92(3)°.

As part of the kinetic investigation the substitution reactions between $HfCl_4$ and OxH ligands were followed by means of UV/Vis- and stopped-flow spectroscopy. Five reactions in total were observed for the stepwise coordination of OxH to the hafnium metal ion. From this the following mechanism was proposed:

The **first reaction** (1^{st} and 2^{nd} observable reactions) is a two-step reaction involving the stepwise rapid formation of $[Hf(LL)_2Cl_2]$ with pre-equilibrium K_1 = 40(9) M^{-1} and rate determining second step k_2 = 90(15) $M^{-1}s^{-1}$. The **third** observable reaction followed the usual two-term rate law, $k_{obs3} = k_3[LL'] + k_{-3}$ with k_3 = 6.5(3) $M^{-1}s^{-1}$ and k_{-3} = 1.4(1) x 10^{-3} s^{-1} yielding an equilibrium constant K_3 = 4(3) x 10^3 M^{-1}. The **forth** reaction is proposed to be the ring closure of the five membered chelated metallocycle with K_4 = 6(2) x 10^2 M^{-1} and k_3 = 5.80(7) x 10^{-3} $M^{-1}s^{-1}$. The **fifth** and final reaction was concluded to be the formation of the tetrakis complex, $[Hf(L,L')_4]$ that was isolated in the synthesis. The last process followed a normal two-term rate law, $k_{obs5} = k_5[LL'] + k_{-5}$ with k_5 = 0.073(9) $M^{-1}s^{-1}$ and k_{-5} = 2.3(2) x 10^{-4} s^{-1} producing an equilibrium constant, K_5 = 320(50) M^{-1}.

Opsomming

Sleutelwoorde: *Hafnium; Sirkonium; bidentate ligande; skeiding; sintese; kristallografiese karakterisering; kinetika, meganistiese studie.*

Hafnium en sirkonium vertoon baie soortgelyke chemiese eienskappe en kom saam in die natuur voor. sirkoniumerts (oor die algemeen na verwys as sirkoon) bevat altyd 1 – 3% hafnium, en die skeiding van sirkonium en hafnium is uiters moeilik as gevolg van die ooreenkomste in hul chemiese gedrag.

Die doel van hierdie studie was die ondersoek van die cheleringsgedrag van hafnium met verskillende organiese bidentate ligande bv. trifluoroasetielasetoon (tfaaH), heksafluoroasetielasetoon (hfaaH) en 8-hidroksiekinolien (OxH) en die karaterisering van nuwe verbindings is deur middel van enkel kristal X-straal kristallografie, KMR- en UV/Vis spektroskopie. Enige verskil in oplossingsgedrag met betrekking tot reaksiemeganisme, oplosbaarheid, koördinasiemode, ewewigsgedrag, ens., kan moontlik gebruik word in die ontwikkeling van unieke skeidingstegnieke vir die twee metale.

Die strukture van drie nuwe komplekse, naamlik $[Hf(tfaa)_4]$, $[Hf(OH)(hfaa)_3]_2$ en $[Hf(Ox)_4]$ is opgelos. Dit het die identifikasie van die produkte van kinetiese studies help verklaar en die beskikbare voorbeelde van hierdie skaars komplekse in die literatuur uitgebrei. Die kristallografiese karakterisering van hierdie komplekse is voorgelê en vergelyk met beskikbare literatuur. Beide $[Hf(tfaa)_4]$ en $[Hf(OH)(hfaa)_3]_2$ kristaliseer in die monokliniese ruimtegroep, *C*2/*c* met Z = 4. $[Hf(Ox)_4]$ kristaliseer in `n trikliniese ruimtegroep, $P\bar{1}$, met Z = 2. Al drie die strukture sluit oplosmiddelmolekule as deel van die basiese molekulêre eenheid in. Die ko-kristalisering van die oplosmiddelmolekuul beperk, of meng nie waarneembaar in met enige beduidende fisiese eienskappe van die gesolveerde kristalyne moïeteit nie. $[Hf(tfaa)_4]$ is deur agt O atome van die vier tfaa ligande gekoördineer, met `n gemiddelde Hf–O afstand van 2.172(26) Å en O–Hf–O bythoek van 75.62(7)°. Die hfaa ligande van $[Hf(OH)(hfaa)_3]_2$ vorm drie seslid metalloringe met `n gemiddelde Hf–O bindingsafstand van 2.190(21) Å en O–Hf–O bythoek van 75.3(5)°. $[Hf(Ox)_4]$

is gekoördineer deur vier O en N atome wat vier vyflid metalloringe vorm met gemiddelde Hf─O en Hf─N bindingsafstande van onderskeidelik 2.095(13) Å en 2.399(15) Å, en `n O─Hf─N byt hoek van 70.92(3)°.

As deel van hierdie kinetiese studie is die substitusiereaksie tussen $HfCl_4$ en OxH ligande deur middel van UV/Vis- en vloeistop spektroskopie gevolg. Vyf reaksies is in totaal waargeneem vir die stapsgewyse koördinasie van OxH aan die hafnium metaal kern. Hieruit word die volgende meganisme voorgestel:

Die **eerste reaksie** (1^{ste} en 2^{de} waarneembare reaksies) is `n tweestap reaksie wat die stapsgewyse vinnige vorming van $[Hf(LL)_2Cl_2]$ met voorekwilibrium K_1 = 40(9) M^{-1} en tempobepalende tweede stap k_2 = 90(15) $M^{-1}s^{-1}$. Die **derde** waarneembare reaksie volg die gewone tweeterm tempowet, $k_{obs3} = k_3[LL'] + k_{-3}$ met k_3 = 6.5(3) $M^{-1}s^{-1}$ en k_{-3} = 1.4(1) x 10^{-3} s^{-1} wat `n ewewigskonstante van K_3 =4(3) x 10^3 M^{-1} lewer. Die **vierde** reaksie is moontlik die ringsluiting van die vyflid chelaatmetalloring met K_4 = 6(2) x 10^2 M^{-1} en k_3 = 5.80(7) x 10^{-3} $M^{-1}s^{-1}$. Die **vyfde** en finale reaksie is voorgestel as die vorming van die tetrakis kompleks, $[Hf(L,L')_4]$ wat in die sintese geïsoleer is. Hierdie laaste proses volg `n normale tweeterm tempowet, $k_{obs5} = k_5[LL'] + k_{-5}$ met $k_5$ = 0.073(9) $M^{-1}s^{-1}$ en $k_{-5}$ = 2.3(2) x $10^{-4}$ $s^{-1}$ wat `n ewewigskonstante, K_5 = 320(50) M^{-1} lewer.

1 Introduction and Aim

1.1 History of Hafnium

While developing his periodic table in 1869, Mendeleev found that position number 72 was vacant. He postulated that the atomic weight of the 72nd element (Hf) would be near 180 and will be situated below zirconium in his table. Mendeleev further speculated that this element would have similar properties to that of zirconium, and that these two elements would probably occur together in nature.[1] Element no. 72 (Hafnium) was first predicted by Bohr's theory to be a Group IV element and its presence in zirconium minerals was confirmed by Coster and von Hevesy in 1923, using Moseley's technique of identification by means of X-ray spectroscopy.[2]

Coster and von Hevesy reported on January 20, 1923, in a letter addressed to Nature[3] the discovery of the new element and proposed the name Hafnium. This name was taken from the word 'Hafnia', the Latin name for the city of Copenhagen, in which the investigation was carried out. The work being done at the Institute for Theoretical Physics was under the direction of Niels Bohr.

Pure metallic hafnium was first obtained by sodium reduction[1] from hafnium fluorides, where they were isolated by means of fractional crystallization. Hönigschmid undertook the challenge to determine the atomic weight of hafnium by preparing the tetrabromide and determining the ratio of $HfBr_4$: 4Ag. The average atomic weight was found to be 178.06, taking into account that the presence of *ca.* 1% ZrO_2 lowers the atomic weight slightly. [4]

[1] von Hevesy G., *Chem. Rev*., **2**, 1, 1925.

[2] Coster D., *Phil. Mag.,* **46,** 856, 1923.

[3] Coster D. and von Hevesy G., *Nature,* **111**, 79, 1923.

[4] Hönigschmid and Zintl, *Z. Anorg.Chem.,* **140**, 335, 1924.

Pure hafnium and zirconium metals have wide application in the nuclear industry because of their unique thermal neutron absorption cross-sections (NAC), mechanical strength and resistance to corrosion associated with nuclear reactors operating at elevated temperatures. Hafnium has a very high absorption cross-sections for thermal neutron capturing (*ca*. 600 times that of zirconium)[5] and acts as a "poison" for its zirconium counterpart in the nuclear industry.

The separation of hafnium and zirconium is very difficult because of the fact that these two elements are so similar in terms of their chemistry. One could almost go so far as to describe these elements as chemical twins. The only other major chemical difference between hafnium and zirconium is their density. The density of zirconium is almost half that of hafnium.

Metals with high neutron capture cross-sections are capable of absorbing many neutrons without fissioning themselves. These metals are used in nuclear reactors to control the flux (rate of fission) in nuclear reactors.

It was already mentioned above that it is essential to have hafnium and zirconium in pure form for it to be useful in the nuclear industry. Pure metallic zirconium is used as a fuel-rod cladding material, while hafnium in its pure form, is used as a control rod (the chemistry and application of cladding materials and control rods are discussed in detail in Chapter 2)

[5] Weast R. C., *CRC Handbook of Chemistry and Physics*, 63rd Ed., The Chemical Rubber Publishing Company, USA, 1982.

1.2 Separation of Hafnium and Zirconium

*Picture obtained from: Venetskii. S.I., *Metallurg*. **4**, 44, 1972.

It is clear from the previous section that it would be advantageous to obtain hafnium and zirconium as pure as possible for nuclear power applications. A search of the available literature revealed that several separation techniques exist and these are briefly summarized below[6,7,8] (*discussed in more detail in Chapter 2*):

- Kroll process
- Ion exchange
- Solvent extraction
- Fractional distillation

Of the four techniques, only the Kroll process has been successfully implemented on an industrial and economically viable level. This creates a need for new research to improve existing techniques or for designing new ones.

[6] Overholser L. G., Barton C. J. and Grimes W.R., *US Atomic Energy Commission Reports* **Y431**, 23, 1949.

[7] Vinarov I. V., *Russ. Chem. Rev.*, **36**, 522, 1967.

[8] Mallikarjunan R. and Sehra J. C., *Bulletin of Materials Science*, **12**, 407, 1989.

1.3 Aim of this Study

A search done on applicable literature revealed that there is very little knowledge of the chelation behaviour of hafnium and zirconium with different bidentate ligands. The available pool of structural studies (X-ray crystallographic, NMR- and UV/Vis spectroscopy) is limited, so that thus any relevance in this regard could add to the knowledge base, and therefore potential separation techniques of these metals.

The aim of this study is therefore to investigate the chelating behaviour of hafnium with different organic bidentate ligands and compare it with zirconium (a parallel study done by M. Steyn, M.Sc., UFS, 2009[9]). If hafnium and zirconium show differences in their chelating behaviour, either by reaction rates, solubilities, coordination modes, equilibrium behaviour, *etc*., it could possibly be exploited as a novel separation technique for the two metals. The elucidation of the reaction mechanisms for these chelating reactions can also prove valuable if significant differences are observed for the two metals.

As part of the study the bidentate ligands, trifluoroacetylacetone (tfaaH), hexafluoroacetylacetone (hfaaH) and 8-hydroxyquinoline (OxH) where selected for various reasons (*see* Figure 1.1 for the structures of those ligands).

1) Electron withdrawing CF_3 *vs*. electron donating CH_3 moieties (tfaaH *vs*. hfaaH),
2) Electronic influences from aromatic ring systems as found in OxH,
3) Five (OxH) *vs*. six (tfaaH and hfaaH) membered chelating systems, and
4) Variations in donor atoms (O,O' *vs*. N,O).

[9] Steyn M., Steyl G. and Roodt A., *M.Sc*. *Thesis*, University of the Free State, 2009.

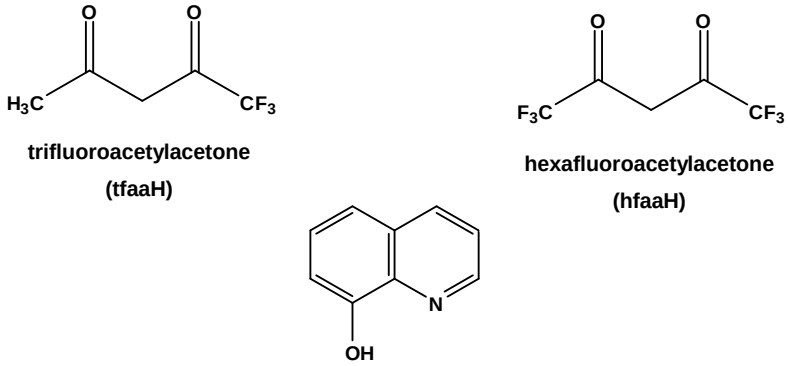

Figure 1.1: Bidentate ligands selected for this study.

It is also important to note that zirconium-free hafnium was used throughout this study in order to investigate possible differences in the chemistry of hafnium and zirconium. Once differences (if any) are identified, the techniques could be applied to zircon to check if the metal separation is feasible for industrial application.

<u>The following aims were set for this study</u>:

- The synthesis of model complexes such as $[HfCl_n(tfaa)_{4-n}]$, $[HfCl_n(hfaa)_{4-n}]$ and $[HfCl_n(Ox)_{4-n}]$, where *n* is the number of equivalent ligands added.

- The characterization of these complexes by means of ^{1}H,^{13}C and ^{19}F NMR and single crystal X-ray crystallography.

- To study the reaction kinetics and determine the mechanism of the formation of $[HfX_n(L,L')_{4-n}]$ complexes by means of UV/Vis- and stopped-flow techniques.

2 Literature Overview of Hafnium

2.1 History of Hafnium

Hafnium was first accurately predicted by Niels Bohr by his theory (*see* Appendix A *for the full derivation of Bohr's Theory*). Soon after, this new silvery element was discovered by a Dutch physicist Dirk Coster and Hungarian chemist Georg von Hevesy in 1923. Its main source is as a by-product from obtaining pure zirconium. All natural occurring zirconium minerals contain between 0.5 and 5% hafnium. Due to lanthanide contraction, zirconium and hafnium have essentially identical atomic and ionic radii (1.44 and 0.86 Å for Zr and Zr^{4+}; 1.44 and 0.85 Å for Hf and Hf^{4+})[1] making their chemistries similar.

2.2 Nuclear Properties of Hafnium and Zirconium

The separation of hafnium and zirconium has become vital in the nuclear power industry, as zirconium is a common fuel-rod cladding alloy material, with desirable properties of low neutron capture cross-section and high chemical stability at high temperatures. However, because of hafnium's high neutron absorbing properties, zirconium is far less useful for nuclear reactor material applications if it contains any amount of hafnium impurities.

[1] Cotton F. A., Wilkinson G., Murillo C. A. and Bochmann M., *Advanced Inorganic Chemistry*, 6th Ed., Wiley-Interscience Publications, New York, 1999.

Table 2.1 and Table 2.2 lists the stable isotopes of hafnium and zirconium together with data on natural abundance, atomic mass and thermal neutron capture cross-section.[2]

Table 2.1: Stable isotopes and some selected properties of $_{72}$Hf.

Isotopes	Natural Abundance	Atomic mass	Neutron capture cross-section (barns)
^{174}Hf	0.18%	173.94	400
^{176}Hf	5.20%	175.94	30
^{177}Hf	18.50%	176.94	370
^{178}Hf	27.14%	177.94	80
^{179}Hf*	13.75%	178.9	(0.2 + 65)
^{180}Hf	35.24%	179.95	10
Average		**178.49**	**105**

*Two isomers for ^{179}Hf

Table 2.2: Stable isotopes together with some selected properties of $_{40}$Zr

Isotopes	Natural Abundance	atomic mass	Neutron capture cross-section (barns)
^{90}Zr	51.46%	89.90	0.1
^{91}Zr	11.23%	90.91	1.0
^{92}Zr	17.11%	91.90	0.2
^{94}Zr	17.40%	93.91	0.1
^{96}Zr	2.80%	95.91	0.1
Average		**91.22**	**0.18**

These unique properties make both hafnium and zirconium ideal for manufacturing *control rods* and *cladding materials,* respectively.

[2] Weast R. C., *CRC Handbook of Chemistry and Physics*, 48th Ed., The Chemical Rubber Publishing Company, Cleveland, 1967-8.

2.2.1 Control Rods

Control rods are manufactured from very robust chemical elements which are capable of absorbing countless numbers of neutrons at relatively high temperatures without fissioning themselves. The elements used in control rods must also be extremely corrosion resistant as they are mainly submerged in water.

Control rods are usually combined in control rod assemblies and inserted into guide tubes within the fuel elements. These rods are then inserted into the core of a nuclear reactor in order to control the neutron flux (fission) or to shut down the reactor, as shown in Figure 2.1.

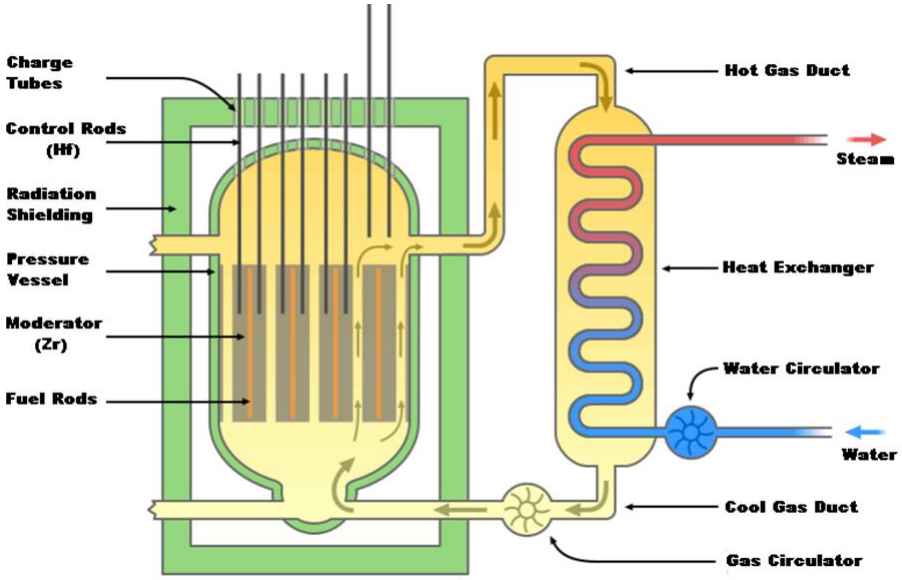

Figure 2.1: Diagrammatical representation of a nuclear reactor.[3]

[3] Image of Nuclear Reactor adapted from: http://commons.wikimedia.org/wiki/Image:Magnox_reactor_schematic.svg (Last accessed 25/09/08).

Hafnium's unique neutron absorbing properties and corrosion resistance makes it a very attractive element for control rods.[4] Silver, indium, cadmium, boron, cobalt, gadolinium and europium also have sufficiently high neutron capture cross-sections suitable for control rods, each with a different affinity for neutrons. Due to these slight differences in their absorbing properties the compositions of the control rods can be designed specifically for the neutron spectrum of the reactor it is suppose to control, *e.g.* Breeder reactors operate with "fast" neutrons and light water reactors (Boiling Water Reactors (BWR) and Pressurised Water Reactors (PWR) with "thermal" neutrons).

Chemical shim, which is a soluble neutron absorber (for instance boric acid) can also be added to a reactor's coolant to allow for complete extraction of the control rods during stationary power operation, thereby ensuring an even power and flux distribution over the entire core.

The control rods are mainly used for fast alterations, like shutdown and start-up of the nuclear reactors.

2.2.2 Cladding Materials

The very low neutron absorbing character (*ca*. 600 times smaller than its hafnium counterpart, *see* Tables 2.1 and 2.2) of zirconium makes it an attractive element as a cladding material in nuclear reactors. Cladding materials must be corrosion-resistant with very low thermal neutron cross-sections.

Cladding is often achieved by bonding different metals through extruding these metals through a die or by pressing sheets together under high pressure, as illustrated in Figure 2.2.[5]

[4] Keller H. W., Ballenberger J. M., Hollein, D. A. and Hott C., *Nucl. Technol.*, **59**, 3, 476, 1982.

[5] Image of extruding of metals through a die from: http://www.ent.ohiou.edu/~raub/manufacturing/extrus6.jpg (Last accessed 17/02/2009).

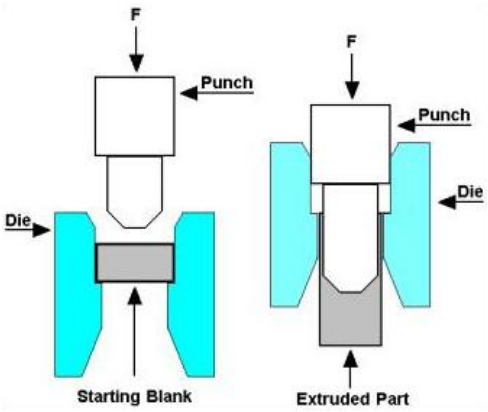

Figure 2.2: Graphic illustration of extruding (pilgering) of metals through a die.[5]

The cladding material is the outer layer of the fuel rods in nuclear reactors which separates the coolant and nuclear fuel from one another. This prevents radioactive fission fragments from escaping from the fuel and thereby contaminating the coolant.

2.3 Separation Techniques

Due to the unique nuclear properties of both hafnium and zirconium, it has become a highly lucrative business to produce pure metallic zirconium and hafnium. As mentioned earlier, hafnium is a naturally occurring impurity (0.5-5%) in zirconium minerals, which necessitates the separation of these two elements, but due to their overall chemical similarities, separation is very difficult. There are several known methods of separation of zirconium and hafnium; the earliest known among these involved the fractional crystallization of ammonium fluoride metal salts and the fractional distillation of the metal chloride. However, these methods are not suitable for industrial scale production. Methods currently used in the industry for separation are summarized below:

2.3.1 Kroll Process[6]

The Kroll process is a pyrometallurgical industrial process first used to produce metallic titanium. In 1945, after W. J. Kroll moved to the United States, he continued to refine his process for the separation of hafnium and zirconium. During this process zircon, $ZrSiO_4$, is combined with carbon in a furnace to convert the hafnium and zirconium to their corresponding carbides, which is in turn treated with chlorine gas to form their corresponding metal tetrachlorides. Both the hafnium and zirconium tetrachlorides are very sensitive to hydrolysis. The tetrachlorides, $HfCl_4$ and $ZrCl_4$, are then reduced with magnesium and purified by sublimation in an inert atmosphere. The reaction scheme involved in converting hafnium/zirconium oxides to their corresponding metals are illustrated in Scheme 2.1, where M = Hf and Zr.

$$MO_2(s) + 2C(s) + Cl_2 \rightleftharpoons MCl_4(g) + 2CO(g) \quad \textbf{. . . Eq. 2.1}$$

$$MCl_4(g) + 2Mg(l) \rightleftharpoons M(s) + 2MgCl_2 \quad \textbf{. . . Eq. 2.2}$$

Scheme 2.1: The reaction scheme involved in converting hafnium and zirconium oxides to their corresponding metals.

2.3.2 Liquid-Liquid Extraction[7]

Liquid-liquid extraction is a method that is used to separate compounds based on their relative solubilities in two different immiscible liquids, usually water and an organic solvent. With this technique a soluble compound is usually separated from an insoluble compound. In other words, only one substance from the reaction mixture dissolves in the organic phase and the other compound in the water phase.

[6] Gilbert H. L. and Barr M. M., *J. Electrochem. Soc.,* 102, **5**, 243, 1955.

[7] Madhavan R., *Optimize Liquid-Liquid Extraction*. Available: http://www.cheresources.com/extraction.shtml. (Last accessed 25/11/2008).

2.3.3 Ion-Exchange Separation[8]

Ion exchange separation is a type of extraction technique where an ion is transferred from an aqueous phase to the organic phase; another ion is then transferred in the opposite direction to maintain equilibrium in the charge balance.

Mixtures of HfO_2 and ZrO_2 have been effectively separated by means of ion-exchange methods. This method has been applied to oxide mixtures containing *ca*. 20% HfO_2. The oxide mixtures is first dissolved in sulphuric- and hydrofluoric acid, and then fumed to dryness. The residue is dissolved in concentrated hydrochloric acid and the hydroxides are precipitated with ammonium hydroxide. The precipitated hydroxides are then converted to oxychlorides by dissolving it again in hydrochloric acid. Perchloric acid containing 40 cm^3 of "Dowex 50" is slowly added to the oxychlorides. After 30 min. the supernatant liquid is siphoned off and the resin slurry added to the top of the exchanged column ("Dowex 50" of 100-200 mesh, packed in a column) and washed with 6 M hydrochloric acid to convert it to the acid form. Pure hafnium is then collected in the eluant**.**

2.3.4 Extractive Distillation[9]

Extractive distillation is used when the volatilities of the two components in a reaction mixture are nearly the same, making normal distillation techniques impossible. In this method a high boiling, relatively non-volatile and miscible solvent that does not form any azeotropic mixtures with any of the compounds inside the reaction mixture, must be used. The solvent chosen interacts differently with the compounds in the reaction mixture, thereby causing their relative volatilities to change and making separation of the reaction mixture possible by distillation. The most essential part of extractive distillation is to select the correct solvent as it is the active species which alters the

[8] Newnham I. E., *J. Am. Chem. Soc*., **73**, 12, 5899, 1951.

[9] Yee D. F. C., *In Depth Look at Extractive Distillation*. Available: http://www.cheresources.com/extrdist.shtml (Last accessed 25/11/2008).

relative volatilities of the compounds. It must however be kept in mind that the solvent should also be easily removed from the product left behind after distillation.

2.4 Bidentate Ligand Complexes of Hafnium

As stated earlier in Chapter 1 the aim of this study is to investigate other possible means of separation than those described above. The utilization of bidentate ligand systems was selected for this purpose, to enable preparation of a range of complexes with possible different physical properties thus allowing separation. Literature shows a few such complexes where Hf and Zr exist and these are discussed in the following paragraphs. It is also noted from literature that this approach was not considered as a possible means of separation to date. The generalised step-wise reaction mechanism of hafnium halo complexes reacting with O,O'- or N,O-donating bidentate ligands is presented in Scheme 2.2,[10] where (L,L') = bidentate ligand and X = halogens.

$[HfX_4] + (L,L') \rightleftharpoons [HfX_3(L,L')] + X^-$ **... Eq. 2.3**

$[HfX_3(L,L')] + (L,L') \rightleftharpoons [HfX_2(L,L')_2] + X^-$ **... Eq. 2.4**

$[HfX_2(L,L')_2] + (L,L') \rightleftharpoons [Hf\text{-}X_1(L,L')_3] + X^-$ **... Eq. 2.5**

$[Hf\text{-}X(L,L')_3] + (L,L') \rightleftharpoons [Hf(L,L')_4] + X^-$ **... Eq. 2.6**

Scheme 2.2: General reaction sequence of hafnium halo complexes reacting with O,O'- or N,O-donating bidentate ligands.

[10] Hubert-Pfalzgraf L. G., Touati N., Pasko S. V., Vaissermann J. and Abrutis A., *Polyhedron*, **24**, 3066, 2005.

Hafnium(IV) and zirconium(IV) tetrahalides react with β-diketones under anhydrous Schlenk conditions[11] to yield substitution product(s) plus hydrogen halide(s). In organic solvents the di-substituted products ([Hf(L,L')$_2$]) are obtained, and at higher temperatures the reaction gives the tri- and tetra substituted products, where (L,L') = bzbz (dibenzoylmethanato)[12], thd (tetramethylheptanedionato)[10] and tod (trimethyloctanedionato)[13]. More recently, β-diketonate complexes have been synthesized and studied as precursors for decomposition of $HfSi_xO_y$ films by metal-organic chemical vapour deposition (MOCVD).[14]

Hafnium(IV) and zirconium(IV) tetrahalides also react readily with N,O-bidentate ligands to form a variety of mono- to tetra-substituted (1:1 – 1:4) adducts.[15] These types of complexes are generally prepared by mixing solutions or suspensions of the starting reagents in a polar organic solvent at room temperature. The complexes are mainly moisture-sensitive, white and yellow solids, and are quite insoluble in most organic solvents.

2.5 Hafnium and Zirconium Halide Complexes

Both hafnium(IV) and zirconium(IV) halides form crystalline solids with very high-melting points which contain a variety of geometries. The two main structural geometries are referred to as the α- and β forms, the dodecahedral and antiprismatic geometries, respectively,[16] *see* Figure 2.3. The other geometry that these structures

[11] Shriver D. F. and Drezdzon M. A., *The Manipulations of Air-Sensitive Compounds*, 2nd Ed., Wiley-Interscience Publications, New York, 1986.

[12] Pinnavaia T. J. and Fray C., *Inorganic Chemistry*, **7**, 3, 502, 1968.

[13] Pasko S. V., Hubert-Pfalzgraf L. G., Abrutis A., Richard P., Bartasyte A. and Kaziauskiene V., *J. Mater. Chem*., **14**, 1245, 2004.

[14] Zherikova K. V., Morozova N. B., Kurat'eva N. V., Baidina I. A., Stabnikov P. A. and Igumenov I. K., *J. Struct. Chem.*, **46**, 6, 1039, 2005.

[15] Frazer M. J. and Rimmer B., *J. Chem. Soc*., **A**, 2273, 1968.

[16] Cotton F. A., Wilkinson G. and Gaus P. L., *Basic Inorganic Chemistry,* 3rd Ed., John Wiley and Sons, New York, 1995.

can adopt in the very rare case, is the cubic geometry. Hafnium(IV) and zirconium(IV) tetrahalides are interlinked together by sharing halides to produce infinite zig-zag chains of MX_6 octahedra (M = Hf and Zr, X = Br and Cl).[17] In the gas phase, these tetrahalides exists as monomeric regular tetrahedral molecules, where M–X bond distances decrease appreciably as X varies in order Cl > Br > I.[18]

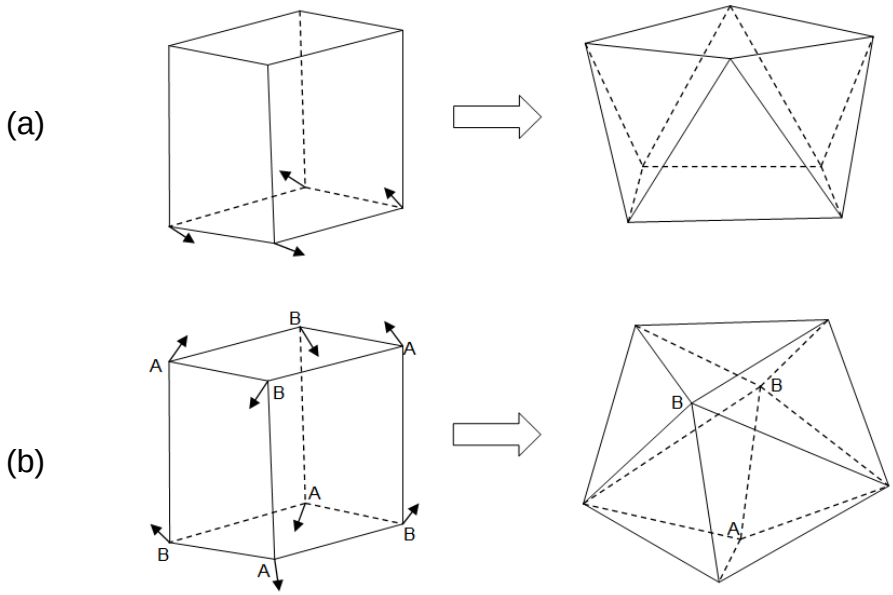

Figure 2.3: The three main geometries for eight-coordinated complexes: The cube with its two principle distortions (a) ***Square antiprism,*** (b) ***Dodecahedron.***

2.6 Bidentate Ligands

2.6.1 Hafnium and zirconium complexes containing β-Diketones

Metal complexes of β-diketones are known for all non-radioactive transition metals. Hafnium and zirconium are unique in that it can form complexes in which the metal may exhibit six, seven or eight coordination numbers.[12] β-diketones have also been successfully used for extracting metals in organic media and are well known ligands

[17] Krebs B., *J. Anorg. Allg. Chem*., **378**, 263, 1970.

[18] Clark R. J. H., Hunter B. K. and Rippon M., *Inorg. Chem*., **11**, 56, 1972.

for a variety metals in catalyst systems.[19,20] It has also been shown that β-diketone complexes with the titanium triad (Ti, Zr, and Hf), show antitumor activity.[21] More recently, β-diketonate complexes have been synthesized and studied by Zherikova *et al.*[14,22] as precursors for the decomposition of $HfSi_xO_y$ films.

Due to the large variety of physiochemical properties, high dielectric constants, catalytic properties, chemical inertness and corrosion resistance, these compounds are extensively studied and used in a wide range of applications such as for oxygen detector sensors, memory chips and solid oxide fuel cells, to name a few.

2.6.1.1 Synthesis of β-Diketones

β-diketone, acting as O,O'-bidentate ligands, are generally synthesized by utilizing a Claisen-condensation reaction,[23] whereby a desired ketone, which possesses an α-hydrogen, reacts with an appropriate acylation reagent (acid chloride, acid anhydride or ester) in the presence of a suitable base (*see* Scheme 2.3).

[19] Cullen W. R., Rettig S. J. and Wickenheizer E. B., *J. Organomet. Chem.*, **370**, 141, 1989.

[20] Banach T. E., Berti C., Colonna M., Fiorini M., Marianucci E., Messori M., Pilati F. and Toselli M., *Polymer*, **42**, 7511, 2001.

[21] Bischoff H., Berger M. R., Keppler B. K. and Schmähl D., *J. Cancer Res. Clin. Oncol.*, **113**, 446, 1987.

[22] Zherikova K. V., Morozova N. B., Baidina I. A., Alekseev V. I. and Igumenov I. K., *J. Struct. Chem.*, **47**, 1, 82, 2006.

[23] Hauser C. R., Swamer F. W. and Adams J. T., *Organic Reactions*, John Wiley and Sons, **8**, 61, 1954.

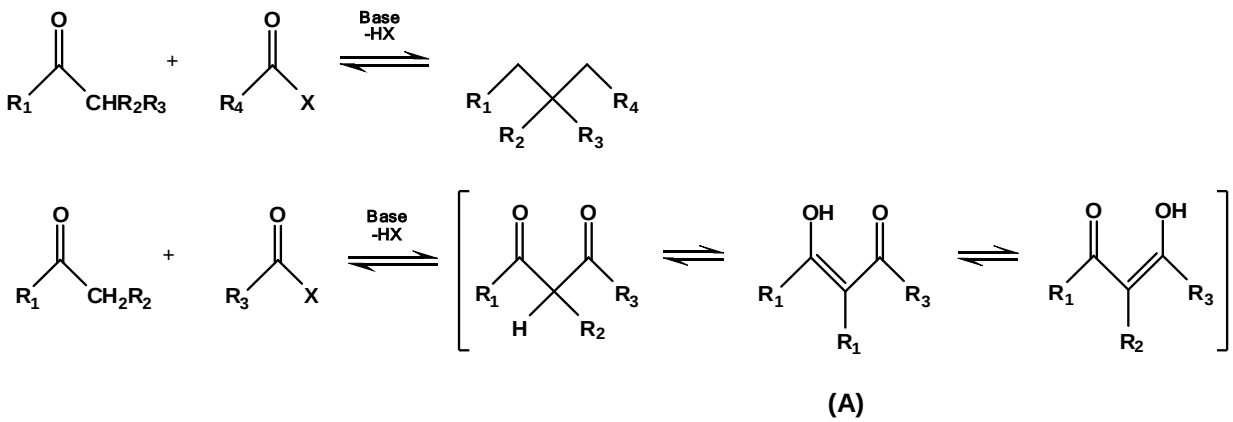

Scheme 2.3: Generalised synthetic scheme for β-diketones.

The most common bases employed for the synthesis of β-diketone ligands are NaOH, alkyl oxides (R-OM, M = alkali metal), hydrides, alkali metals, amides and even sterically hindered bases such as lithiumdiisopropylamide (LDA). Ketones which contain strong electron donating R-groups, need stronger bases like amines for the associated β-diketones to form, while side reactions can dramatically influence the yield of the β-diketones.

A few side reactions that can occur are:

- Self condensation of the ketone (aldol reaction),[24]
- β-keto-ester formation, particularly if the acelate of the ketone is unreactive and,[25]
- Synthesis of bis-β-diketones from succinic- and maloic acid esters may lead to the Stobbe-reaction.[26]

[24] Nielson A. T. and Houlihan W. J., *Organic Reactions*, Robert E. Krieger Publishing Company, New York, **16**, 20, 1975.

[25] Morrison R. T. and Boyd R. N., *Organic Chemistry,* Allyn and Bacon Inc., 5th Ed., 922, 1987.

[26] Johnson W. S. and Daud G. H., *Organic Reactions*, John Wiley and Sons, **6**, 2, 1951.

2.6.1.2 Keto-Enol Tautomerism in β-Diketones

Hydrogen bonding and proton transfer are probably some of the most important behavioural aspects concerning structural and reactivity of simple compounds[27] and complex substances.[28] β-diketone compounds exhibit both of these features and is probably one of the finest examples of keto-enol tautomerism. This special kind of isomerism occurs when a carbonyl α-hydrogen rapidly equilibrates with its corresponding enol (*see* (A) in Scheme 2.3).[29] Note that tautomers are different compounds (isomers) with different structures, while resonance forms are different representations of the same structure. Keto-enol tautomerism has been extensively studied via IR, UV/Vis, NMR and bromide titration to investigate the tautomeric equilibrium.[30] The tautomeric equilibrium for pentane-2,4-dione (acetylacetone) and its derivatives have been recognized for a long time.[31] Several factors can influence the position of the keto-enol equilibrium, especially steric and electronic effects of the substituents and the nature of the solvent.[32, 33] An electron withdrawing group such as trifluoromethyl, which is also relevant to this study, leads to higher percentages of the enol tautomer in solution because these groups attract electron density from the enolic ring through induction. Related NMR studies have been reported on the tautomerism of β-diketones.[34, 35, 36]

[27] Calvin M. and Wilson K. W., *J. Am. Chem. Soc*., **65**, 2003, 1945.

[28] Holm R. H. and Cotton F. A., *J. Am. Chem. Soc*., **80**, 5658, 1958.

[29] McMurry J., *Organic Chemisty*, 6th Ed., Thomson Brooks/Cole, Belmont, 2004.

[30] Burdett J. L. and Rogers M. T., *J. Am. Chem. Soc*., **86**, 2105, 1964.

[31] Jarries H. J. and Parry G., *J. Am. Chem. Soc*., **31**, 233, 1978.

[32] Jarret H., Sadler M. and Shoolery J., *J. Am. Chem. Soc*., **21**, 2092, 1953.

[33] Reeves L., *Can. J. Chem*., **35**, 1351, 1957.

[34] Luz G. Z. and Mazur Y., *J. Am. Chem. Soc*., **89**, 1183, 1967.

[35] Nonhebel D. C., *Tetrahedron*, **24**, 1869, 1968.

[36] Isaazson D. and Morokuma K. J., *J. Am. Chem. Soc*., **102,** 4453, 1975.

2.6.1.3 Derivatives of β-Diketones

The backbone of β-diketones can be modified in a variety of ways to obtain a range of completely new classes of compounds. Some of these β-diketone derivatives are the mono-thio-β-diketone (a),[37] dithio-β-diketone (b)[38] and enaminone (c) [39] as shown in Figure 2.4 below.

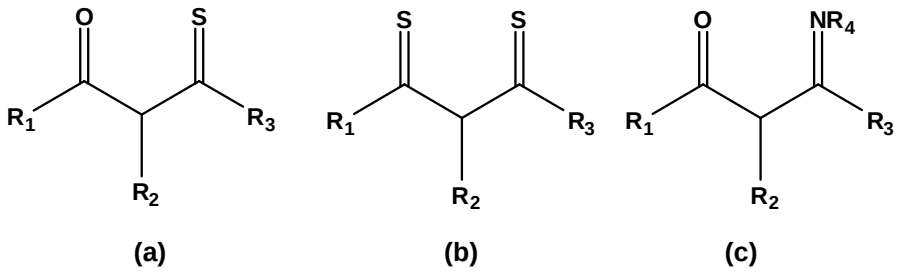

Figure 2.4: Modified backbones of β-diketone systems.

2.6.2 Hafnium and Zirconium Complexes Containing Mono(diketonates), [M(*L,L'*)X_3]

Only a handful of mono-acetylacetonates of the Ti triad have been prepared and isolated in the past, *e.g*. [$HfCl_3$(acac)],[40] [$Zr(OR)_3$(acac)][41] and [$Zr(OR)(NO_3)_2$(acac)][42] (R = C_2H_5, C_3H_7, C_4H_9). Note that [$HfCl_3$(acac)] was isolated as the THF adduct [M(L,L')$Cl_3 \cdot C_4H_8O$].

[37] Silver M. E., Chun H. K. and Fay R. C., *Inorg. Chem*., **21**, 3765, 1982.

[38] Bousman K. S., Tocane P.J. and Welch J. T., Inorg. Chim. Acta., 357, 3871, 2004.

[39] Jones D., Roberts A., Cavell K., Keim W., Englert U., Skelton B. W. and White A. H., *J. Chem. Soc. Dalton Trans.*, 255, 1998.

[40] Brianina E. M. and Mortikova E. I., *Russ. Chem. Bull*., **16**, 2418, 2005.

[41] Brianina E. M. and Freidlina R. K., *Izvest. Akad. Nauk SSSR, Otdel Khim. Nauk*, 1595, 1961.

[42] Brianina E. M., Freidlina R. K. and Nesmeyanov A. N., *Izvest. Akad. Nauk SSSR, Otdel Khim. Nauk*, 63, 1960.

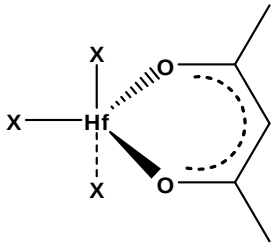

Figure 2.5: Graphic illustration of the Mono-β-diketonato metal complexes, $[M(L,L')X_3]$, where X = Cl, NO_3 and OR, R = C_2H_5, C_3H_7, C_4H_9.

2.6.3 Hafnium and Zirconium Complexes Containing Bis-(diketonates), $[M(L,L')_2X_2]$

Bis-β-diketonato complexes have an octahedral coordination and can occur in both *cis*- and *trans*-configurations as illustrated in Figure 2.6.

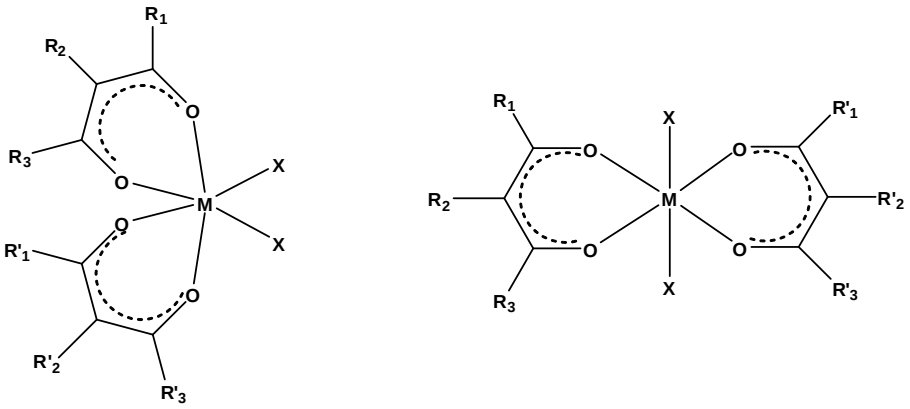

(a) Cis-conformation ***(b) Trans-conformation***

Figure 2.6: Structures of bis-β-diketonato metal complexes, $[M(L,L')_2X_2]$, in the *cis*- and *trans*-conformations, X = Br, Cl, OR or $(C_5H_5)^-$, M = Hf^{IV} and Zr^{IV}.

IR spectra of $[M(acac)_2Cl_2]$ complexes feature two ν(M-Cl) stretching frequencies,[43] pointing to an octahedral cis-conformation. The cis-configuration is the most stable

[43] Fay J. P. and Pinnavaia T. J., *Inorg. Chem.,* **7**, 508, 1968.

isomer, although the trans-configuration may sometimes be favourable due to steric effects on the O,O'-backbone. The reason for the higher stability of the *cis*-configuration can be attributed to the π-back donation into the three metal *d*-orbitals (d_{xy}, d_{xz} and d_x^2), whereas for the *trans*-configuration only two *d*-orbitals (d_{xy} *and* d_{xz}) are occupied.[44] Bis-β-diketonato metal complexes, $[M(L,L')_2X_2]$, (M = Zr and Hf) which contain the same halides, are shown to be isomorphous by X-ray powder diffraction. $[M(acac)_2Cl_2]$ complexes are fluxional in solution, and the intermolecular ligand exchange occurs very fast, even at 143K, so that the non-equivalent acac-methyl protons could not be resolved.[43] The ligand rearrangements in bis-β-diketonato metal complexes are much slower when the halides are replaced by more bulky alkoxide groups. These complexes are readily prepared by reacting two moles of acacH with one mole $[M(OR)_4]$, to produce $[M(OR)_2(acac)_2]$ and 2ROH.[45] NMR spectra however indicated that *cis*-octahedral species were also present. A large variety of chlorocyclopentadienylbis(β-diketonato)metal(IV) derivatives, $[(C_5H_5)_2MX_2]$, (X = F,[46,47] Cl,[48,] Br[49] and I,[50] metal = Ti, Zr and Hf) have also been synthesized and studied.

Over the years bis-β-diketonato complexes of titanium, zirconium and hafnium have been investigated in depth, due to their unique antitumor activity properties.[51,52] The structures studied are shown in Figure 2.7.

[44] Bradley D. C. and Holloway C. E., *J. Chem. Soc., Chem. Commun*., 284, 1965.

[45] Brantley D. C. and Radford D., *Prog. Inorg. Chem*., **2,** 303, 1960.

[46] Bruce P. M., Kingston B. M., Lappert M .F., Spalding T. R. and Srivastava R. C., *J. Chem. Soc.* ***A***., 2106, 1969.

[47] Druce P. M., Kingston B. M., Lappert M. F., Srivastava R. C., Frazes M. J. and Newton W. E., *J. Chem. Soc.* ***A*****.,** 2814, 1969.

[48] Wilkinson G., Pauson P. L., Birmingham J. M. and Cotton F. A., *J. Am. Chem. Soc*., **75**, 1011, 1953.

[49] Reid A. F. and Wailes P. C., *J. Organomet. Chem*., **2,** 329, 1964.

[50] Reid A. F. and Wailes P. C., *J. Organomet. Chem*., **5,** 1213, 1966.

[51] Keller H. J., Kepler B. K. and Schmähl D., *Arzneimittel Forsch*, **32**, 8, 806, 1982.

[52] Keller H. J., Kepler B. K. and Schmähl D., *J. Cancer Res. Clin. Oncol*, **105**, 109, 1983.

A significant reduction in tumors was detected with $[Hf(bzac)_2Cl_2]$ (bzac = 1-phenylbutane-1,3-dionato), whereas the zirconium analogue, $[Zr(bzac)_2Cl_2]$, showed no reduction in tumor size at all. However, $[Hf(bzac)_2Cl_2]$ was still not as active as $[Ti(bzac)_2Cl_2]$ and $[Ti(bzac)_2(OEt)_2]$.[21]

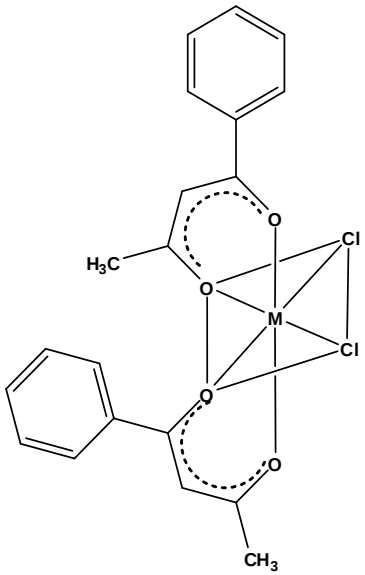

Figure 2.7: Schematic structure of the tumor-inhibiting bis-β-diketonato metal complexes with M = Ti, Zr and Hf.

Fleeting *et al*.[53] synthesized several bis-β-diketonato metal complexes $[M(OPr^i)_2(thd)_2]$, M = Zr and Hf and OPr^i = isopropoxide) to manufacture and provide better precursors for the decomposition of various materials. X-ray diffraction confirmed that the structures are isomorphous.

More recently, Hubert-Pfalzgraf *et al*.[10] synthesized bis-β-diketonato hafnium complexes, $[Hf(thd)_2Cl_2]$, where thd = tetramethylheptanedione, also as precursors for metal-organic chemical vapour deposition (MOCVD) of hafnium silicate films due to their thermodynamic stability properties. Various substitution reactions was applied to $[Hf(thd)_2Cl_2]$ to produce hafnium siliciates, $[Hf\{N(SiMe_3)_2\}_2(thd)_2]$, $[Hf(OSiMe_3)_2(thd)_2]$ and $[Hf(OSi^tBuMe_2)(thd)_2]$, in high yields.

[53] Fleeting K. A., O'Brien P., Otway D. J., White A. J. P., Williams D. J. and Jones C., *Inorg. Chem*., 38, 1432, 1999.

The precursors typically used for MOCVD include hafnium β-diketonates as mentioned above[54,55], alkoxides[56] and fluorinated β-diketonates.[55,57]

The general synthesis for bis-β-diketonato metal complexes with M = Ti, Zr and Hf comprises of mixing the corresponding metal tetrahalide and β-diketone in an organic solvent under anhydrous conditions, according to Scheme 2.4.

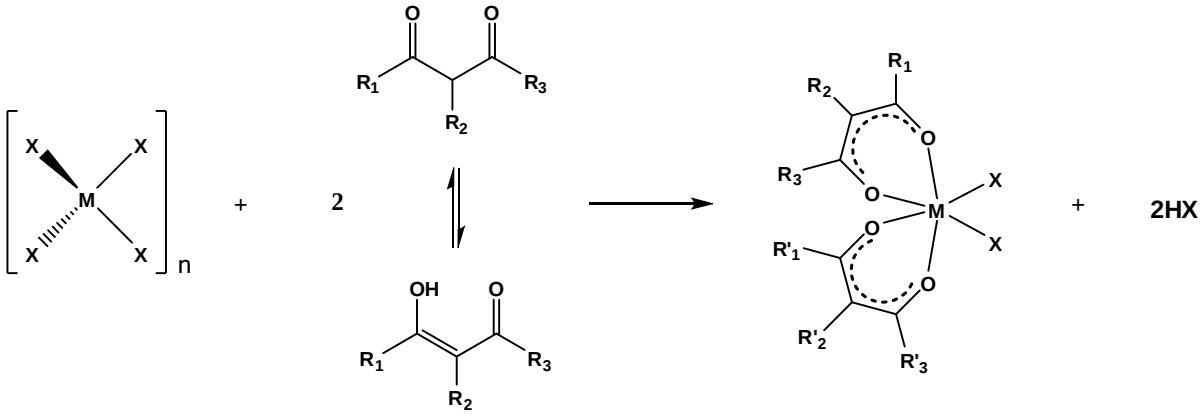

Scheme 2.4: General synthesis of $[M(L,L')_2X_2]$ complexes with M = Ti^{IV}, Hf^{IV} and Zr^{IV}.

Bis-β-diketonato metal complexes are highly susceptible to atmospheric moisture and are easily hydrolysed due to the easily replaceable group X (X = halide or alcohol) by an aqueous group as illustrated in Scheme 2.5.[58]

[54] Si J., Desu S. B. and Tsai C. Y., *J. Mater. Res*., **9**, 1721, 1994.

[55] Balog M., Schieber M., Patai S. and Michman M., *J. Cryst. Growth,* **17**, 298, 1972.

[56] Xue Z., Vaartstra B. A., Caulton K. G., Chisholm M. H. and Jones D. L., *Eur. J. Solid State Inorg. Chem*., ***29***, 213, 1992.

[57] Hwang C. S. and Kim H. J., *J. Mater. Res*., **8**, 1361, 1993.

[58] Keppler B. K. and Heim M. E., *Drugs of the Future*, **3**, 638, 1988.

The resistance against hydrolysis depends on group X in the following order:

$$F > Cl > Br > I$$

$$[M(L,L')_2X_2] \overset{+H_2O}{\rightleftharpoons} [M(H_2O)(L,L')_2X]^+X^- \quad \text{. . . Eq. 2.7}$$

$$[M(H_2O)(L,L')_2X]^+X^- \overset{-HX}{\rightleftharpoons} [M(HO)(L,L')_2X] + HX \quad \text{. . . Eq. 2.8}$$

$$[M(HO)(L,L')_2X] \overset{+H_2O}{\rightleftharpoons} [M(OH)(H_2O)(L,L')_2]^+X^- \quad \text{. . . Eq. 2.9}$$

$$[M(OH)(H_2O)(L,L')_2]^+X^- \overset{-HX}{\rightleftharpoons} [M(OH)_2(L,L')_2] + HX \quad \text{. . . Eq. 2.10}$$

$$[M(OH)_2(L,L')_2] \overset{-H_2O}{\rightleftharpoons} \text{Polymers} \quad \text{. . . Eq. 2.11}$$

$$\text{Polymers} \longrightarrow MO_2 \quad \text{. . . Eq. 2.12}$$

Scheme 2.5: Hydrolysis of bis-β-diketonato metal complexes

2.6.4 Hafnium and Zirconium Complexes Containing Tris-(diketonates), [M(*L,L'*)$_3$X]

The first tris-β-diketonato metal complexes were synthesized on the basis of its chemical properties as ionic salts, $[M(L,L')_3]^+ Cl^-$ which contains six coordinated metal centres.[59] From there on, a number of derivatives have been prepared, $[M(L,L')_3Cl]$, L,L' = acac, bzac and dbm; M = Zr and Hf, which are all seven coordinated, monomeric, non-electrolyte compounds.[60] Only the $[M(dbm)_3Cl]$ species could be ionized to $[M(dbm)_3]^+(FeCl_4)^-$, however $[M(acac)_3I]$ demonstrated significant ionic conduction in tetrahydrofuran and nitromethane to produce the corresponding solvated cations. NMR spectra confirmed rapid intermolecular exchange of the β-

[59] Morgan G. T. and Bowen A. R., *J. Chem. Soc*., **125,** 1252, 1924.

[60] Cox M., Lewis J. and Nyholm R. S., *J. Chem. Soc*. 6113, 1964.

diketone ligands at 143 K.[12] All the seven coordinated $M(acac)_3X$ complexes showed two or more non-equivalent methyl groups. A single methyl resonance indicated that the chelate rings undergo rapid configurational rearrangements, which exchange methyl groups between the different non-equivalent environments. This phenomenon is also observed for the eight coordinated, $M(L,L')_4$, complexes.[61] Unfortunately IR- and Raman Spectra (*see* Table 2.3) could not yield any information on stereochemistry.

Table 2.3: Selected Infrared and Raman Spectra of tris-β-diketonato metal complexes.[43]

Compound		ν_s(C=O)	ν_{as}(C=O)	ν_{as}(C=O)	ν_s(C=C)	π(C-H)	ν_s(M-O)	ν_{as}(M-O)	ν(M-X)
$Zr(acac)Cl_3$	IR Raman	1581 vs, 1568 vs Obs	1532	1381 s	1283 s 1292 vs, p	788 m	449 sh 448 s, p	432 s 431 s	314 s
$Hf(acac)Cl_3$	IR Raman	1579 vs, 1570 vs Obs	1533	1387 s	1287 s 1293 vs, p	790 m	454 sh 452s, p	432 s 433 sh	293 s
$Zr(acac)Br_3$	IR Raman	1580 Obs	1534	1381 s	1283 s 1292 vs, p	788 m	449 sh 449 s, p	434 s 430	164 w
$Hf(acac)Br_3$	IR Raman	1574 vs, 1565 vs Obs	1532	1386 s	1278 s 1291 vs, p	791 m	454 w 452 s, p	433 s 430	166w
$Zr(acac)I_3$	IR	1562 vs	1533	1380 s	1285 s	790 m	452 sh	438 s	93 w

***Notes**: All spectra were obtained in dichloromethane; obs = region obscured by solvent, vs = very stong, s = strong, m = medium, w = weak, sh = shoulder and p = polarized.*

The molecular structure of $[Hf(thd)_3Cl]$ was obtained by Hubert-Pfalzgraf and co-workers[10] for the MOCVD precursor of hafnium silicate films. This tri-substituted complex, $[Hf(thd)_3Cl]$, was obtained with the same procedure followed for the di-substituted complex. In the case of the tri-substituted complex, 3 moles bidentate ligand (thdH) was added to 1 mole hafnium tetrachloride in toluene, whereas 2 moles of the bidentate ligand (thdH) was added to obtain the di-substituted complex. The compound, $Hf(thd)_3Cl$ (*see* Figure 2.8) crystallized in the monoclinic space group, $P2_1/m$, where the hafnium(IV) is seven coordinated. The coordination polyhedron of the hafnium(IV) atom showed a distorted *capped trigonal prism*.

[61] Pinnavaia T. J. and Fray C., *Inorg. Chem.*, **5**, 233, 1968.

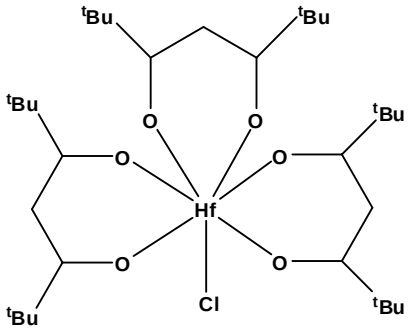

Figure 2.8: The two-dimensional structure of $Hf(thd)_3Cl$.

2.6.5 Hafnium and Zirconium Complexes Containing Tetrakis(diketonates), [M(*L,L'*)$_4$]

Until recently the x-ray crystal structures of acetylacetonate hafnium complexes had not been determined. Previously, only the acetylacetonate zirconium complexes, $[Zr(acac)_4]$,[62] and $[Zr(bzbz)_4]$,[63] crystal structures were reported. Both these structures have an eight-coordinated complex with a slightly distorted square antiprismatic geometry which was studied in depth by Chun and co-workers.

Lowe *et al.*[64] has shown by means of electron diffraction that the hafnium analogue, $[Hf(acac)_4]$, is isomorphous with $[Zr(acac)_4]$, where both structures have a D_2 antiprismatic coordination polyhedron geometry. Since then a number of these homoleptic compounds, $[M(tfaa)_4]$ (M = Zr and Hf)[65] and $[Zr(hfaa)_4]$,[66] have been synthesized. The molecular structure for $[Zr(hfaa)_4]$ was confirmed through X-ray diffraction, and it was established that the complex was an eight-coordinated monomer.

[62] Silverton J. V. and Hoard J. L., *Inorg. Chem*., **2**, 243, 1963.

[63] Chun H. K., Steffen W. L. and Fay R. C., *Inorg. Chem*., **18**, 2458, 1979.

[64] Lowe L. M., Prestwich W. V. and Zmora H., *Can. J. Phys*., **53**, 1327, 1975.

[65] Matsubara N. and Kuwamoto T., *Inorg. Chem*., **24,** 2697, 1985.

[66] Calderazzo F., Englert U., Maichle-Mossmer C., Marchetti F., Pampaloni G., Petroni D., Pinzino C., Strahle J. and Tripepi G., *Inorg. Chim. Acta*., **270**, 177, 1998.

Kinetic studies[67,68] on the exchange of [M(acac)$_4$] (M = Zr and Hf) with free acetylacetone ligands, indicated that the process proceeds *via* a nine-coordinated intermediate. ^{1}H and ^{19}F NMR kinetics were performed on mixtures of [M(acac)$_4$] and [M(tfaa)$_4$], which yielded equilibrium mixtures containing five different compounds, [M(acac)$_4$], [M(acac)$_3$(tfaa)], [M(acac)$_2$(tfaa)$_2$], [M(acac)(tfaa)$_3$] and [M(tfaa)$_4$] (M = Zr and Hf).[69] Therefore, two types of ligand exchange were identified for the equilibrium system:

1. The first type involving the exchange between the acetylacetone ligands and trifluoroacetylacetone groups:

$$M(acac)_3(\underline{tfaa}) + M(acac)_2(tfaa)_2 \rightleftharpoons M(acac)_4 + M(acac)(\underline{tfaa})_3 \quad \textbf{. . . Eq. 2.13}$$

or

$$M(acac)_3(\underline{tfaa}) + M(acac)_2(tfaa)_2 \rightleftharpoons M(acac)_2(tfaa)_2 + M(acac)_3(\underline{tfaa}) \quad \textbf{. . . Eq. 2.14}$$

2. The second route involves the exchange between the acetylacetone ligands and acetylacetone groups:

$$M(acac)_2(\underline{acac})'(tfaa) + M(acac)_2(tfaa)_2 \rightleftharpoons M(acac)_3(tfaa) + M(acac)(\underline{acac})'(tfaa)_2 \quad \textbf{. . . Eq. 2.15}$$

or

$$M(acac)_2(tfaa)(\underline{tfaa})' + M(acac)(tfaa)_3 \rightleftharpoons M(acac)_2(tfaa)_2 + M(acac)(tfaa)_2(\underline{tfaa})' \quad \textbf{. . . Eq. 2.16}$$

[67] Jung W. S. and Nakagawa T., *Inorg. Chim. Acta.,* **209**, 79, 1993.

[68] Jung W. S., Ishizaki H. and Tomiyasu H., *J. Chem. Soc., Dalton Trans.,* 1077, 1995.

[69] Adams A. C. and Larsen E. M., *Inorg. Chem.*, **5**, 2, 228, 1966.

It is interesting to note that the equilibrium constants, K_n, for the formation of the mixed ligand complexes, is directly proportional to the differences in the degree of fluorination of the two diketonate ligands.

Fay *et al*.[43] described the prevalence of $[M(L,L')_n(L,L')'_{4-n}]$ species due to entropy effects but was unsuccessful in detecting geometrical isomers utilizing NMR at 168K, due to the fast intermolecular ligand rearrangements in the $[M(L,L')_4]$ complex.

Recently, a wide range of volatile tetrakis-diketonate metal complexes have been prepared by Zherikova *et al.*[14,70] through reacting anhydrous hafnium chloride, $[HfCl_4]$, with an excess of β-diketones in an inert solvent under reflux and purified by zone vacuum sublimation. (a) $[Hf(acac)_4]$, (b) $[Hf(tfaa)_4]$ and (c) $[Hf(ptac)_4]$ was successfully synthesized (*see* Figure 2.9) to be used for the preparation of hafnium dioxide films and oxide coatings.

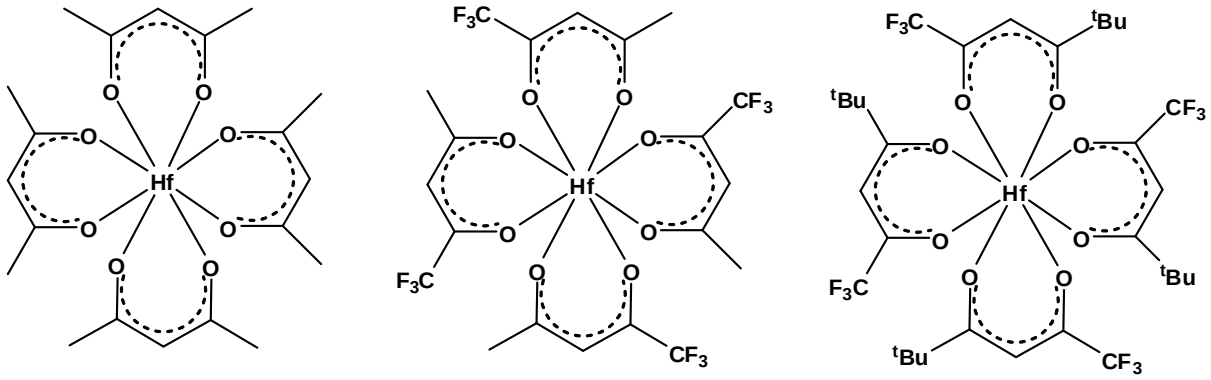

(a) $[Hf(acac)_4]$ **(b)** $[Hf(tfaa)_4]$ **(c)** $[Hf(ptac)_4]$

Figure 2.9: Complexes successfully synthesized by Zherikova *et al.*

All three molecular structures above formed isolated mononuclear complexes, where their four β-diketonate ligands made four six-membered chelate metallocycles in each complex. The crystal structures of $[Hf(acac)_4]$ and $[Hf(ptac)_4]$ are isomorphous

[70] Zherikova K. V., Morozova N. B., Baidina I. A., Peresypkina E.V. and Igumenov I. K., *J. Struct. Chem.*, **47**, 3, 570, 2006.

to the $[Zr(acac)_4]$ and $[Zr(ptac)_4]$ analogues of which crystal structures were obtained by Allard in 1976[71] and Zherikova *et al.,*[72] respectively. The crystal structure of $[Hf(tfaa)_4]$ is not available in literature.

The hexafluoroacetylacetonato hafnium(IV) complex has been synthesized and characterized by Zherikova *et al*. in 2006.[22] The published molecular structure of discrete centrosymmetric dimers $[Hf(OH)(hfaa)_3]_2$ is represented in Figure 2.10.

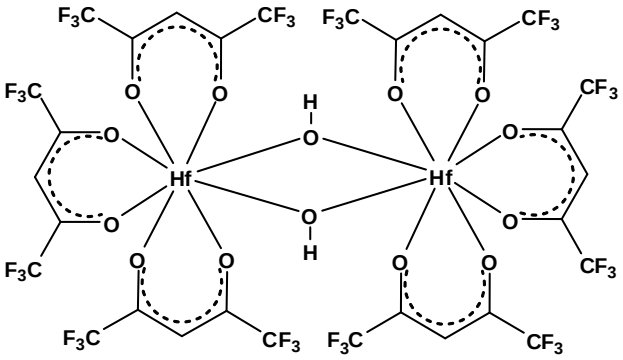

Figure 2.10: Dimeric complex, $[Hf(OH)(hfaa)_3]_2$, synthesized by Zherikova *et al*.

Hexafluoroacetylacetonato hafnium(IV) is one of the very few complexes which is not isomorphous to its zirconium counterpart. Literature revealed that $Zr(hfaa)_4$, has a monomeric structure with a slightly distorted antiprism coordination polyhedron about the hafnium atom.

[71] Allard B., *J. Inorg. Nucl. Chem.,* **38**, 2109, 1976.

[72] Zherikova K. V., Morozova N. B., Kurat'eva N. V., Baidina I. A., Stabnikov P. A. and Igumenov I. K., *J. Struct. Chem.*, **48**, 3, 513, 2007.

2.6.6 Hafnium and Zirconium Complexes Containing Quinones (N,O-Bidentate Ligands)

8-hydroxyquinolinate, Ox, can be considered as a combination of catecholate and 2,2'-bipyridine as illustrated in Figure 2.11.

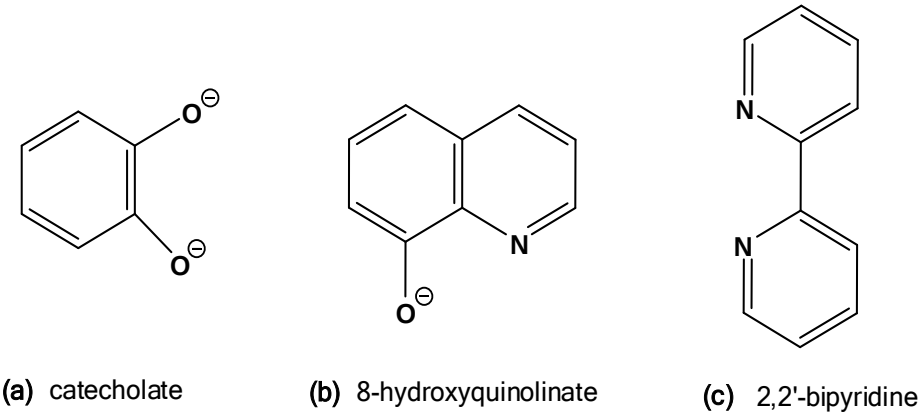

(a) catecholate **(b)** 8-hydroxyquinolinate **(c)** 2,2'-bipyridine

Figure 2.11: Comparison of the chelating elements of catecholate, 8-hydroxyquinoline and 2,2'-bipyridine.

8-Hydroxyquinoline in its deprotonated form, possesses one phenolate unit of catecholate and one pyridine donor of the bipyridine, therefore making it monoanionic and bridges the gap between the dianionic catecholate and the neutral bipyridine. 8-Hydroxyquinoline and its derivatives are generally synthesized by the Doebner-Miller[73], Friedländer[74] or the Skraup[75] synthesis. Substituents on the quinoline can be introduced during the synthesis or by modifying the various positions of the parent molecule, OxH, as illustrated in Scheme 2.6(a) and (b), respectively.

[73] Doebner O. and Miller W. V., *Chem. Ber.,* **16**, 1664, 1883.

[74] Cheng C. C. and Yan S.J., *Org. React.,* **28**, 37, 1982.

[75] Skraup Z.H., *Chem. Monatsschr.,* **2**, 139, 1881.

(a)

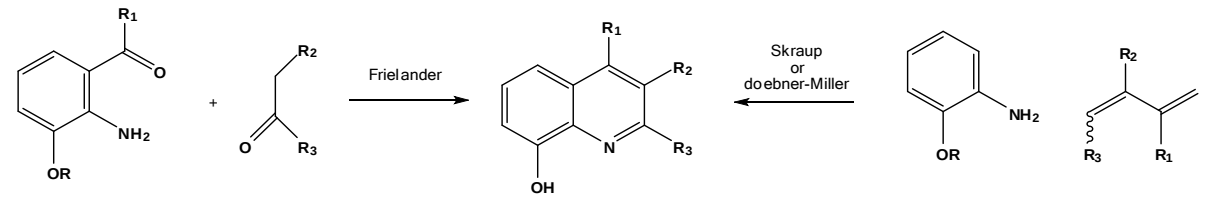

(b)

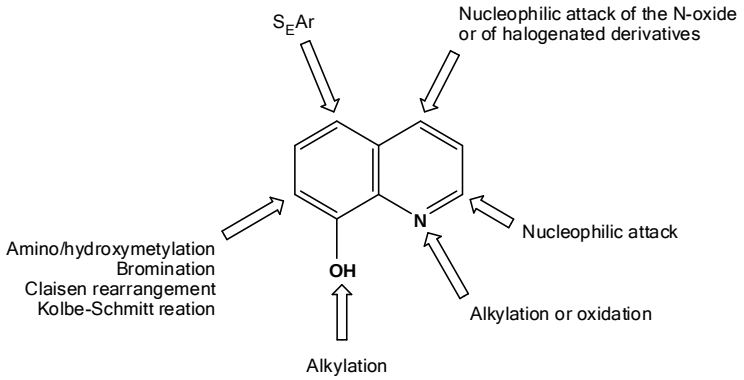

Scheme 2.6: Preparation of different 8-hydroxyquinoline derivatives, (a), and possible functionilization of the 8-Hydroxyquinoline, (b).

8-Hydroxyquinoline is a colourless, crystalline, solid, which is almost insoluble in water but forms sparingly soluble derivatives with metallic ions. Depending on the coordination number, OxH can coordinate to the metal to form different $[M(Ox)_2]$, $[M(Ox)_3]$ and $[M(Ox)_4]$ adducts. By using complex-forming reagents or by proper control of the pH in solutions, various separations of metal complexes can be carried out by means of quantitative precipitation of the metal oxinates.[76]

Hafnium(IV) and zirconium(IV) halides react readily with N,O-bidentate ligands to form a variety of mono- to tetra-substituted (1:1 – 1:4) adducts as mentioned earlier in Section 2.4. In literature it is reported that eight equivalents of OxH reacts in THF with zirconium and hafnium chlorides at elevated temperatures to produce tetrakis-8-quinolinate metal complexes, $M(Ox)_4$. $M(Ox)_4$[15] (M = Zr and Hf, Figure 2.12) is hydrolytically and thermally very stable. IR spectra confirmed the 8-hydroxyquinolate

[76] Jeffery G. H., Basset J., Mendham J. and Denney R. C., *Vogel's textbook of Quantitative Chemical Analysis*, 5th Ed., Longman Scientific and Technical, New York, 1989.

groups to be bidentate and X-ray powder diffraction verified that the zirconium- and hafnium tetrakis-8-quinolinate are isomorphous.

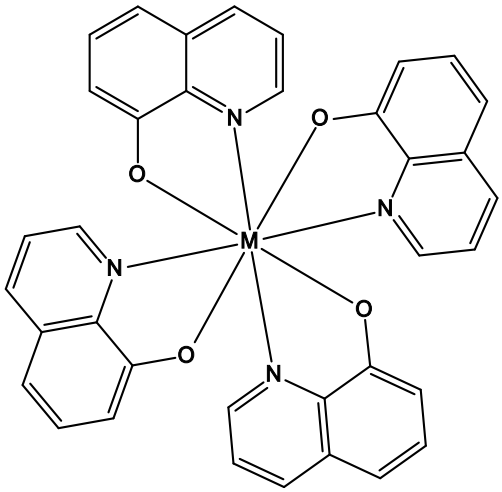

Figure 2.12: Tetrakis(8-quinolinato) metal complexes, $M(Ox)_4$, synthesized by Frazer *et al*.[93]

The X-ray crystal structure of tetrakis(8-quinolinato)zirconium(IV) was solved by Lewis *et al*.[77] while no single crystal structures of the corresponding hafnium quinolate have been reported yet.

[77] Lewis D. F. and Fay R. C., *J. Chem. Soc., Chem. Commun*., 1046, 1974.

3 Basic Theory of IR, NMR, UV/Vis and X-Ray Diffraction

3.1 Introduction

The complexes, O,O'- and N,O-bidentate ligands coordinated to Hf(IV) and synthesized in this study was fully characterized by various spectroscopic techniques, including infrared (IR), ultraviolet-visible (UV/Vis) and nuclear magnetic resonance (NMR) spectroscopy. These techniques are of great importance to the scientist for the identification and characterization of starting, intermediate and final products.

Three complexes synthesized in this study were also characterized by X-ray diffraction which will be discussed in detail in Chapter 5. The basic theory of the techniques utilized in this study is briefly discussed in this chapter.

3.2 Infrared Spectroscopy

3.2.1 Background

Infrared (IR) spectroscopy is a quick, relatively cheap and reliable method to identify and quantify a large range of complexes. Almost all organic and inorganic compounds containing covalent bonds, except for some homonuclear molecules, absorb infrared radiation. The infrared region in the electromagnetic spectrum extends from 14 000 cm^{-1} to 10 cm^{-1}, where the mid-infrared region (4 000 cm^{-1} to 400 cm^{-1}) is of the most interest for chemical analysis. This region corresponds to changes in vibrational energies within the molecules. The far infrared region (400 cm^{-1} to 10 cm^{-1}) is mainly used for analyzing inorganic compounds which contain heavy atoms.

Infrared spectroscopy alone is seldom, if ever, used to identify new and unknown compounds, and is mainly used for indentifying certain functional groups with single bonds (C-H, O-H and C-Cl), double bonds (C=O, C=N and N=O) and triple bonds (C≡C and C≡N).

3.2.2 Theory[1]

When a beam of electromagnetic radiation of intensity I_o is passed through a complex, it can be either absorbed or transmitted, depending upon the frequency of the light source, ν, and the structure of the molecule it encounters.

When a molecule absorbs radiation it gains energy as it undergoes a quantum transition from one energy state ($E_{initial}$) to another (E_{final}). The frequency of the absorbed radiation is related to the energy by Planck's law:

$$E_{final} - E_{initial} = \Delta E = \boldsymbol{\lambda\nu} = \frac{\boldsymbol{hc}}{\boldsymbol{\lambda}} \qquad \textbf{...Eq. 3.1}$$

ΔE is the difference in energy between two quantized states ($E_{initial}$ and E_{final}). The amount of radiation that a molecule absorbs to be excited from $E_{initial}$ to E_{final} is emitted at the same radiation frequency, ν, (as in Eq. 3.1) when it relapses back from E_{final} to $E_{initial}$.

IR radiations can excite rotational, vibrational and even electronic energy levels if these levels are close enough to each other. Rotational energy levels are relatively close to each other, resulting in the fact that transitions between them occur at much lower frequencies, needing less energy than transitions between the vibrational and electronic energy levels as shown in Figure 3.1.[2]

[1] Nakamoto K., *Infrared Spectra of Inorganic and Coordination Compounds*, 2nd Ed., John Wiley and Sons Inc., New York, 1970.

[2] Image obtained from:
http://hyperphysics.phy-astr.gsu.edu/Hbase/molecule/molec.html (Last accessed 14/11/2008).

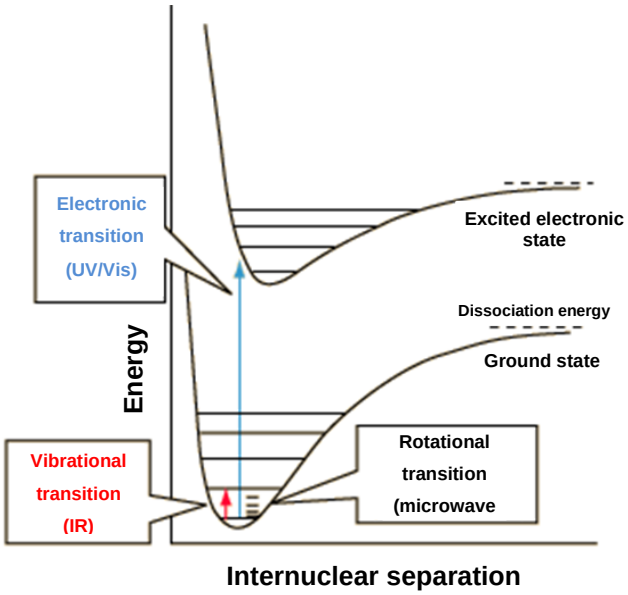

Figure 3.1: Energy levels of a diatomic molecule.

3.2.3 Molecular Vibrations

All molecules vibrate, even at a temperature of absolute zero, due to nuclear vibrations. Figure 3.2 shows the normal modes of vibration (characteristic absorptions) in a formaldehyde (IUPAC name methanal) molecule, where the arrows indicate the direction of the harmonic motions carried out by each individual nucleus. In general a polyatomic molecule with n atoms, has $3n - 6$ or, if linear, $3n - 5$ distinct vibrations, [1] and each vibration can be associated with motion in a particular group. These various vibrations absorb the infrared beam at characteristic frequencies to produce absorption bands. Methanal can be used as a good example (OCH_2, $n = 4$, thus $3n - 6 =$ *6 vibrations involved*).

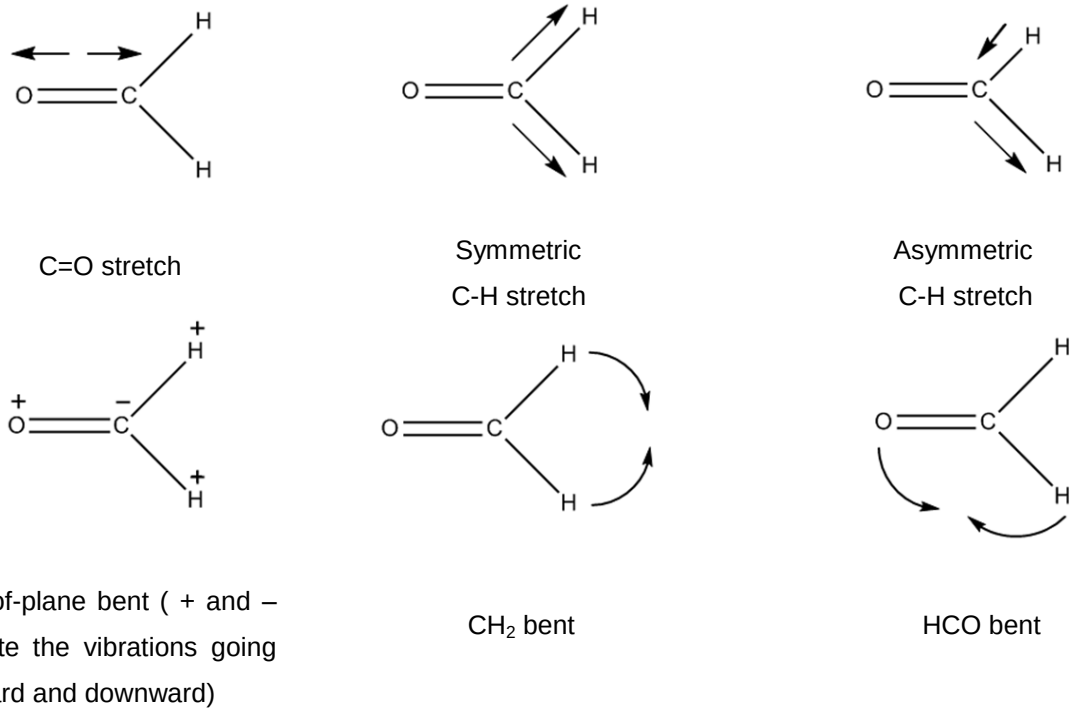

Figure 3.2: Normal modes of vibration in a methanal molecule.

It is quite evident that even for a very simple molecule, such as methanal, it can become very complicated and complex to determine all the molecular vibrations. Fortunately it is almost never necessary to assign each vibration for IR spectroscopy to be useful.

3.2.4 Infrared Activity

As mentioned above, almost all organic and inorganic compounds containing covalent bonds, absorb infrared radiation except for some homonuclear molecules. For a molecule to be infrared active, there must be a change of dipole moment during the vibrations[3]. Therefore a homonuclear diatomic molecule such as H_2, N_2 and O_2 will not absorb infrared radiation because these molecules have no net

[3] Nakanishi K. and Solomon P. H., *Infrared Absorption Spectroscopy*, 2nd Ed., Holden-Day, Inc., San Francisco, 1977.

change in the dipole moment and stretching of these bonds do not produce a change in dipole moment. It is important to understand that it is not necessary for a molecule to have a permanent dipole moment to be infrared active. An example is the linear centrosymmetric CO_2 molecule, which has no permanent dipole movement.

The symmetric stretch in the CO_2 molecule will not be infrared active but the asymmetric stretch will produce a change in dipole moment and therefore make it infrared active (*see* Figure 3.3).

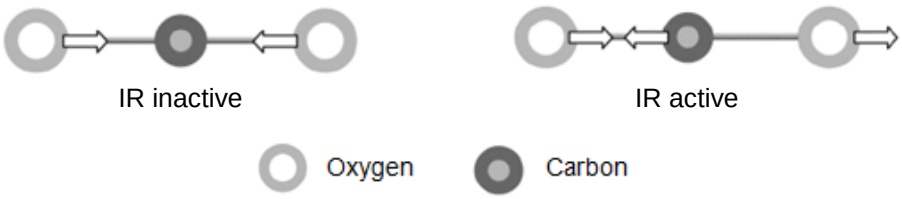

Figure 3.3: Symmetric and asymmetric stretching vibrations of a CO_2 molecule

3.2.5 Interpreting IR Spectra via Fingerprinting

Typical vibrations of functional groups make infrared spectroscopy a powerful analytical tool. Functional groups are groups of atoms that absorb IR radiation in approximately the same region in a variety of compounds. The absorption bands of these functional groups are somewhat, but not much affected by the rest of the molecule. This allows one to relate absorption band position with a particular functional group and compare it to known and published groups, very much like a *fingerprint* of a human being (*see* Figure 3.4).[3]

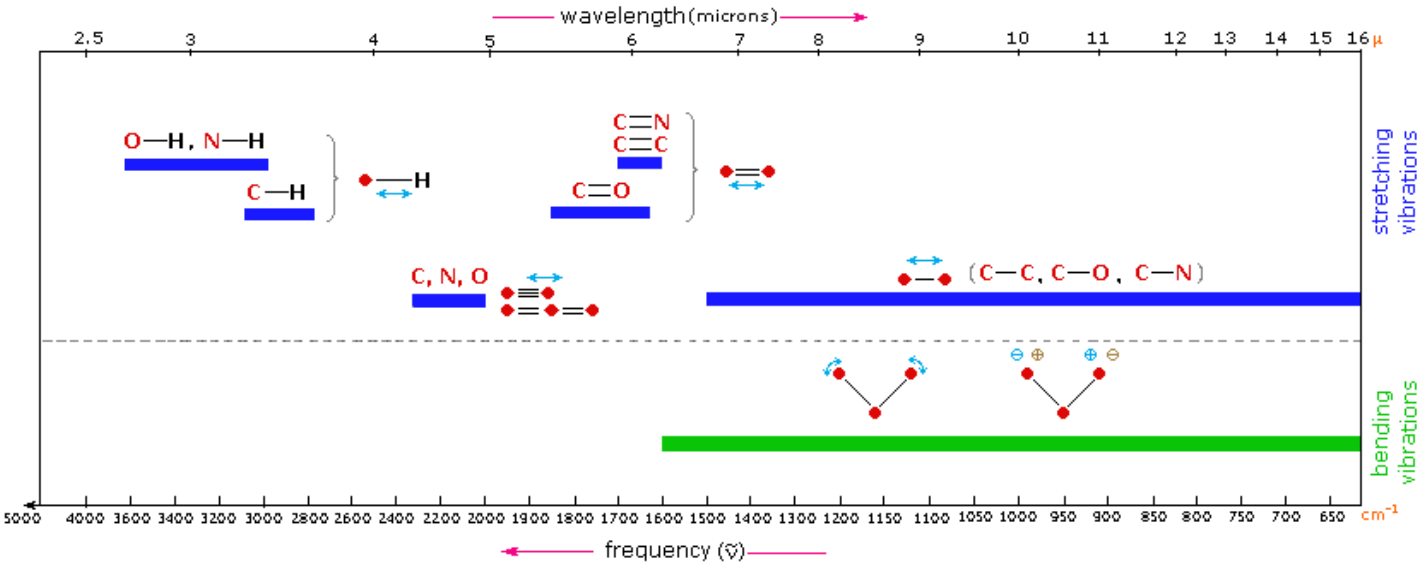

Figure 3.4: Stretching and bending vibrations of some functional groups[3]

There are many different tables like the above, available for reference in literature. When assigning different peaks off functional groups in the infrared region, it is usually the stretching vibrations and not the bending vibrations which are most useful for analysis.

3.3 Nuclear Magnetic Resonance (NMR) Spectroscopy

3.3.1 Introduction

Nuclear Magnetic Resonance (NMR) spectroscopy has been a powerful non-destructive analytic tool for chemists since 1946, when two independent research groups invented NMR for the first time. Both research groups were jointly awarded the Noble Prize for Physics in 1952. In 1991 the NMR spectroscopist, R.R. Ernst from Zürich, was awarded the Noble Prize for Chemistry for his pioneering work on NMR techniques. Since then, NMR spectroscopy became one of the most powerful analytical techniques.

The main purpose for NMR spectroscopy is usually the determination of molecular structures in a non-destructive way. NMR spectroscopy can produce very good structural information about an unknown complex in a relatively short amount of time, needing less than a milligram of the unknown complex.

Due to the major success of NMR spectroscopy over the years, it has become one of the most powerful and indispensible tool for chemists, biochemists, physicists and is used as an application in medical sciences.

3.3.2 Theory

Before understanding NMR spectroscopy, one must first understand how a nucleus, which has a certain nuclear angular momentum, *P*, and magnetic moment, μ, will behave in a strong static magnetic field.

Angular momentum, *P*, means that a nucleus has a spin property. If we assume that nuclei rotates about an axis like the earth rotates on its own axis, it must have an angular momentum. This angular momentum is quantized by Eq. 3.2.[4]

$$\boldsymbol{P} = \sqrt{\boldsymbol{I}(\boldsymbol{I}+\mathbf{1})}\boldsymbol{\hbar} \qquad \textbf{.....Eq. 3.2}$$

Where $\hbar = h/2\pi$, h = Planck's constant (6.6256 x 10^{-34} J.s) and I the angular momentum (spin) quantum number or just simply nuclear spin. The nuclear spin values can range from ½ up to 6 in increments of ½'s. This value depends on the nucleus' atomic mass and atomic number.

[4] Harris K. R., *Nuclear Magnetic Resonance Spectroscopy*, Longman Group UK Ltd., England, 1986.

The overall spin (*I*) can be determined by using Table 3.1 below.[5]

Table 3.1: The spin quantum number (*I*) is determined by evaluating the atomic mass and number of a molecule**.**

Atomic mass	Atomic number	Spin quantum number (I)
uneven	even or uneven	1/2, 3/2, 5/2, ...
even	even	0
even	uneven	1, 2, 3, 4, ...

Also associated with angular momentum, *P*, is a magnetic moment, μ, as given by Eq. 3.3.

$$\mu = \gamma P \qquad \text{... Eq. 3.3}$$

The proportionality factor, γ, is a constant value for each nuclide and is called the gyromagnetic ratio. The gyromagnetic ratio is again directly proportional to the theoretical sensitivity of a nuclide to NMR (*large* γ *values give better detection*).

In the absence of an external magnetic field, nuclei will have random orientations. If however, an external magnetic field (B_0) is applied to such nuclei they adopt specific orientations relative to the applied field, a phenomenon referred to as directional quantization[5]. A nucleus with a nuclear spin, *I,* will have (2*I* +1) discrete orientations ranging from *I* to -*I* in steps of 1.[6]

The orientations are defined by a magnetic quantum number (m_I), thus a nucleus with a nuclear spin of a ½ will have two possible orientations e.g. *I* = ½ and *I* = -½ (*see* Figure 3.5).

[5] Lynden-Bell R. M., Harris R. K., *Nuclear Magnetic Resonance Spectroscopy*, Thomas Nelson and Sons (South Africa) (Proprietary) Ltd., Cape Town, 1969.

[6] Hore P. J., *Nuclear Magnetic Resonance*, Oxford University Press Inc., New York, 1995.

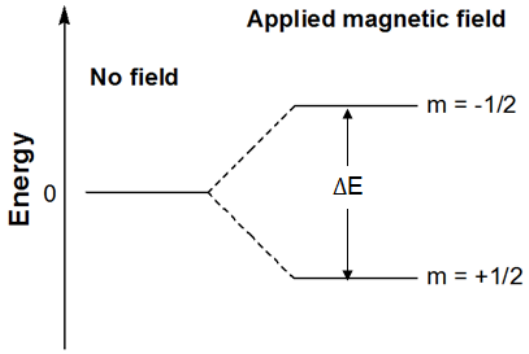

Figure 3.5: Energy levels for a nucleus with spin quantum number ½**.**

A spinning nucleus in a static external magnetic field (B_0) interacts with the magnetic dipole moment (μ) to cause the nuclear dipoles to spin about its axis processing around the magnetic field (B_0) to resemble the behaviour of a spinning top.

The precession frequency, or better known as the Lamor frequency, υ_L, is directly proportional to the applied external magnetic field, B_0.

$$\upsilon_L = \left|\frac{\gamma}{2\pi}\right| B_0 \qquad \textbf{.....Eq. 3.4}$$

For a nucleus with 2I+1 possible orientations there are 2I+1 energy levels. These energy levels are also better known as nuclear Zeeman levels. The relative energy of each orientation is dependent on its magnetic quantum number (m_I)

$$E = -m\gamma\hbar B_0 \qquad \textbf{.....Eq. 3.5}$$

For example, a nucleus with I = ½ will then have two Zeeman levels in a static magnetic field which corresponds with the two m_i values (+½ which is parallel to the applied field and -½ which is anti-parallel to the applied field) as illustrated in Figure 3.6.

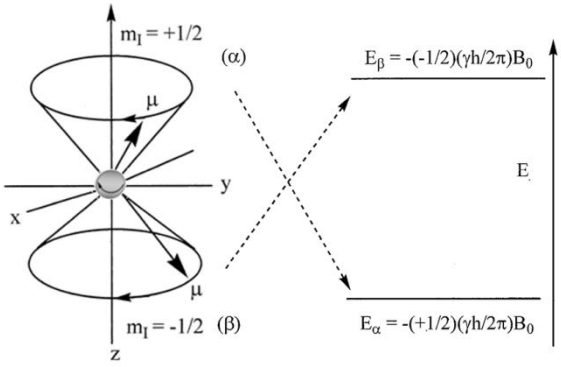

Figure 3.6: A graphic illustration of the two Zeeman levels for a nucleus with I = ½.

The energy difference between the two levels is determined by Eq. 3.6.

$$\Delta E = \gamma \hbar B_0 \qquad \textbf{.....Eq. 3.6}$$

The magnetic field experienced at the nucleus is not equal to the applied magnetic field due to negatively charged electrons moving in spherical orbitals (s-orbitals) about the nucleus and generating a local magnetic field perpendicular to the applied magnetic field, B_o, as shown in Figure 3.7.

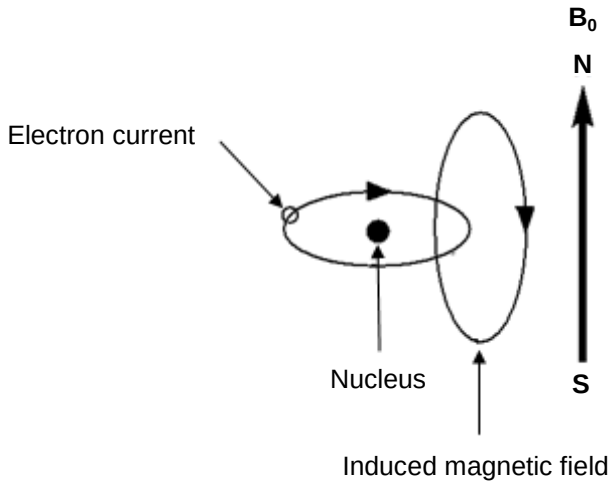

Figure 3.7: Schematic illustration of nuclear shielding.

The result is that the nucleus does not experience the applied magnetic field but rather an effective magnetic field (H_0) resonating at a lower Larmor frequency (ν), which is the applied field modified by the environment of the nucleus (e.g. electron density, proximity of other nuclei, etc.).[7] This phenomenon is known as nuclear shielding (chemical shift, δ) and varies from nucleus to nucleus. Molecules containing electrons in non-spherical orbitals like *p*- and *d*-orbitals produce relatively large magnetic fields in the nucleus compared to spherical s orbitals. The last mentioned orbitals produce low field shift, deshielding, where non-spherical orbitals produce high field shift, shielding. Many factors can influence the chemical shift but the inductive- and anisotropic effects are the main contributors.

- ***Inductive*- and anisotropic *effects* can be summarized as follows**:
  - ***Inductive effects:***

    Electron donating groups increase the electron density around the nucleus which causes shielding. Electron withdrawing groups on the other hand decrease the electron density around the nucleus and therefore cause deshielding, *see* Figure 3.8.

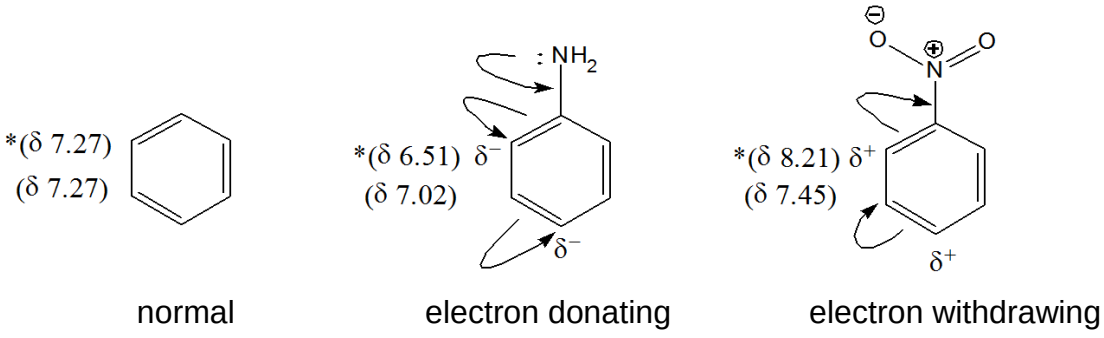

Figure 3.8: Illustration of Inductive effects due to electron- donating and withdrawing groups.

  - **Anisotropic *effects:***

    A local magnetic field is generated by the delocalization of π-electrons in a molecule which may influence the applied magnetic field, causing the

[7] Friebolin H., *Basic One- and Two-Dimensional NMR Spectroscopy*, 2nd Ed., VCH Publishers, New York, 1993.

protons to resonate at higher or lower chemical shifts, effectively shielding and deshielding respectively, as indicated in Figure 3.9.

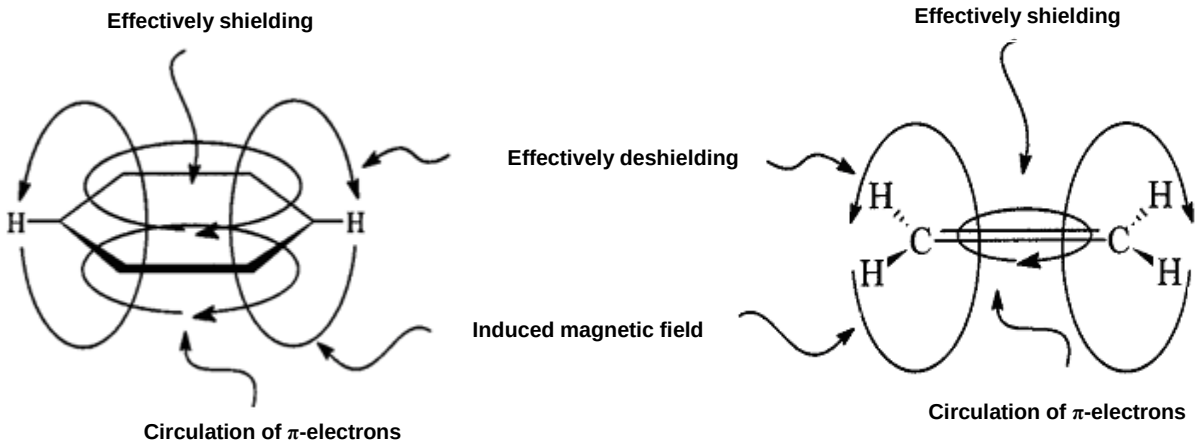

Figure 3.9: Delocalization of π-electrons in a molecule to produce a local magnetic field.

The resonant signals of a proton can also be affected by interactions *via* bonding electrons of nearby protons. This interaction causes mutual splitting (multiplicity) of their resonant signals into two or more lines which is the result of an interaction between the magnetic moments of neighbouring protons. This phenomenon is known as *spin-spin coupling.* The multiplicity of spin-spin coupling is totally dependent on the amount of neighbouring protons in the case of ^{1}H NMR.

The following rules can be followed when interpreting multiplicity:

- A proton with *n* equivalent neighbouring protons will split into (*n*+1) lines,
- A proton with *n* non-equivalent neighbouring protons will split into (2^{n}) lines,
- Equivalent protons do not interact with each other (no splitting).

The spacing between the peaks of the splitted resonant signals is measured in Hertz and is commonly known as the *coupling constant (J).* The coupling constant is totally independent of the applied field and only dependant on the number of bonds between (1-4 bonds) the coupled protons and structural characteristics of the molecule.

3.4 Ultraviolet-Visible Spectroscopy

3.4.1 Introduction

Ultraviolet-visible spectroscopy (UV/Vis) is based on the absorbance of energy in the same way as IR spectroscopy. In the case of UV/Vis it is the transition between electronic states that is monitored, whereas in IR spectroscopy, transitions between the vibrational and rotational states are monitored. The UV/Vis wavelengths range from 200-400 nm for UV and 400-800 nm for the visible region in the electromagnetic spectrum.

The absorption of UV or visible radiation corresponds to the excitation of valence (outer) electrons. There are a few main types of electronic transitions which can be considered in UV/Vis, e.g. transitions involving single (σ) single bonding-, double or triple (π) bonding- and non bonding (*n*, lone pair electrons) orbitals.

As a molecule is radiated with energy, the valence electrons are excited from a **highest occupied molecular orbital** (HOMO) to the **lowest unoccupied molecular orbital** (LUMO)[8] as illustrated in Figure 3.10.

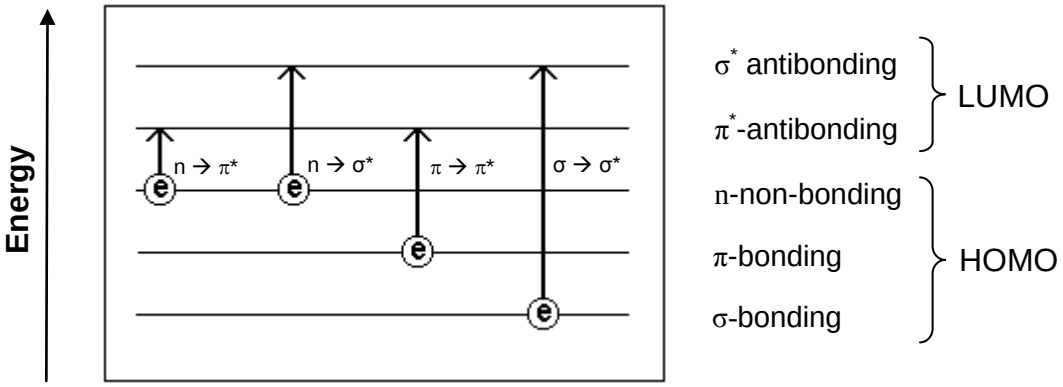

Figure 3.10: Possible electronic transitions of π, σ, and n electrons from LUMO to HOMO.

[8] Pavia D. L., Lampman G. M. and Kriz, G.S., *Introduction to Spectroscopy*, 3rd Ed., Thomson Learning Inc., New York, 2001.

Figure 3.10 indicates that there are four main types of electronic transitions e.g. **n → π***, **n→ σ***, **π → π***, and **σ → σ***, where **n → π*** needs the least amount of energy to be excited and σ → σ* the highest amount of energy. The energies required to excite the valence electron from HOMO to LUMO are proportional to the electron's bonding strength on its atom. To excite σ → σ*, one needs relatively large amounts of energy and therefore it is not typically observed in a UV/Vis spectrum.

Wavelengths of absorbance peaks can yield some useful information about the types of bonds and functional groups in the molecule. However UV/Vis cannot be used for a specific test for any given compound because factors such as solvent, pH, temperature and concentration can influence the absorption spectra of compounds under examination. Due to the ineffectiveness of UV/Vis to obtain significant structural information, it is necessary to utilize other analytical tools. IR-spectroscopy, NMR-spectroscopy and X-ray crystallography can be used to support the UV/Vis information obtained. UV/Vis spectroscopy is mainly used for quantitative analyses such as the determination of reaction mechanism by following the formation and disappearance of coloured reaction mixtures.[9]

3.5 Theoretical Principals of Chemical Kinetics

3.5.1 Kinetic Investigations

Kinetic investigations are most often carried out with the purpose of gaining insight into the mechanism by which the chemical changes occur, thus observing the manner in which a specific system changes from one state to another and the time required for the transition. Kinetic studies are usually carried out by using standard UV/Vis spectrophotometer techniques. One shortcoming of these types of techniques is their inability to follow very fast reactions. To overcome this major problem, various flow techniques can be utilized for the rate determination of very

[9] Rao C. N. R., *Ultra-Violet and Visible Spectroscopy*, *Chemical Applications*, 2nd Ed., Butterworth and Co Publishers Ltd., England, 1967.

fast reactions in solution. The most frequently used technique by far is the *stopped-flow* method.

Factors such as pressure, temperature and concentration variations, homogeneity of the system, sensitivity to air and light, etc., can all play a significant role and affect on the reaction mechanism and rate of the reaction taking place.

It is well known that every compound, due to its unique characteristics, absorbs ultraviolet (UV) or visible (Vis.) light in a different fashion. Thus a homogenous sample will absorb a certain quantity of an incident beam of monochromatic light with an intensity of I_0, resulting in a transmitted intensity beam, I_{trs}, emitted from the sample.

This phenomenon is better known as the Beer-Lambert law, which gives the relationship between the concentration, *c*, of a single absorbing species, the intensity of the incident monochromatic light, I_0, and the transmitted intensity[10], I_{trs}.

$$Log_{10}\frac{I_0}{I_{trs}} = \varepsilon cl = A \qquad \text{. . .Eq. 3.7}$$

where *l* = path length, ε = molar decadic absorption or extinction coefficient and A = absorbance. From this it follows that the absorbance is a linear function of concentration but the percentage absorbance is not. The total absorbance of a solution is simply the sum of the individual absorbencies of each species, i.e.

$$A = \sum \varepsilon cl \qquad \text{. . . Eq. 3.8}$$

[10] Atkins P. W., *Physical Chemistry,* Oxford University Press Inc., Oxford, 1994.

3.5.2 Reaction Rate and Rate Orders

Consider the general reaction:

$$aA + bB \rightarrow cC + dD \qquad \text{. . . Eq. 3.9}$$

A, B, C and D denote reactants and products and a, b, c and d coefficients in the balanced chemical equation. In a closed system, the rate of the above reaction can be defined as the rate of change with time *t* of the concentration of one of the reactants or of one of the products of the reaction. If [A], [B], [C] and [D] are the concentrations, the rate r of the reaction is given by Eq. 3.10.

$$r = -\frac{d[A]}{dt} = -\frac{d[B]}{dt} = \frac{d[C]}{dt} = \frac{d[D]}{dt} = k[A]^{\alpha}[B]^{\beta} \qquad \text{. . . Eq. 3.10}$$

where α = the order of the reaction with respect to substance A,

β = the order of the reaction with respect to substance B,

α + β = the overall order of the reaction and

k = rate constant.

In Eq. 3.10, k, α and β are independent of concentration and time. k is the rate constant with a unit dependent on the reaction order. α and β are the partial orders respective to A and B. The overall order is the sum of all partial orders and then donated with the symbol *n*.

Kinetic experiments are carried out during the time interval from t_0 to t_e, when the reactant and product concentrations are changing continuously. Thermodynamic methods on the other hand operate in the region beyond t_e, when the bulk concentrations for reactants and products have become constant and the chemical system is at equilibrium or steady state. The distinction between the two types of methods is illustrated in Eq. 3.11 and Figure 3.11 which shows the progress of a reaction over time.

$$A \rightleftharpoons B \qquad \text{. . . Eq. 3.11}$$

The concentration of a reactant, [A], starts at zero time, t_0, with an initial [A_0] concentration which decreases to a zero or some equilibrium value [A_∞] asymptotically as time elapse to time t_e (equilibrium time). The total opposite is observed for the formation of product, B.[11]

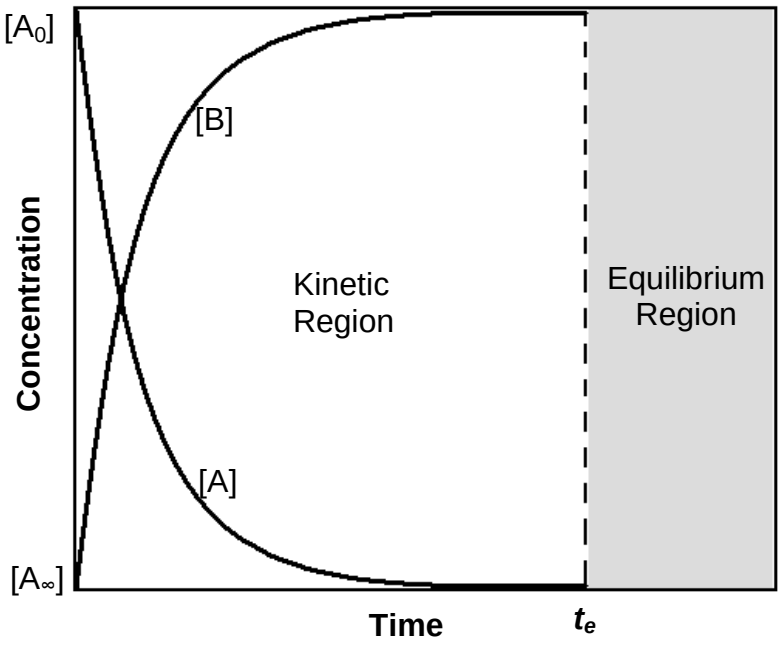

Figure 3.11: Change in concentration of reactant, [A], and product, [B], as a function of time. Until time t_e the reactant and product concentration are continuously changing and is known as the kinetic regime. After t_e, the reactant and product concentrations are static.

[11] Skoog D. A., West D. M., Holler F. J. and Crouch S. R., *Fundamentals of Analytical Chemistry*, 8th Ed., Brooks/Cole, London, 2004.

3.5.2.1 The Rate Law for nth-Order Reaction

The simplest case in mathematical analysis of reaction kinetics is the spontaneous irreversible decomposition of a species A producing the following first order reaction,[12]

$$A \xrightarrow{k} B \qquad \text{. . .Eq. 3.12}$$

The form of the rate expression becomes:

$$r = -\frac{d[A]}{dt} = k[A]^n \qquad \text{. . . Eq. 3.13}$$

A first order reaction (*n=1*) is one in which the rate of the reaction is proportional to the concentration of the reacting substances. By rearranging the equation above, Eq. 3.14 is obtained.

$$\frac{d[A]}{[A]^n} = -kdt \qquad \text{. . . Eq. 3.14}$$

The integral of this equation from time zero, t_0, when [A] = $[A]_0$, to time t, when [A] = $[A]_t$, is:

$$-\int_{[A_0]}^{[A]} \frac{d[A]}{[A]^n} = k\int_0^t dt \qquad \text{. . . Eq. 3.15}$$

In Eq. 3.15, $[A_0]$ = initial concentration at t = 0 and [A] = concentration at time t, respectively. Evaluation of the integrals where *n = 1* gives:

$$\ln\frac{[A]_t}{[A]_0} = -kt \qquad \text{. . . Eq. 3.16}$$

[12] Moore J. W. and Pearson R. G., *Kinetics and Mechanisms*, 3rd Ed., John Wiley and Sons, Inc., New York, 1981.

Finally, by taking the exponential of both sides of Eq. 3.16, we obtain the first-order rate expression:

$$[A]_t = [A]_0 e^{-kt} \quad \text{. . . Eq. 3.17}$$

There are several possible reaction orders, such as zero (*as indicated above*), first and second order. The integrated form of the common rate expression for zero, first and second order reaction is given in Table 3.2.

Table 3.2: Rate constants of 0, 1st and 2nd order reactions.

Order	Rate constants
0	$[A]_t = [A]_0 - kt$
1	$Ln[A]_t = -kt + ln[A]_0$ or $[A] = [A]_0 e^{-kt}$
2	$\frac{1}{[A]_t} = kt + \frac{1}{[A]_0}$

The rate equations are generally obtained by fitting the experimentally determined concentration-time rates to each of the integrated expressions in turn. A linear plot is only obtained if the correct integrated rate law is used. The rate constant, k, can then be determined from the slope of the line.[13]

[13] Jordan R. B., *Reaction Mechanisms of Inorganic and Organometallic Systems*, Oxford University Press., Inc., Oxford, 1991.

3.5.3 Reaction half-lives

Another very important quantity is the reaction *half-life*, $t_{1/2}$, which is the time required for the reactant concentration to decay to one-half of its initial value. For a first-order reaction ($A \rightarrow B$, $t = t_{1/2}$ when $[A] = \frac{1}{2}[A]_0$), the half-life can be calculated by substituting $t = t_{1/2}$ and $[A] = \frac{1}{2}[A]_0$ into $[A] = [A]_0 e^{-k_1 t}$, to produce Eq. 3.18.

$$\frac{1}{2}[A]_0 = [A]_0 e^{-k_1 t_{1/2}} \quad \text{or} \quad t_{1/2} = \frac{\ln 2}{k_1} = \frac{0.693}{k_1} \qquad \textbf{. . . Eq. 3.18}$$

The most useful property of the *half-life* is that, by virtue of the exponential decrease in concentration, the reaction will consume equal fractions of [A] in consecutive periods of time $t_{1/2}$. The half-life for other rate equation can be similarly defined.

Table 3.3 gives a brief summary of the most common half-life equations.

Table 3.3: The half-life equations of 0, 1st, 2nd and 3rd order reactions.

Order	**Half-life ($t_{1/2}$)**
0	$\frac{\frac{1}{2}[A_0]}{k_0}$
1	$\frac{\ln 2}{k_1}$
2	$\frac{1}{k_2[A_0]}$
3	$\frac{3}{2k_3[A_0]^2}$

3.6 Transition-State Theory

Some exothermic reactions occur readily (almost instantaneously), whereas other reactions are very slow, even to the point of being undetectable. This indicates that an intermediate transition state must be involved (*see* Figure 3.12*)*. Every reaction in which bonds are broken will have a high energy transition state that must be reached before any products can form. The energy needed to raise the reactant to the transition state energy level is called the activation energy, E_a. For any general elementary reaction a plot of potential energy *versus* the reaction, a coordinate will be as follows:

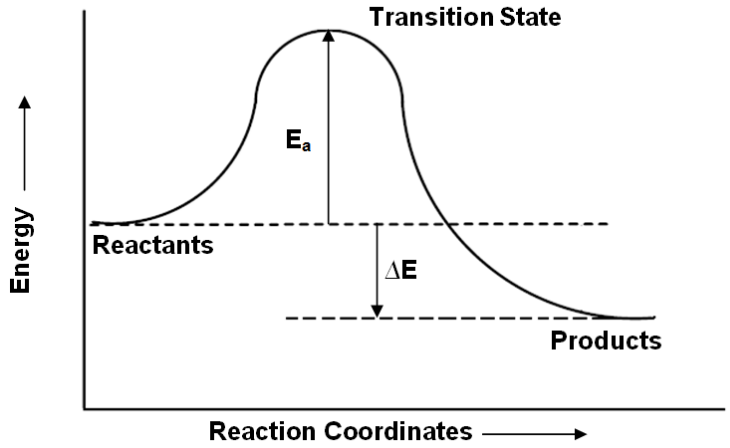

Figure 3.12: Activation energy of reactants, intermediates and products.

The rate of chemical reactions increases with temperatures as mentioned earlier. Generally, the dependence of the rate constant k on temperature, follows the Arrhenius equation.[14]

$$k = A\ e^{\left(-\frac{E_a}{RT}\right)} \qquad \text{. . . Eq. 3.19}$$

E_a is the activation energy and is useful in determining the mechanism of the reaction. The higher the activation energy, the slower the reaction will be at any given temperature. In practice, the reaction rate increased by a factor of 2-3 for each

[14] Arrhenius S. Z., *Phys. Chem.,* **4**, *226*, 1889.

10K increase in temperature.[12] Other activation parameters such as $\Delta H^{\neq}$, $\Delta S^{\neq}$, $\Delta G^{\neq}$ and $\Delta V^{\neq}$ can also be determined, where $\Delta G^{\neq}$, $\Delta H^{\neq}$, $\Delta S^{\neq}$ and $\Delta V^{\neq}$ are the standard molar free energy, enthalpy, entropy and volume differences between the activated complex and the reactants. The sign and magnitude of these activation (thermodynamic) parameters are also often used to indicate the mechanism of a reaction.

The transition state theory postulates that the reaction can be described by the following sequence, where the reaction rate is given by the rate of decomposition to the activated complex to form the products.

$$A + B \overset{K_c^{\neq}}{\rightleftharpoons} [A \cdot B]^{\neq} \overset{k}{\rightarrow} \text{products} \qquad \textbf{. . . Eq. 3.20}$$

The rate constant is then given by Eq. 3.20 according to this theory: where $K_c^{\neq}$ = equilibrium constant, R = gas constant, h = Planck's constant, N = Avogadro's number and T = absolute temperature.

$$k = \left(\frac{RT}{Nh}\right) K_c^{\neq} \qquad \textbf{. . . Eq. 3.21}$$

The information of this activated complex is governed by thermodynamic considerations similar to those of ordinary chemical equilibria. The free energy of $\Delta G^{\neq}$ can therefore be defined in normal thermodynamics by;

$$\Delta G^{\neq} = -RT \ln K_c^{\neq}$$
$$= \Delta H^{*} - T\Delta S^{\neq} \qquad \textbf{. . . Eq. 3.22}$$

Combining Eq 3.21 and Eq 3.22 and then rewriting the obtained equation in its logarithmic form, leads to the Eyring equation:[15]

$$\ln\left(\frac{k}{T}\right) = \ln\left(\frac{k}{h}\right) - \frac{-\Delta H^{\neq}}{RT} + \frac{\Delta S^{\neq}}{R} \qquad \textbf{. . . Eq. 3.23}$$

[15] Laidler K. J. and Meiser J. H., *Physical Chemistry*, The Benjamin/Cummings Publishing Company, California, 1982.

In the Eyring relation, a plot of ln(k/T) *vs* 1/T is linear with a slope of ($-\Delta H^{\neq}/R$) and $\Delta S^{\neq}$ can be calculated from the intercept. Both the Arrhenius and Eyring plots are used to obtain similar results.[16] The rate constant at varying temperatures can thus be calculated by using an established Eyring plot. Non-linear Arrhenius and Eyring plots are unusual, where deviations from a linear plot usually indicate reaction involving parallel, equilibria, or *consecutive reactions*.[17]

3.7 X-Ray Crystallography

3.7.1 Introduction

In 1912 a German physicist, Max Von Laue, first predicted that crystals would exhibit diffraction qualities when bombarded with X-ray beams. This phenomenon is known today as X-ray diffraction and occurs when the X-ray wavelength (λ) and interatomic distance (*d*) of the crystal lattice have the same order of magnitude (*ca.* 10^{-10} m or 1 Å). At first these diffraction patterns were of no use to Von Laue because no data could be obtained from it. A year later W.L. Bragg presented a simple explanation (Bragg's Law) for the angles observed in diffracted X-ray beams and successfully analyzed the first crystalline structures of potassium chloride and sodium chloride by X-ray crystallography.[18] This new technique opened a wide range of opportunities in the field of X-ray crystallography for physicists and chemists.

The atoms in a crystal are not distributed randomly, but arranged in a highly ordered manner relative to each other. There are several different types of crystalline structures, (fourteen Bravais lattices, grouped into the seven crystal systems with a total of 230 different space groups) depending on the geometry of the atom arrangements. A solid is only a *crystal* if the atoms in the solid are arranged in such a way that their positions are exactly periodic, meaning that if an atom is translated

[16] McAteer C. H. and Moore P., *J. Chem. Soc., Dalton Trans*., 353, 1983.

[17] Wilkins R. G., *Kinetics and Mechanism of Reactions of Transition Metal Complexes*, 2nd Ed., VCH Publishers, Inc., New York, 1991.

[18] Bragg W. L., *Proceedings of the Royal Society,* **A89,** 248, 1914.

by any vector, T, joining the two atoms, the crystal remains invariant (*see* Figure 3.13).[19]

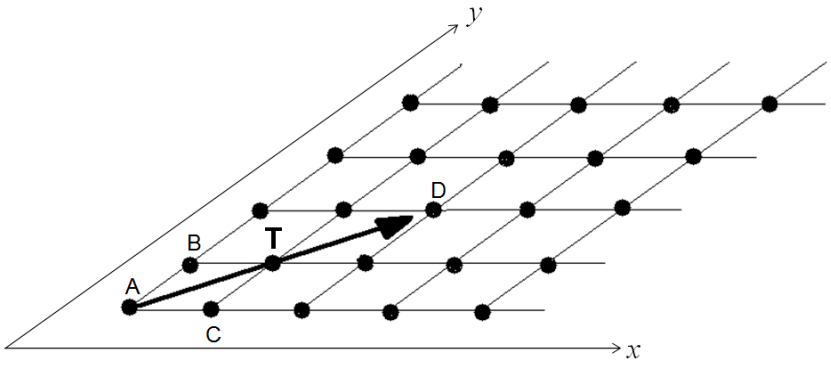

Figure 3.13: A representation of a crystal solid with all the atoms arranged periodically. The atomic arrangement in the crystal looks exactly the same at position A and D when position A is translated with a vector, T, to position D.

A *lattice* is defined by three fundamental translation vectors x, y and z, such that the atomic arrangement in a structure looks the same in every respect when viewed from any other point or in lighter terms, a lattice is a regular periodic arrangement of a point in space. A *unit cell* is the smallest group of atoms whose three-dimensional repetition at regular periodic arrangements, produces the crystal lattice. The unit cell consists of three sides and angles, **a**, **b**, **c** as well as α, β, γ respectively. The orientation and position of a plane in a lattice is specified by its Miller index e.g. (*h, k, l*) value. Miller indexes specify an infinite set of equivalent planes and not just one plane. This is very important when studying X-ray diffraction because a diffracted beam is the result of scattering from large numbers of equivalent parallel planes, *h,k,l* plane.

[19] Kittel C., *Introduction to Solid State Physics*, Wiley and Sons, Inc., USA, 1971.

3.7.2 Scattering from a Crystal (Diffraction Conditions)

If we consider an incident X-ray beam, *k*, which is reflected, *k'*, from the surface of a crystal, Δk is defined as the change of the wave vector on scattering (as indicated in Figure 3.14).

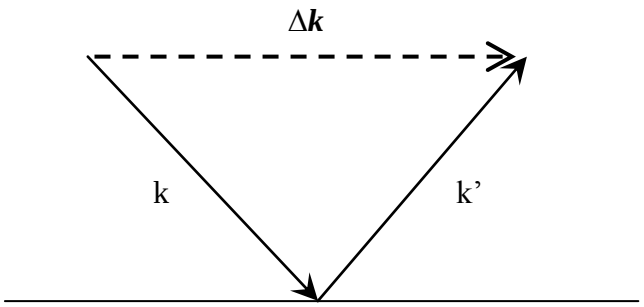

Figure 3.14: Schematic presentation of the scattering vector Δk *such that* $k + \Delta k = k'$. *(For ideal scattering* $k' = k$*).*

Atoms separated by the primitive vectors a, b and c of a crystal lattice will have constructive interference only if the following three equations are satisfied simultaneously:

$$\Delta \boldsymbol{k} \cdot \mathbf{a} = h2\pi$$

$$\Delta \boldsymbol{k} \cdot \mathbf{b} = k2\pi$$

$$\Delta \boldsymbol{k} \cdot \mathbf{c} = l2\pi \qquad \textbf{...Eq. 3.24}$$

where h, k and l is any sets of integers and when written in terms of angles these equations become respectively:

$$\mathbf{a}(\cos\alpha - \cos\alpha_0) = h\lambda$$

$$\mathbf{b}(\cos\beta - \cos\beta_0) = k\lambda$$

$$\mathbf{c}(\cos\gamma - \cos\gamma_0) = l\lambda \qquad \textbf{...Eq. 3.25}$$

α_0, β_0 and γ_0 in Eq. 3.25 are the angels of the incident beam, *k,* and α, β and γ the angles of the diffracted beam, *k'.* Equations 3.24 and 3.25 are known as the **Laue**

equations for the diffraction maxima, after the German physicist, Max Von Laue, who derived them and can be rewritten into what is known as Bragg's law.[20]

3.7.3 Bragg's Law

W.L. Bragg assumed that when a monochromatic X-ray beam is incident on the surface of a crystal, it is reflected. Reflection only occurs when the incident beam has certain values, which depend on the wavelength and lattice constants of the crystal. If we consider a series of parallel lattice planes spaced at equal distances, d, apart from each other, the path difference for X-ray diffracted from adjacent (parallel) planes is $2d\sin\theta$. Constructive interference of the reflected X-ray beams from successive parallel planes can only occur if the path differences are integral numbers n of the wavelength, λ, of the X-ray beam e.g.

$$2d \sin\theta = n\lambda \qquad \textbf{...Eq. 3.26}$$

This phenomenon is known as Bragg's law and is used to correct the difference in phase that exists because of X-rays reflected from different planes. It is important to note that all reflections from the parallel planes are assumed to be specular and that only certain θ values of the reflections add up in phase, to produce strong reflected (diffracted) beams which can be collected simultaneously at a distant detector.

There are three standard methods of diffraction utilized in crystallography for the determinations of different crystal structures e.g. Laue-, rotating-, crystal- and powder method.

[20] Arndt U. W. and Wonacott A. J., *The Rotation Method in Crystallography*, North-Holland, 1997.

3.7.3.1 Laue Method

In this method a single crystal is bombarded with X-ray beams with a continuous wavelength while the crystal is held stationary. The Laue method is excellent for determining crystal symmetry and orientation as well as defects and imperfections in the crystal structure.

3.7.3.2 Rotating-Crystal Method

In the rotating-crystal method, a single crystal is radiated with a monochromatic X-ray beam while the crystal is rotated about a permanent axis. There are several different variations of the rotating-crystal method utilized these days for the determination of absolute crystal structures at different temperatures and for the configuration of enzymes.

3.7.3.3 Powder Method

In the powder method the specimen is (powder or fine-grained polycrystalline) contained in a thin-walled capillary tube and is bombarded with a monochromatic X-ray beam. The main advantage of this method is that there is no need for a single crystal to be grown, which can be quite difficult at times.

3.7.4 The Structure Factor

The possible reflections from a crystal are described by the reciprocal lattice points (*hkl*) which reflection intensities depends on various factors of the content of the cell. The structure factor, $\boldsymbol{F_j}$, is used to obtain a value which corresponds to the ability and intensity of X-rays to be diffracted from a specific plane. The position of the j^{th} atom, within a unit cell expressed in terms of fractional coordinates, is given by Eq. 3.27, where x_j, y_j *and* z_j *are constants.*

$$R_j = x_j a + y_j b + z_j c \qquad \textbf{...Eq. 3.27}$$

A new set of basis vectors a*, b* and c* can be used as a basis for a new lattice, whose vectors can be given by:

$$G_j = ha^* + kb^* + lc^* \qquad \textbf{...Eq. 3.28}$$

Eq. 3.28 is known as the *reciprocal lattice* and the *a**, b* and c* the *reciprocal basis vectors.* The mathematical relationships between the lattice and reciprocal basis are given as followed:

$$\begin{aligned} a^* \cdot a &= 2\pi, \quad & a^* \cdot b &= a^* \cdot c = 0, \\ b^* \cdot b &= 2\pi, \quad & b^* \cdot a &= b^* \cdot c = 0, \\ c^* \cdot c &= 2\pi, \quad & c^* \cdot a &= c^* \cdot b = 0 \end{aligned} \qquad \textbf{...Eq. 3.29}$$

.

If we consider an X-ray beam scattered from a one-dimensional mono-atomic lattice, the overall scattering of all the atoms (j) in the unit cell relative to that of a single electron, is express by the structure factor, F_{hkl},

$$F_{hkl} = \sum_{j=1}^{N} f_j \exp[i2\pi r.s] \qquad \textbf{. . . Eq. 3.30}$$

By incorporating the reciprocal lattice equations, Eq. 3.30, into the overall scattering of all the atoms (*j*) in a three dimensional unit cell, the following equation is obtained:[21]

$$F_{hkl} = \sum_{j=1}^{N} f_j \exp\left[i2\pi\left(hx_j + ky_j + lz_j\right)\right] \qquad \textbf{. . . Eq. 3.31}$$

In the case of a cento-symmetric unit cell, Eq. 3.32, can be rewritten as:

$$F_{hkl} = \sum_{j=1}^{N} f_j \cos\left[i2\pi\left(hx_j + ky_j + lz_j\right)\right] \qquad \textbf{. . . Eq. 3.32}$$

[21] Ladd M. F. C. and Palmer R. A., *Structure Determination by X-ray Crystallography*, Plenum Press, New York, 1977.

From the above equation it is obvious that the structure factor is only dependent on the relative position of the atoms in the cell and their scattering factors. Where each term in the above equation describes a wave with amplitude of f_j and phase of $2\pi(hx_j + ky_j + lz_j)$, meaning that the position of the atoms in a crystal determines the phase dependence between the diffracted rays from each atom contributing to the diffraction.[22] The intensities of the diffracted X-rays are directly proportional to F^2 because the energies in cosines waves are proportional to the square of the amplitudes of the waves and therefore:

$$I_0(hkl) \propto [F_0(hkl)]^2 \qquad \textbf{. . . Eq. 3.33}$$

I_0 and F_0 are the experimentally observed quantities. This phenomena makes it possible to link and compare the intensities of reflected X-rays, I_0, to the structure properties of a crystal by F_0. Reflected X-rays are caused by electrons associated within the atoms in a crystal, which makes it possible to determine a crystal structure. Electron density can be expressed as a function of position, ρ(X,Y,Z) since atoms with higher atomic numbers yield greater concentrations of electrons than atoms with lower atomic numbers. Due to the relation between electron density and structure factor Eq. 3.34 is obtained.

$$F_{hkl} = \int \rho(x,y,z)\, exp\left[i2\pi\left(hx_n + ky_n + lz_n\right)\right] dV \qquad \textbf{. . . Eq. 3.34}$$

3.7.5 'Phase Problem'

The determination of a crystal structure requires both the amplitude, f_j, and the phase of the structure factor as described in Eq. 3.32. Due to the limitation X-ray technology it is only possible to emit monochromatic X-rays and not coherent X-rays. Consequently, the X-rays emitted start out with dispersed phases, making it impossible to acquire the phases of the reflected X-rays. Unfortunately these phases contribute more to the informational content of X-ray diffraction patterns than the corresponding amplitudes. This inability to determine the phase is commonly

[22] Azaroff L. V., *Elements of X-ray Crystallography*, McGraw-Hill Inc., New York, 1968.

known as the “phase problem” or “lost phases” and can easily be overcome by utilizing a number of different methods. There are two main methods to recover the phases using the data obtained by standard equipment, e.g. the direct method and Patterson function.

3.7.5.1 Direct Method

The direct method estimates the initial- and expanding phases from measured X-ray intensities, by using mathematical formulae like triple relations. This method yields the best results for compounds where only light atoms are present.

3.7.5.2 Patterson Function

The Patterson Function is only applied for compounds containing heavier atoms or when a major part of the structure is already known. The Patterson Function or Patterson Map resembles a map of electron density with positive electron density peaks in various positions, which is defined by Eq. 3.35, where *V* represents the volume of the unit cell.[23]

$$P(u,v,w)=V^{-1}\sum_{h}\sum_{k}\sum_{l}(F_{hkl})^{2}\,exp[-i2\pi(hu+kv+lw)] \qquad \textbf{. . . Eq. 3.35}$$

The positions of these peaks are not the positions of the atoms in the structure but a function of vectors between pairs of atoms in the structure, implying that the Patterson Function only produces information on where the atoms lie relative to each other and not relative to the unit cell origin. The Patterson Function will provide the position of one or two of the heavier atoms in the unit cell and then the rest of the structure can be analysed by other techniques.

[23] Stout G. H. and Jensen L. H., *X-ray Structure Determination: A Practical Guide*, The Macmillan Company, London, 1968.

3.7.6 Least Squares Refinement

The least squares refinement is a method used to compare experimental data with modelled data, to obtain a degree of similarity between them. For crystal structure refinement, the similarities between the experimental (observed) structural factor, $|F_0|$, and calculated structural factor, $|F_c|$, is compared in terms of the *residual index* or *R-factor*[23] via Eq. 3.36.

$$R=\frac{\Sigma\left||F_0|-|F_c|\right|}{\Sigma|F_0|} \qquad \text{. . . Eq. 3.36}$$

R-factor values below 1 indicate that a well defined crystal structure was obtained from the data collected. An even better refinement can be obtained by incorporating a weighting factor for each reflection, *w*, which is a reliability factor of the different measured data. This gives rise to a new residual factor which is extensively used for determining crystal structures.

$$wR^2=\frac{\Sigma w(F_0^2-F_c^2)^2}{\Sigma w(F_0^2)^2} \qquad \text{. . . Eq. 3.37}$$

4 Synthesis and Spectroscopic Characterisation of Hafnium Compounds

4.1 Introduction

The synthesis of various new hafnium complexes is described in this chapter. Complex characterizations were performed by using various techniques, including IR-, UV/Vis- and NMR spectroscopy.

The chemical behaviour of hafnium and zirconium is almost identical; it forms complexes of the same geometry and same parameters (size, lipophilicity, dipole moment, ionic mobility, etc). With this in mind, various hafnium compounds containing O,O'- and N,O-bidentate ligands were synthesized to investigate possible differences in coordination modes between hafnium and its zirconium counterpart. Miss. M. Steyn is currently investigating this in her M.Sc. Chemistry thesis, at the University of the Free State, South Africa, 2009.

As mentioned in Chapter 2, only a small number of hafnium complexes with O,O'- and N,O-bidentate ligands have been reported previously, but no attention has been given to solution kinetic studies. Since no literature method was found that purposely investigates and discusses the dependence of hafnium complex formation on the specific reaction conditions, a range of methods were attempted during this project.

Thus, the aim of this part of the study was to explore the synthesis of hafnium complexes with chosen O,O'- and N,O-bidentate ligands and to establish their formation kinetic behaviour in solution.

4.2 Experimental

All reagents used for the synthesis and characterization were of analytical grade and were purchased from Sigma-Aldrich, South Africa, unless otherwise stated. Reagents were used as received, without further purification. All organic solvents were dried and distilled before use.

The CO stretching frequencies of the complexes were obtained from infrared spectra recorded on a Bruker Tensor 27 Standard System spectrophotometer with a laser range of 4000 – 370 cm^{-1} and analysed with the Bruker OPUS – NT software (32 scans, 4 cm^{-1} resolution Blackman – Harris 3 – Term apodisation). Samples were analyzed as solid state species *via* ATR infrared spectrophotometry. All data were recorded at room temperature.

^{1}H NMR spectra were obtained in C_6D_6 (deuterated Benzene), referenced to the C_6D_6 solvent peak – 7.16 ppm, on a Bruker 300 MHz nuclear magnetic resonance spectrometer, while ^{19}F NMR spectra were obtained in C_7D_8 (deuterated Toluene), referenced to α,α,α-Trifluorotoluene – 564.77 MHz, on a Bruker 600 MHz spectrometer.

4.2.1 Direct Bench Top Approach

Due to insufficient specialized glassware, a preliminary direct bench top synthetic procedure was attempted to try and synthesize compounds with the mentioned (*see* Section 1.3) bidentate ligands coordinated to $HfCl_4$.

Syntheses were performed under argon, using a single line manifold with no vacuum line present. Solvents were dried by passing it through alumina, while glassware and other apparatus were cleaned and dried in an oven for 2 hours at 110 ºC. This approach was taken to establish initial parameters for the synthesis, such as amounts of starting materials to be used, solvents conditions for refluxing and recrystallisation. A noticeable HCl gas odour was detected during the reaction. This

is ascribed to the hydrogen of the bidentate ligand reacting with the chlorides of the $HfCl_4$ (*see Scheme 4.1*).

$$HfCl_4(s) + 1eq\ (L,L')H \xleftrightarrow[\Delta]{Toluene} HfCl_3(L,L') + 1eq\ HCl(g)$$

$$HfCl_4(s) + 2eq\ (L,L')H \xleftrightarrow[\Delta]{Toluene} HfCl_2(L,L')_2 + 2eq\ HCl(g)$$

$$HfCl_4(s) + 3eq\ (L,L')H \xleftrightarrow[\Delta]{Toluene} HfCl(L,L')_3 + 3eq\ HCl(g)$$

$$HfCl_4(s) + 4eq\ (L,L')H \xleftrightarrow[\Delta]{Toluene} Hf(L,L')_4 + 4eq\ HCl(g)$$

L,L' = bidentate ligand

Scheme 4.1: Synthesis reaction scheme.

The extent of the detected gas in these preliminary attempts may cause a major problem if the starting reagent is changed to HfF_4. With the use of HfF_4, hydrofluoric acid gas will be liberated, which is more poisonous than its HCl analogue. Another problem envisaged, is that hydrofluoric acid is not compatible with glass equipment and glass erosion will occur. There are several proposed ways to prevent formation of hydrofluoric acid, one of these would be to use a halogen salt precipitation technique. This is done by substituting the hydrogen on the bidentate ligand with a alkali metal like sodium (Na) or lithium (Li). Thus when the bidentate ligand reacts with the metal centre NaF will be formed instead of HF, therefore making it possible to work with glass equipment. The salt precipitate can easily be removed by an appropriate solvent.

$$HfX_4(s) + 1eq\ Li/Na(L,L') \xleftrightarrow[\Delta]{Toluene} HfX_3(L,L') + 1eq\ Li/NaX(s)$$

4.2.1.1 Synthesis of TfaaNa

The ligand salt (tfaaNa) was prepared by adding 1,1,1-trifluoroacetylacetone, tfaaH, (6.05 cm^3, 50 mmol) drop wise to NaOH (2.02 g, 50 mmol) over a period of 3 minutes. The resulting solids were washed with toluene to produce an isotropic mixture and then dried *in vacuo* (*see* Reaction 4.1).

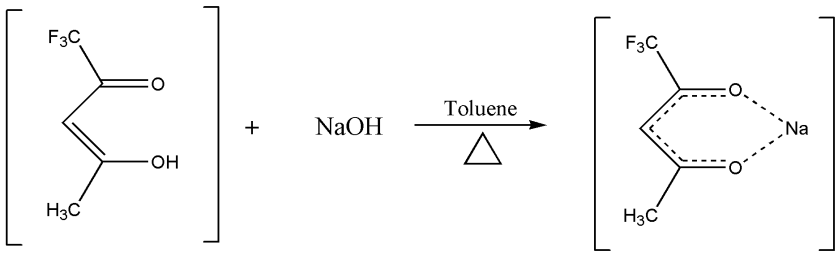

Reaction 4.1: Synthesis reaction scheme of tfaaNa

From the IR spectra (*see* Figure 4.1) it is obvious that tfaaH was converted to the sodium salt [tfaaNa] as the CO peak of the tfaaH had shifted *ca.* 41cm^{-1}, while the rest of the fingerprint of tfaaH remained fairly intact.

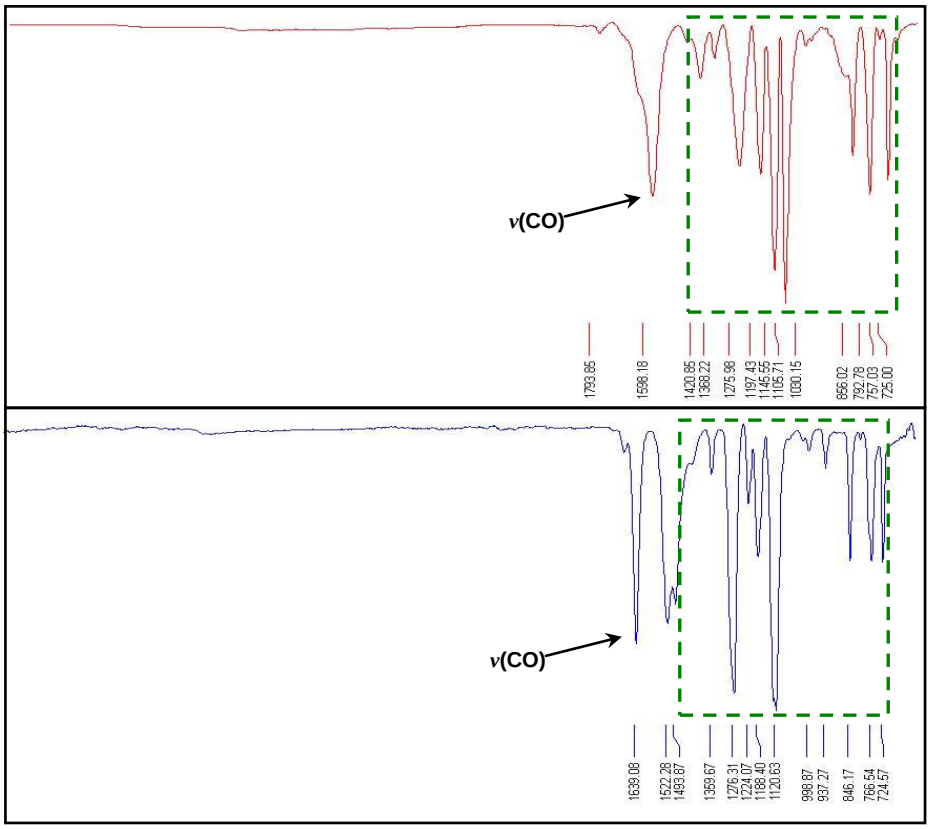

Figure 4.1: IR Spectra of tfaaH and tfaaNa

4.2.2 Schlenk Synthesis

After establishing initial parameters for the synthesis of the various hafnium compounds for this study and obtaining sufficient glassware for Schlenk synthesis, we were able to start doing anhydrous chemistry.

All manipulations of air and moisture sensitive compounds were performed by means of standard Schlenk techniques[1] under argon gas and with a double line glass manifold.

[1] Shriver D. F. and Drezdzon M. A., *The Manipulations of Air-Sensitive Compounds*, 2nd Ed., Wiley-Interscience Publications, New York, 1986.

Throughout the applicable literature the synthetic methodology of hafnium halo complexes containing O,O'- or N,O-donating bidentate ligands, can be represented by the previous general reaction scheme (Scheme 4.1).

Literature indicates that the reaction is a step-wise substitution reaction where one bidentate ligand is substituted for one halogen.[2,3] The research in this study indicates that the 1:1 ratio compounds cannot be isolated, while the 1:2, 1:3 and 1:4 compounds appear to be readily synthesized. Due to this preliminary observation, we did not pursue the synthesis of the 1:1 ratio, metal to ligand complexes.

4.2.2.1 Attempted Synthesis of $[Hf(tfaa)_2Cl_2]$

TfaaNa (0.246 g, 1.4 mmol) was added to a suspension of $HfCl_4$ (0.211 g, 0.66 mmol) in toluene (10 ml). Dissolution gave a slightly yellow solution after 10 min, and after refluxing for *ca*. 20 h, the crude product was filtered and washed with toluene. The filtrate was slowly recrystallised at 253 K. (Yield: 157 mg, 43%)

Spectroscopic data: ^{19}F NMR (Toluene-d_7) : δ = -75.95 (s, 1F); ^{1}H NMR (Benzene-d_6) : δ = 1.66 (s, 3H), 5.86 (s, 1H).
IR (ATR): ν(CO) = 1537 cm^{-1};
UV/Vis: λ_{max} = 324 nm.

[2] Pinnavaia T. J. and Fray R. C., *Inorganic Chemistry*, **7**, 502, 1968.

[3] Hubert-Pfalzgraf L. G., Touati N., Pasko S., Vaissermann J. and Abrutis A., *Polyhedron*, **24**, 3066, 2005.

4.2.2.2 Attempted Synthesis of [Hf(tfaa)$_3$Cl]

TfaaNa (0.344 g, 2.0 mmol) was added to a suspension of $HfCl_4$ (0.201 g, 0.63 mmol) in toluene (10 ml). The dissolution turned into a slightly yellow solution after 10 min, and after refluxing for *ca.* 20 h, the crude product was filtered and washed with toluene. The filtrate was slowly recrystallised at 253 K. (Yield: 266 mg, 63%)

Spectroscopic data: ^{19}F NMR (Toluene-d_7): δ = -75.95 (s, 1F); ^{1}H NMR (Benzene-d_6) : δ = 1.65 (s, 3H), 5.85 (s, 1H)
IR (ATR): ν(CO) = 1530 cm^{-1};
UV/Vis: λ_{max} = 320 nm.

4.2.2.3 Synthesis of [Hf(tfaa)$_4$]

TfaaNa (0.459 g, 2.6 mmol) was added to a suspension of $HfCl_4$ (0.207 g, 0.66 mmol) in toluene (10 ml). The dissolution turned into a slightly yellow solution after 10 min, and after refluxing for *ca*. 20 h, the crude product was filtered and washed with toluene. The filtrate was slowly recrystallised at 253 K. (Yield: 440 mg, 86%)

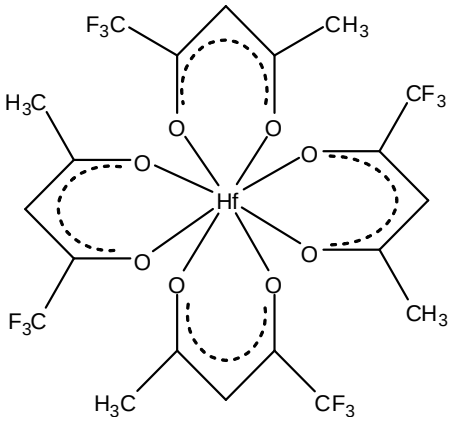

Spectroscopic data: ^{19}F NMR (Toluene-d_7): δ = -75.95 (s, 1F); ^{1}H NMR (Benzene-d_6) : δ = 1.66 (s, 3H), 5.86 (s, 1H).
IR (ATR): ν(CO) = 1533 cm^{-1};
UV/Vis: λ_{max} = 323 nm.

After completion of this synthetic phase, very little could be confirmed about the extent of coordination of the bidentate ligand to hafnium. Neither IR nor ^{1}H and ^{19}F NMR spectroscopy could provide any useful information about the coordination of the ligand to the metal. Crystallographic results (*see* Chapter 5.4 for a detailed discussion of the single crystal structure of product 4.2.2.3) confirmed that a tetrakis-coordinated hafnium complex, with the four β-diketonate ligands coordinating to the hafnium, was isolated in the solid phase.

The synthesis of the $HfCl_4(hfaa)_{4-n}$ involved the same modified Schlenk technique as motioned above, but this time the ligands was added drop-wise to the metal starting material over a period of about 30 minutes. This method was used in an attempt to allow all possible hafnium starting material to react with the bidentate ligands over time. It was hoped that the slower addition of the ligand to the starting metal material might yield bis- and tris(diketonates).

4.2.2.4 Attempted Synthesis of $[Hf(hfaa)_2Cl_2]$

The compound $[Hf_2Cl_2(hfaa)_2]$ was synthesized by adding 1,1,1,5,5,5-hexafluoroacetylacetone, hfaaH, (270µL, 1.9 mmol) drop-wise to a suspension of $HfCl_4$ (306 mg, 0.96 mmol) in toluene (10 ml). The dissolution turned into a slightly white solution after 20 min. After refluxing for *ca*. 12 h the crude product was filtered and evaporated *via* vacuum and then the product was purified by fractional recrystallization from acetone at 253 K. The compound was isolated as a colourless crystalline substance. (Yield: 139 mg, 22%)

Spectroscopic data: ^{1}H NMR (Acetone-d_6): δ = 6.59 (s, 1H), 7.29 (s, 1H);
IR (ATR): ν(CO) = 1532cm^{-1};
UV/Vis: λ_{max} = 316 nm.

4.2.2.5 Attempted Synthesis of [Hf(hfaa)$_3$Cl]

Hexafluoroacetylacetone (350 µL, 2.5 mmol) was added drop-wise to a suspension of $HfCl_4$ (264 mg, 0.82 mmol) in toluene (10 ml). The dissolution turned into a slightly white solution after 20 min. After refluxing for *ca*. 12 h, the crude product was filtered and evaporated via vacuum and then purified by recrystallization from acetone at 253 K. The compound is a colourless crystalline substance. (Yield: 268 mg, 39%)

Spectroscopy data: ^{1}H NMR (Acetone-d_6): δ = 6.59 (s, 1H), 7.29 (s, 1H);
IR (ATR): ν(CO) = 1561 cm^{-1};
UV/Vis: λ_{max} = 321nm.

4.2.2.6 Synthesis of [Hf(hfaa)$_4$]

Hexafluoroacetylacetone (450 µL, 3.3 mmol) was added drop-wise to a suspension of $HfCl_4$ (241 mg, 0.75 mmol) in toluene (10 ml). The dissolution turned into a slightly white solution after 20 min. After refluxing for *ca*. 12 h, the crude product was filtered and evaporated in vacuo. Colourless crystals were obtained after re-crystallisation in acetone at 253 K. The compound created a colourless crystalline substance. (Yield: 408 mg, 43%)

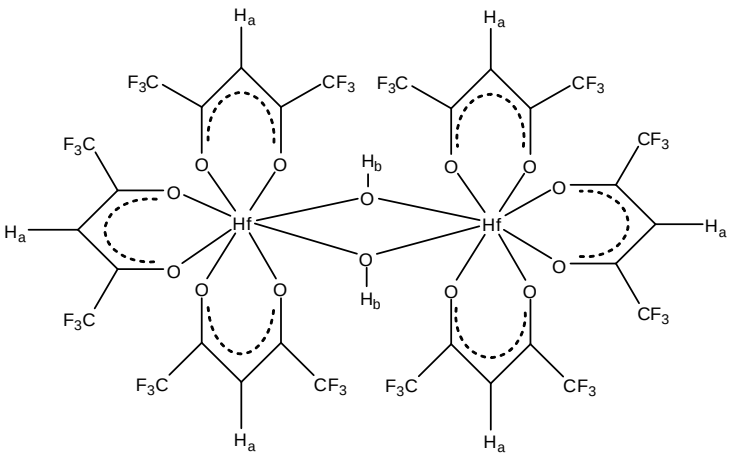

Spectroscopic data: ^{1}H NMR (Acetone-d_6): δ = 6.59 (s, 1H$_a$), 7.29 (s, 1H$_b$);
IR (ATR): ν(CO) = 1553 cm^{-1};
UV/Vis: λ_{max} = 319 nm.

Our attempts in trying to obtain better control over the coordination mode of hafnium were unsuccessful. Again, both IR- and ^{1}H and ^{19}F NMR spectroscopy could not provide any information about the coordination mode of the metal centre. In an attempt to synthesize the tetrakis type compound, Hf(hfaa)$_4$, a dimer hafnium complex (bis(μ_2-Hydroxo)hexakis-(hexafluoroacetylacetonato-κ^2-O,O')-dihafnium(IV), *see* Chapter 5.5 for a complete discussion of its single crystal structure), was isolated.

4.2.3 Other Bench Top Syntheses

N,N-dimethylformamide (DMF) was used as reaction solvent due to its unique properties in the synthesis of 8-hydroxyquinoline hafnium complexes. For the first time, we were able to do bench top synthesis as DMF dissolves all starting materials. One other main advantage using DMF as solvent is the possibility to do solution kinetic studies. Note that these kinetic studies can only be investigated if the reaction solutions are completely homogenous.

4.2.3.1 Attempted Synthesis of [Hf(Ox)$_2$Cl$_2$]

$HfCl_4$ (492 mg, 1.5 x 10^{-4} mol) was dissolved in a minimal amount of DMF. While stirring this solution at room temperature, a solution of 8-hydroxyquinoline, [C_9H_8ON], (446 mg, 3.1 x 10^{-3} mol), also dissolved in a minimal amount of DMF, was added dropwise, resulting in the formation of a bright yellow solution. The solution was left to stand for *ca*. a week for yellow crystals to form. (Yield: 440 mg, 53%)

Spectroscopic data: ^{1}H NMR (Benzene-d_6;): δ = 6.70 (d, 1H, *J* = 6Hz), 7.29 (dd, 2H, *J* = 7.8Hz, 6Hz), 7.36 (t, 2H, *J* = 7.8Hz), 8.13 (d, 1H, *J* = 7.2Hz);
IR (ATR): ν(CO) = 1664 cm^{-1};
UV/Vis: λ_{max} = 382 nm.

4.2.3.2 Attempted Synthesis of [Hf(Ox)$_3$Cl]

$HfCl_4$ (513 mg, 1.6 x 10^{-3} mol) was dissolved in a minimal amount of DMF. While stirring this solution at room temperature, another solution of [C_9H_8ON] (656 mg, 4.5 x 10^{-3} mol) also dissolved in a minimal amount of DMF was slowly added, resulting in formation of a bright yellow solution. The solution was left to stand for *ca*. a week for crystals to form. (Yield: 686 mg, 66%)

Spectroscopy data: ^{1}H NMR (Benzene-d_6;): δ = 6.70 (d, 1H, *J* = 6Hz), 7.29 (dd, 2H, *J* = 7.8Hz, 6Hz), 7.36 (t, 2H, *J* = 7.8Hz), 8.13 (d, 1H, *J* = 7.2Hz);
IR (ATR): ν(CO) = 1663 cm^{-1};
UV/Vis: λ_{max} = 384 nm.

4.2.3.3 Synthesis of [Hf(Ox)$_4$]

$HfCl_4$ (603mg, 1.9x10^{-3} mol) was dissolved in a minimal amount of DMF. While stirring this solution, at room temperature, another solution of [C_9H_8ON] (1.07 g, 7.4 x 10^{-3} mol) also dissolved in a minimal amount of DMF was slowly added, resulting in the formation of a bright yellow solution. The solution was left to stand for *ca*. a week for crystals to form. (Yield: 1.32 g, 92%)

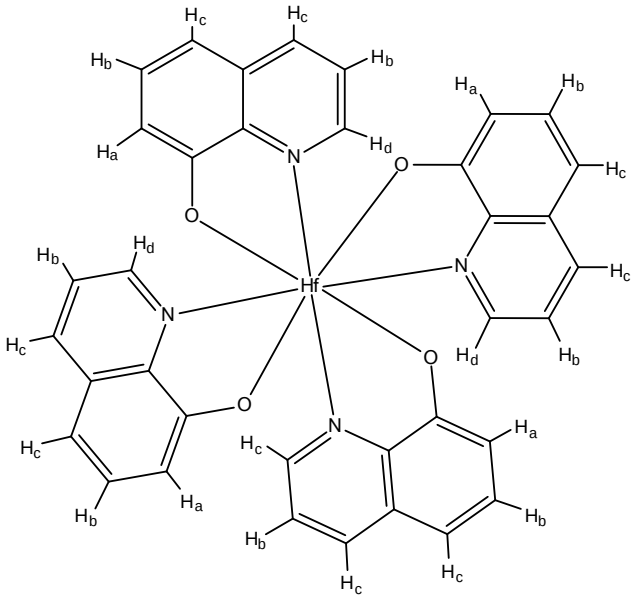

Spectroscopy data: ^{1}H NMR (Benzene-d_6;): δ = 6.70 (d, 1H$_d$, J = 6Hz), 7.29 (dd, 2H$_b$, J = 7.8Hz, 6Hz), 7.36 (t, 2H$_c$, J = 7.8Hz), 8.13 (d, 1H$_a$, J = 7.2Hz);
IR (ATR): ν(CO) 1659 cm^{-1}
UV/Vis: λ_{max} = 381 nm.

4.3 Conclusion

This part of the project has produced valuable information in terms of the coordination chemistry of hafnium toward different O,O'- and N,O-bidentate ligands.

The aims of Chapter 1 were set to investigate the chelating behaviour of hafnium with different organic bidentate ligands and to compare it with zirconium (parallel study of M. Steyn, M.Sc., UFS, 2009[4]) and this produced good results. Three new crystallographic structural determinations were done on [Hf(tfaa)$_4$], [Hf(OH)(hfaa)$_3$]$_2$ and [Hf(Ox)$_4$]. The parallel zirconium study produced two new crystallographic structural identifications, i.e. [Zr(tfaa)$_4$] and [Zr(Ox)$_4$]. An RMS overlay error of *ca*. 2 x 10^{-2} Å was obtained when [Hf(tfaa)$_4$] was superimposed on the isomorphous [Zr(tfaa)$_4$] complex (*see* Section 5.7), illustrating again the similarities in these two metals' chemical behaviour. IR-, NMR- and UV/Vis spectroscopy also produced

[4] Steyn M., Steyl G. and Roodt A., *M.Sc*. *Thesis*, University of the Free State, 2009.

near identical results for all the hafnium and zirconium isomorphous complexes, illustrating that it is:

(i) Difficult to use under these circumstances to distinguish between products,
(ii) Especially if the coordination modes are so similar for both the hafnium and zirconium synthesis.

Although in all cases different ratios of metal:ligand were used, only the tetrakis complex was isolated in most cases, suggesting that the crystallization energy of the tetrakis complex is the lowest in this typical symbiotic system.[5] This explains why so few examples of lower coordinated moieties are available in literature. From the synthetic methods applied, it became clear that isolation of any lower coordinated hafnium complex, intervention into the reaction process will have to be made shortly after it has started. The crystallographic data of the complexes synthesized are discussed in detail in Chapter 5.

Lower coordinated hafnium bidentate complexes have been isolated before by means of sublimation crystallization. Unfortunately, there were no facilities available for this type of crystallization technique, but it certainly leaves scope for future research work.

In order to obtain better insight of how coordination proceeds, we studied the formation kinetics of $[Hf(Ox)_4]$ in solution. These kinetic results are discussed in Chapter 6.

[5] Huheey J. E., Keiter E. A. and Keiter R. L., *Inorganic Chemistry: Principles of Structure and Reactivity*, 4th Ed, John Wiley and Sons, New York, 1993.

5 Crystallographic Study of Hafnium Compounds

5.1 Introduction

In this chapter the solid state characterization of selected hafnium compounds containing O,O'- and N,O-bidentate ligands is presented. Although there are quite a number of crystal structure reports of hafnium in the literature, our search only revealed a handful of complexes containing mixed halo O,O'- and N,O-bidentate ligand complexes of hafnium. Due to the special properties of the quinoline ligands with its two phenyl (six membered) ring systems, the solid state characterization is suspected to yield essential information with respect to the packing orientation and effects as well as interactions observed on a larger scale, *i.e.* hydrogen bonding and π-π stacking.

The complexes investigated in this study, $[Hf(tfaa)_4]$, $[Hf(OH)(hfaa)_3]_2$ and $[Hf(Ox)_4]$, were fully characterized by means of X-ray crystallography and are described in detail.

5.2 Experimental

The X-ray intensity data was collected on a Bruker X8 ApexII 4K Kappa CCD area detector diffractometer, equipped with a graphite monochromator and MoKα fine-focus sealed tube (λ = 0.71073 Å) operated at 2.0 kW (50 kV, 40 mA). The detector was placed at a distance of 4.0 cm from the crystal; the initial unit cell determinations and data collections were done by the SMART[1] software package. A total of 1315

[1] Bruker SMART-NT Version 5.050. *Bruker AXS Inc. Area-Detector Software Package*, Madison, WI, USA, 1998.

frames of 0.3° were collected at 100(2) K in ω, using an exposure time of 10 s frame^{-1} in all three cases. The frames were integrated using a narrow-frame integration algorithm and reduced with the Bruker SAINT-Plus and XPREP software packages[2] respectively. Analysis of the data showed no significant decay during the data collection. Data was corrected for absorption effects by using the multi-scan technique SADABS[3], and the structure was solved by the direct methods package SIR97[4] and refined using the WinGX[5] software package incorporating SHELXL.[6] The final anisotropic full-matrix least-squares refinement was done on F^2. The methine, methylene and aromatic protons were placed in geometrically idealized positions (C–H = 0.93 – 0.98 Å) and constrained to ride on their parent atoms with $U_{iso}(H) = 1.2U_{eq}(C)$. Non-hydrogen atoms were refined with anisotropic displacement parameters. The graphics were done using the DIAMOND[7] program with 30% probability ellipsoids for all non-hydrogen atoms.

[2] Bruker SAINT-Plus Version 7.12 (including XPREP), *Bruker AXS Inc. Area-Detector Integration Software*, Madison, WI, USA, 1999.

[3] Bruker SADABS Version 2004/1. *Bruker AXS Inc. Area Detector Absorption Correction Software*, Madison, WI, USA, 1998.

[4] Altomare A., Burla M. C., Camalli M., Cascarano G. L., Giacovazzo C., Guagliardi A., Moliterni A. G. G., Polidori G. and Spagna R., *J. Appl. Cryst.*, **32**, 115, 1999.

[5] Farrugia L. J., *J. Appl. Cryst.*, **32**, 837, 1999.

[6] Sheldrick G. M., *SHELXL97. Program for crystal structure refinement*, University of Göttingen, Germany, 1997.

[7] Brandenburg K. and Berndt M., DIAMOND Release 3.0c, *Visual Crystal Structure Information System*, CRYSTAL IMPACT, Postfach 1251, D-53002, Bonn, 2005.

5.3 Results

The three complexes were prepared as reported in Chapter 4. $Hf(tfaa)_4$ crystallized from toluene in a monoclinic space group, *C*2/*c* with Z = 4. $[Hf(OH)(hfaa)_3]_2$ also crystallized in a monoclinic space group *C*2/*c* from acetone with Z = 4. $[Hf(Ox)_4]$ crystallized from N,N-dimetylformamide in a triclinic space group, $P\bar{1}$, with Z = 2.

A summary of the general crystal data and refinement parameter is given in Table 5.1 for all three Hf^{IV} complexes. Supplementary data for the atomic coordinates, anisotropic displacement parameters, all bond distances and angles and hydrogen coordinates are given in the Appendix B.

A complete discussion and comparison with related structures will follow later in this chapter. Hydrogen atoms and/or solvent molecules are omitted in some molecular presentations for clarity.

Table 5.1: Crystal data and structure refinement for $[Hf(tfaa)_4]$, $[Hf(OH)(hfaa)_3]_2$ and $[Hf(Ox)_4]$.

Compound	$[Hf(tfaa)_4]$	$[Hf(OH)(hfaa)_3]_2$	$[Hf(Ox)_4]$
Formula weight	975.09	1689.41	819.25
Crystal system	Monoclinic	Monoclinic	Triclinic
Space group	*C*2/*c*	*C*2/*c*	$P\bar{1}$
Unit cell dimensions: **a,** **b,** **c (Å)**	 22.49(15), 8.0642(5), 22.712(2)	 22.129(5), 12.410(5), 19.501(5)	 11.360(5), 12.245(5), 12.504(5)
α, **β,** **γ (°)**	0, 118.211(2), 0	0, 105.197(5), 0	91.817(5), 103.333(5), 99.190(5)
Volume ($Å^3$) / Z	3631.2(5) / 4	5168(3) / 4	1666.5(12) / 2
Density (calculated) (mg/m^3)	1.784	2.171	1.633
Absorption coefficient (mm^{-1})	2.984	4.205 mm^{-1}	3.180 mm^{-1}
F(000)	1920	3192	824
Crystal size (mm)	0.33 x 0.25 x 0.22	0.26 x 0.16 x 0.10	0.36 x 0.44 x 0.33
Theta range for data collection (°)	2.04 to 28.35	1.90 to 28.30	1.87 to 27.00
Index ranges	-30<=h<=26, -10<=k<=10, -29<=l<=30	-25 <= h <= 29, -16 <=k<= 15, -25 <= l <= 15	-14<=h<=14, -15<=k<=15, -15<=l<=15
Reflections collected	18332	24620	28187
Independent reflections/R(int)	4518 [R(int) = 0.0234]	6381 [R(int) = 0.0502]	7242 [R(int) = 0.0369]
Completeness (θ = 28.35°) (%)	99.80	99.5	99.6
Refinement method	Full-matrix least-squares on F^2	Full-matrix least-squares on F^2	Full-matrix least-squares on F^2
Data / restraints / parameters	4518 / 0 / 252	6381 / 5 / 373	7242 / 2 / 471
Goodness of fit on F^2	1.074	1.030	1.081
Final R indices [I>2sigma(I)]	R1 = 0.0185, wR2 = 0.0412	R1 = 0.0418, wR2 = 0.1102	R1 = 0.0216, wR2 = 0.0522
R indices (all data)	R1 = 0.0212, wR2 = 0.0419	R1 = 0.0571, wR2 = 0.1205	R1 = 0.0233, wR2 = 0.0528
Largest diff. peak and hole ($e.Å^{-3}$)	1.123 and -0.909	2.065 and -1.504	1.346 and -0.973

5.4 Crystal Structure of $[Hf(tfaa)_4]\cdot 2C_7H_8$

The crystal structure of $[Hf(C_5H_4F_3O_2)_4]$, $(C_5H_4F_3O_2)$ = tfaa, was first investigated by Zherikova *et al*. in 2005,[8] who prepared the compound through reacting anhydrous hafnium chloride ($HfCl_4$) with an excess of β-diketones in a inert solvent under reflux conditions and purified by zone vacuum sublimation. For the current M.Sc. study, different ratios of metal to ligand were used, but only tetrakis (1:4 ratio) complexes were isolated, suggesting that the crystallization energy of the tetrakis complex is the lowest of all the possible geometries in this typical symbiotic system.[9]

The synthesis of the title compound with resulting colourless single crystals was obtained as reported in Section 4.2.2.3. The numbering scheme of $[Hf(C_5H_4F_3O_2)_4]\cdot 2C_7H_8$ ($[Hf(tfaa)_4]$) is shown in the perspective drawing in Figure 5.1. Table 5.2 presents selected bond lengths, bond angles and torsion angles. Hydrogen atoms and/or solvent molecules are omitted in some molecular presentations for clarity.

[8] Zherikova K. V., Morozova N. B., Kurat'eva N. V., Baidina I. A., Stabnikov P. A. and Igumenov I. K., *J. Struct. Chem.*, **46**, 6, 1039, 2005.

[9] Huheey J. E., Keiter E. A. and Keiter R. L., *Inorganic Chemistry, Principles of Structure and Reactivity*, 4th Ed., HarperCollins College Publishers, New York, 1993.

Table 5.2: Selected geometrical parameters of [Hf(tfaa)$_4$].

Selected bond lengths (Å)	
Hf—O_1	2.1861 (13)
Hf—O_2	2.1527 (13)
Hf—O_3	2.1933 (13)
Hf—O_4	2.1571 (13)
C_1—C_2	1.494 (3)
C_6—C_7	1.496 (3)
C_4—C_5	1.530 (3)
C_9—C_{10}	1.529 (3)
Selected bond angles (°)	
O_3—Hf—O'_3	71.35 (7)
O_1—Hf—O'_1	71.28 (7)
O_2—Hf—O'_3	72.21 (5)
O_4—Hf—O'_1	72.52 (5)
O_4—Hf—O_3	75.54 (5)
O_2—Hf—O_1	75.69 (5)
O_2—Hf—O_3	76.82 (5)
O_4—Hf—O_1	76.79 (5)
O_2—Hf—O_4	80.96 (5)
O_4—Hf—O'_2	111.77 (5)
O_1—Hf—O'_3	121.11 (5)
O_4—Hf—O'_3	141.11 (5)
O_2—Hf—O'_1	141.35 (5)
O_2—Hf—O'_2	141.66 (7)
O_4—Hf—O'_4	142.02 (7)
O_1—Hf—O_3	143.48 (5)
Selected torsion angles (°)	
O_1—C_2—C_4—O_2	1.565(184)
O_3—C_7—C_9—O_4	-0.477(169)
C_{13}—C_{14}—C_{16}—C_{17}	0.158(240)

Symmetry code: (') –x + 1, y, -z + 3/2

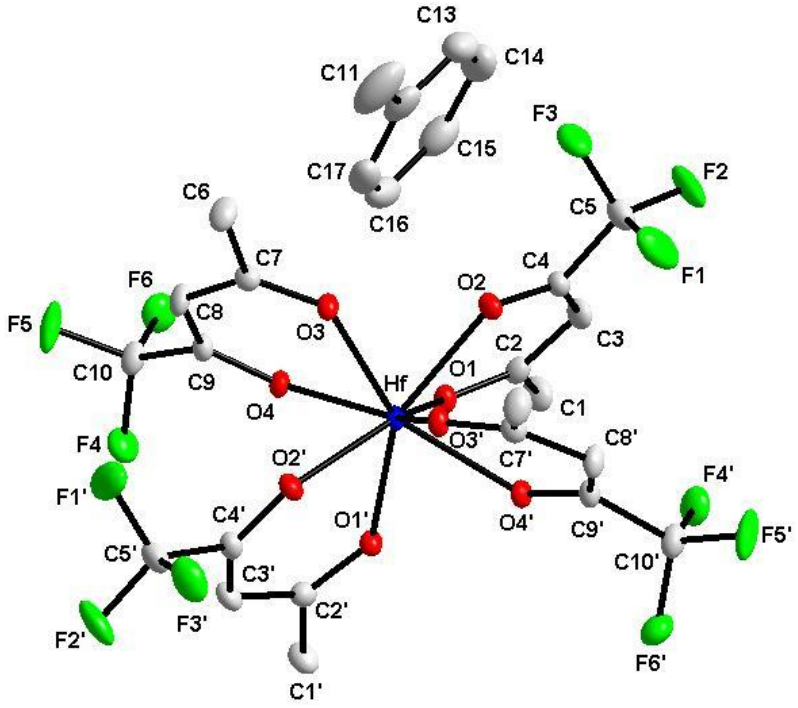

Figure 5.1: Tetrakis(1,1,1-trifluoroacetylacetonato-κ^2-O,O') hafnium(IV) toluene solvate[10] *(30% probability; Hydrogen atoms omitted for clarity, Symmetry code: (') –x + 1, y, -z + 3/2).*

The title compound, tetrakis(trifluoroacetylacetonato)-hafnium(IV) toluene solvate, crystallized as the monoclinic polymorph *C*2/*c* (*Z*=4) with two toluene solvent molecules. The hafnium atoms are situated on a two-fold rotation axis in the unit cell, with the four β-diketonate ligands coordinating to the hafnium, adapting an Archimedean square anti-prismatic coordination environment as illustrated in Figure 5.2.

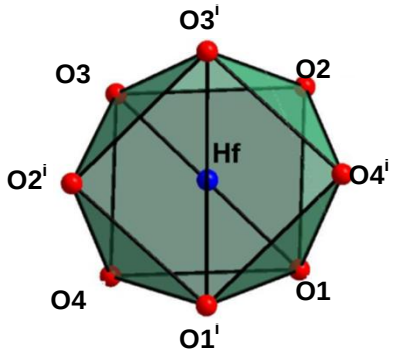

Figure 5.2: Slightly distorted Archimedean antiprism coordination polyhedron surrounding Hf^{IV} atom (*Symmetry code: (') –x + 1, y, -z + 3/2).*

[10] Viljoen J. A., Roodt A. and Muller A. J., *Acta Cryst*., **E64**, m838, 2008.

The Hf—O bond lengths vary from 2.1528(13) Å to 2.1933(13) Å. The average Hf—O distance being 2.172(26) Å and O—Hf—O bite angles of 75.69(5)° and 75.54(5)° are reported. This average bond distance is somewhat larger than the average of 2.146 Å obtained from the Cambridge Structural Database[11] (Data extracted from 18 compounds, yielding 45 observations). Pairs of toluene molecules are π,π-stacked (interplanar distance = 3.650(10) Å, centriod to centriod distance = 4.923(16) Å) in channels formed by the metal complex moieties, parallel to the b-axis as illustrated in Figure 5.3.

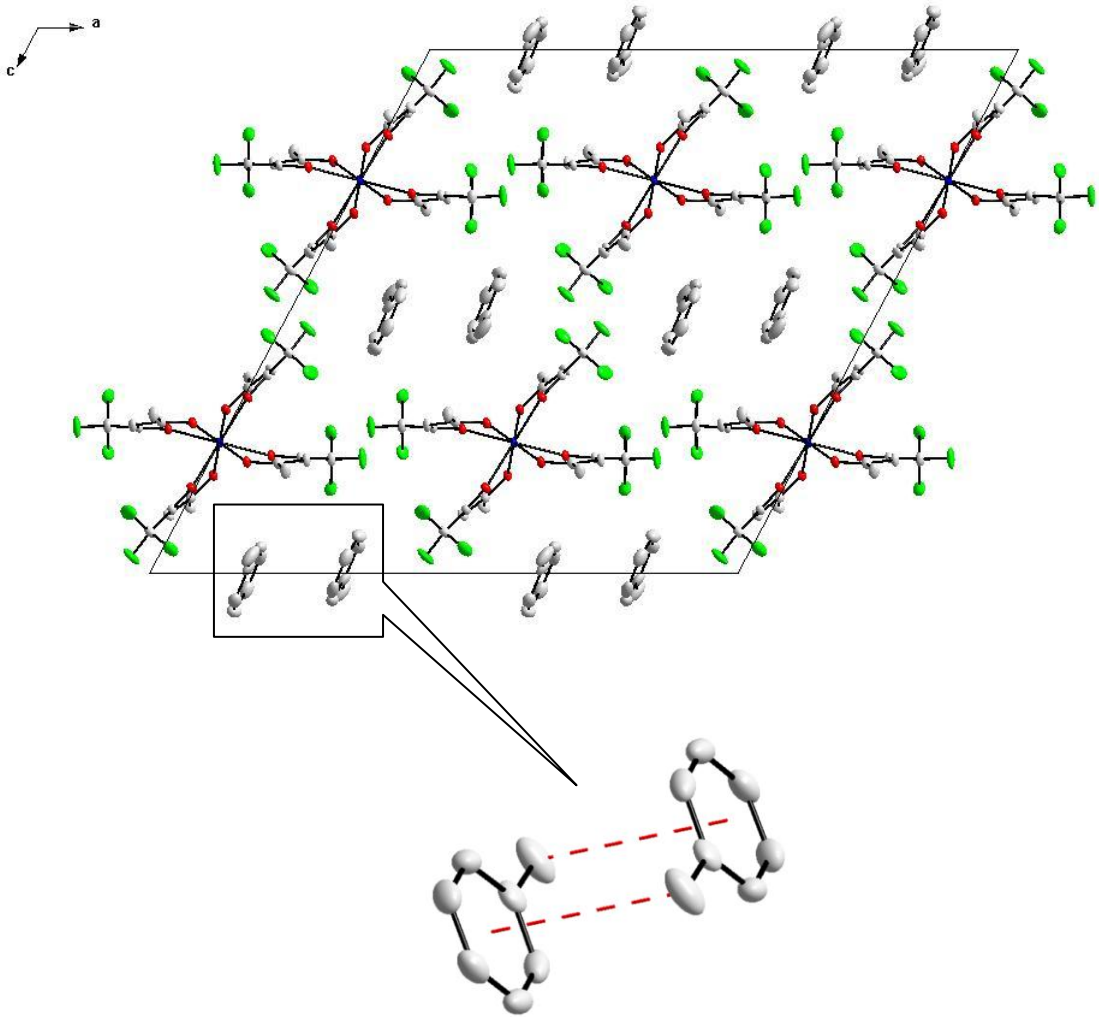

Figure 5.3: Packing diagram of tetrakis(trifluoroacetylacetonato)-hafnium(IV) toluene solvate along the b axis showing π,π-stacking of pairs of toluene molecules.

[11] Cambridge Structural Database (CSD), Version 5.30, November 2008 update, Allen F.H., *Acta Cryst*., **B58**, 380, 2002.

One way to describe the bent nature of the coordinated acac backbone ligand is to construct a plane through O─Hf─O atoms and measure the angle it makes with a plane through coordinated O- and C-atoms of the acac backbone, as illustrated in Figure 5.4.

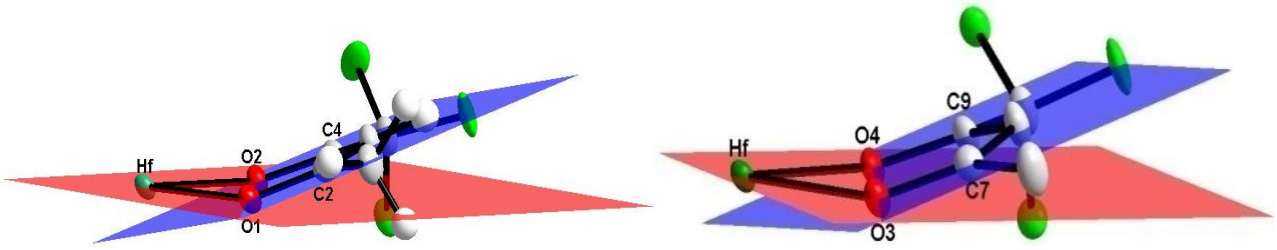

Figure 5.4: Partial structures of $[Hf(C_5H_4F_3O_2)_4 \cdot 2C_7H_8]$ showing graphic illustration of the out of plane bending of the bidentate ligands coordinated to the Hf^{IV} metal centre.

The coordinated ligands are found to bend at the intersection of the two planes formed by the ligand-backbone (O—C—C—C—O) and the O—Hf—O bite angles. The coordinated ligands are bent away from the O—Hf—O planes in an upside-down boat like position. These ligands are not only bent but also slightly twisted. The torsion angle between O_1, O_2, C_2, C_4 and O_3, O_4, C_7, C_9 are -0.477(17)° and 1.565(18)° respectively. All these distortions are listed in Table 5.3. The toluene solvate molecules in the crystal structure are planar, within experimental error, with the average C-C bond distances of 1.378 Å and bond angles of 120° within the anticipated range for phenyl rings.[12]

[12] Lamprecht G. J., Leipoldt J. G. and van Biljon C. P., *Inorg. Chim. Acta*, **88**, 55, 1984.

Table 5.3: Selected dihedral- and torsion angles.

Complex	$[Hf(tfaa)_4]$
Dihedral Angles (°)	
Hf, O_1, O_2 and O_1, O_2, C_2, C_4	18.79(4)
Hf, O_3, O_4 and O_3, O_4, C_7, C_9	19.34(5)
Torsion angles (°)	
O_1, C_2, C_4, O_2	-0.477(17)
O_3, C_7, C_9, O_4	1.565(18)

Weak C-H···F hydrogen bonding intra molecular interactions are also observed and seems to be the reason for the preferred conformation of the CF_3 moiety. The bond distances and angles for all the hydrogen bonds are given in Table 5.4 and illustrated in Figure 5.5.

Table 5.4: Hydrogen-bond geometry (Å, ˚)

D-H...A	d (D-H)	d (H...A)	d (D...A)	D-H…A angle
C_3-H_3···F_2	0.93	2.37	2.712 (2)	102
C_8-H_8···F_5	0.93	2.37	2.721 (2)	102

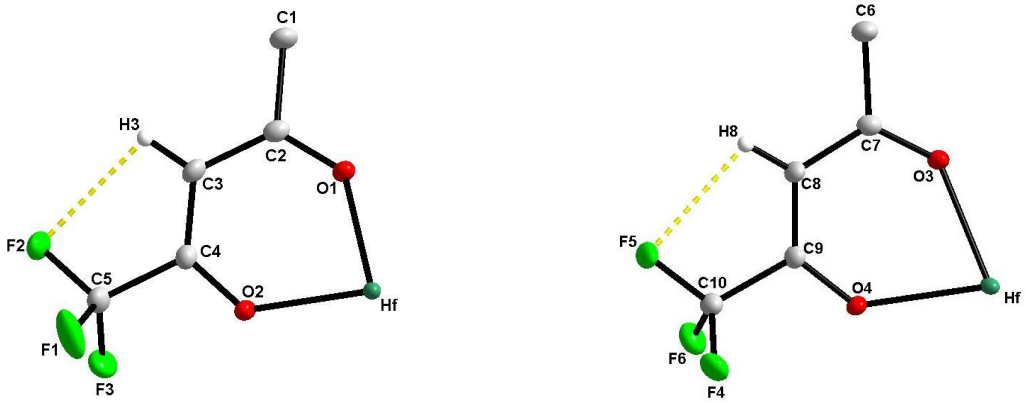

Figure 5.5: Partial structures of $[Hf(C_5H_4F_3O_2)_4 \cdot 2C_7H_8]$ indicating hydrogen bonding between C_3-H_3···F_2 and C_8-H_8···F_5.

5.5 Crystal Structure of $[Hf(OH)(hfaa)_3]_2 \cdot (CH_3)_2CO$

The crystal structure of $[Hf(OH)(C_5HF_6O_2)_3]_2$, $(C_5HF_6O_2)$ = hfaa, was first investigated by Zherikova *et al*.,[13] who prepared the compound through reacting anhydrous hafnium chloride ($HfCl_4$) with an excess of β-diketones in an inert solvent under reflux, and purified by zone vacuum sublimation.

Colourless crystals of the title compound, $[Hf(OH)(hfaa)_3]_2$, were obtained as described in Section 4.2.2.6. $[Hf(OH)(hfaa)_3]_2$ crystallized as the monoclinic polymorph, *C*2/*c,* (*Z*=4) with eight acetone solvent molecules in the unit cell. The numbering scheme of $[Hf(OH)(hfaa)_3]_2$, is shown in the perspective drawing in Figure 5.6, while the most important bond distances and angles are reported in Table 5.5. Hydrogen atoms and/or solvent molecules are omitted in some molecular presentations for clarity.

[13] Zherikova K. V., Morozova N. B., Baidina I. A., Alekseev V. I. and Igumenov I. K., *J. Struct. Chem.*, **47**, 1, 82, 2006.

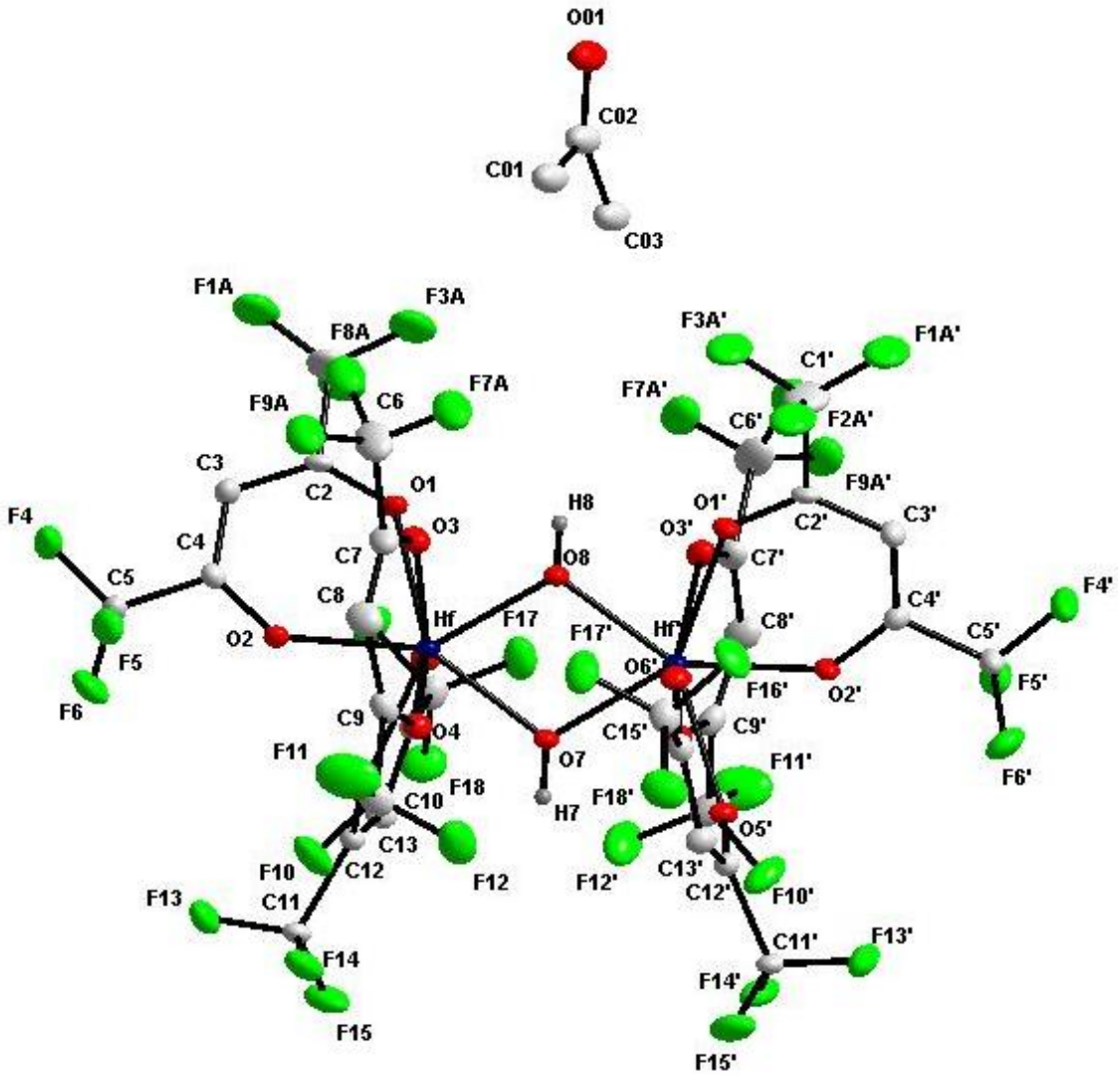

Figure 5.6: Crystal structure of bis(μ^2-hydroxo)-hexakis(hexafluoroacetylacetonato-O,O')-di-hafnium(IV) acetone solvate, $[Hf(OH)(hfaa)_3]_2$ (*30% probability; Hydrogen atoms omitted for clarity).*

The bridged hydroxo atoms are situated on a twofold rotation axis in the unit cell, where the hafnium atoms are octal coordinated, formed by three β-diketonate ligands (hfaa ligands) and two OH-groups, adapting a slightly distorted Archimedean square anti-prismatic coordination environment around the central hafnium atom as illustrated in Figure 5.7.

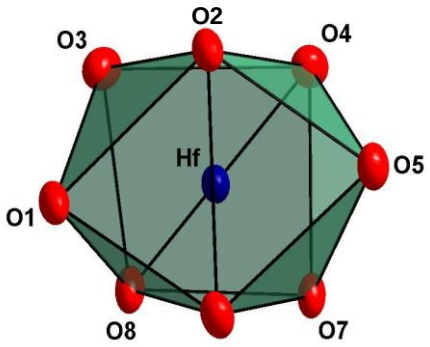

Figure 5.7: Slightly distorted Archimedean antiprism coordination polyhedron surrounding Hf^{IV} atoms.

Table 5.5: Selected geometrical parameters.

Selected bond lengths (Å)		Selected bond lengths cont. (Å)	
Hf—Hf ’	3.5130(7)	C_4—C_5	1.531(18)
Hf—O_1	2.258(8)	C_6—C_7	1.53(2)
Hf—O_2	2.146(9)	C_{11}—C_{12}	1.551(17)
Hf—O_3	2.208(9)	C_{14}—C_{15}	1.523(18)
Hf—O_4	2.150(9)	**Selected bond angles (°)**	
Hf—O_5	2.239(9)	O_1—Hf—O_2	75.8(3)
Hf—O_6	2.136(9)	O_3—Hf—O_4	74.4(3)
Hf—O_7	2.113(7)	O_5—Hf—O_6	75.8(3)
Hf—O_8	2.091(7)	O_7—Hf—O_8	66.6(4)
O_1—C_2	1.239(15)	Hf—O_7—Hf’	112.5(6)
O_2—C_4	1.270(15)	Hf—O_8—Hf’	114.3(6)
O_3—C_7	1.249(16)	**Selected torsion angles (°)**	
O_4—C_9	1.264(16)	O_1—C_2—C_4—O_2	-0.623(23)
O_5—C_{12}	1.239(15)	O_3—C_7—C_9—O4	0.920(23)
O_6—C_{14}	1.277(16)	O_5—C_{12}—C_{14}—O_6	-3.109(23)
C_1—C_2	1.239(15)		

Symmetry code: (‘) 0.5 – x, 0.5 - y , 1 - z

The packing of molecules in solid state $[Hf(OH)(hfaa)_3]_2 \cdot (CH_3)_2CO$ is illustrated in Figure 5.8. In this structure the dimer units are connected by van der Waals interactions, to produce a three dimensional polymeric network, where the average F···F distances are 2.85(21) Å. The different F···F interaction distances are reported in Table 5.6.

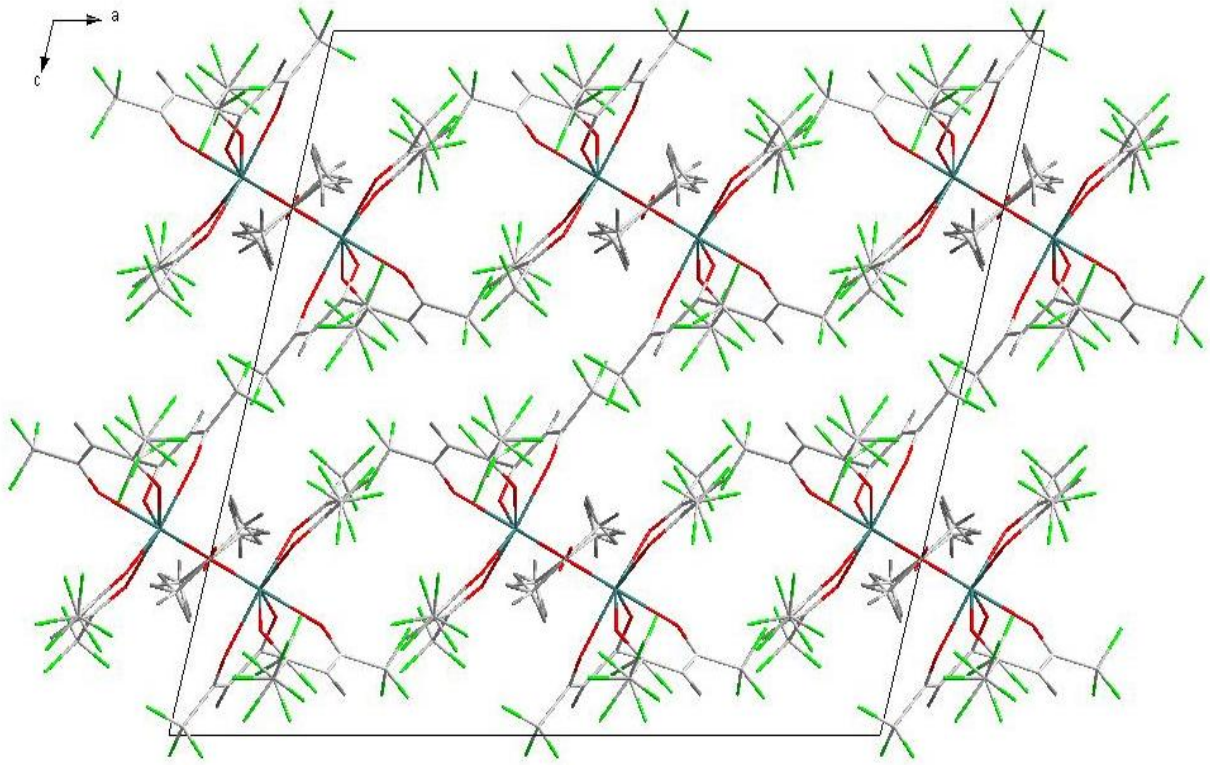

Figure 5.8: Packing of molecules in the crystal structure, illustrating how the dimer units are connected by van der Waals interactions to form a three dimensional polymeric network (*30% probability; Hydrogen atoms and F···F interactions omitted for clarity).*

Table 5.6: F···F interactions distances for $[Hf(OH)(hfaa)_3]_2 \cdot (CH_3)_2CO$.

Van der Waals Interactions	F···F distances
$F_{1B} - F_{15}$	2.883(8)
$F_6 - F_{9B}$	2.868(9)
$F_{7A} - F_{16}$	2.853(9)
$F_{7B} - F_{16}$	2.855(9)
$F_{8B} - F_{10}$	2.714(8)
$F_{9B} - F_{13}$	2.978(9)

The dimer skeleton presents a flat diamond-like structure with Hf—O_7, Hf—O_8 and Hf—Hf' distances of 2.113(7), 2.091(7) and 3.5130(7) respectively, and a bite angle of 66.6(4)°. The hexafluoroacetylacetone ligands form three six-membered metallocycles with an average Hf—O, C—O, C—C_{Me} distances of 2.190(21) Å, 1.256(15) Å and 1.485(16) Å respectively, and an O—Hf—O bite angle of 75.3(5)°. Only one of the chelating metallocycles is flat, while the other two metallocycles are also bent away from the O_3—Hf—O_4 & O_5—Hf—O_6 planes in an upside-down boat position by 15.98° and 8.66° respectively, as illustrated in Figure 5.9.

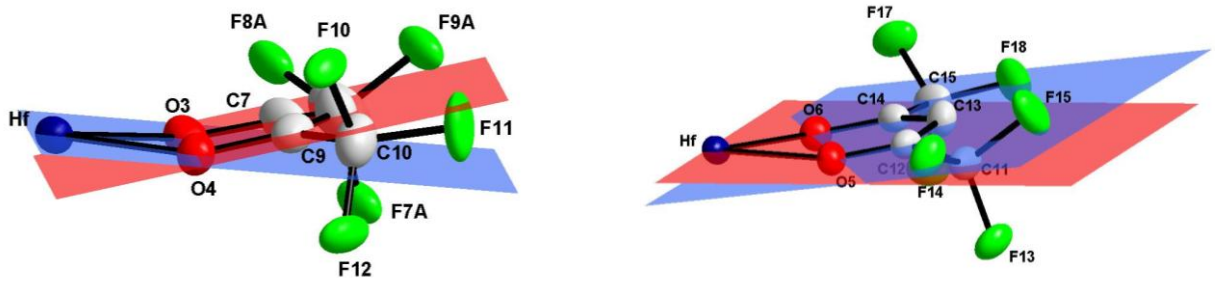

Figure 5.9: Partial structures of $[Hf(OH)(hfaa)_3]_2 \cdot (CH_3)_2CO$ showing graphic illustration of the out of plane bending of the bidentate ligands bonded to the Hf^{IV} metal centre.

One of the metallocycles are twisted to yield a torsion angle of -3.109(23)°. This is possibly due to the close $O_{01}\cdots C_{12}$ (3.0370(5) Å) interaction as illustrated in Figure 5.10.

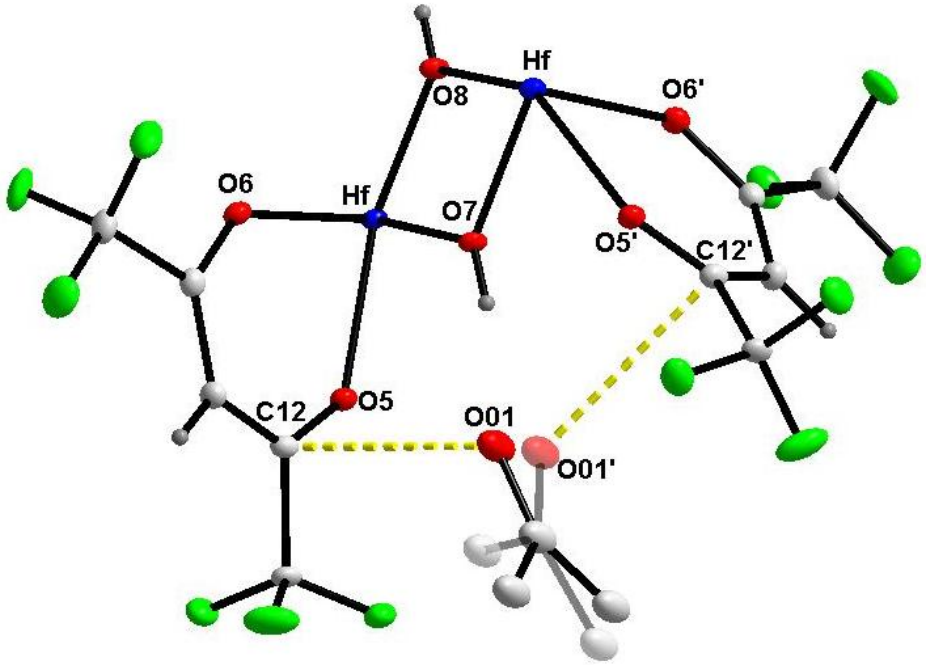

Figure 5.10: Partial structures of $[Hf(OH)(hfaa)_3]_2\cdot(CH_3)_2CO$ illustrating the close $O_{01}\cdots C_{12}$ interaction possibly causing the twisting in the coordinated bidentate ligand.

During the initial refinement cycles, some of the CF_3 moieties showed a somewhat large thermal ellipsoids, indicating loose packing in these regions. These were subsequently refined as disordered, over two positions with a free variable coupled to the occupancy of each moiety to add up to one. The final refinement resulted in ratios of *ca.* 35% and 65%, as indicated in Figure 5.11 below.

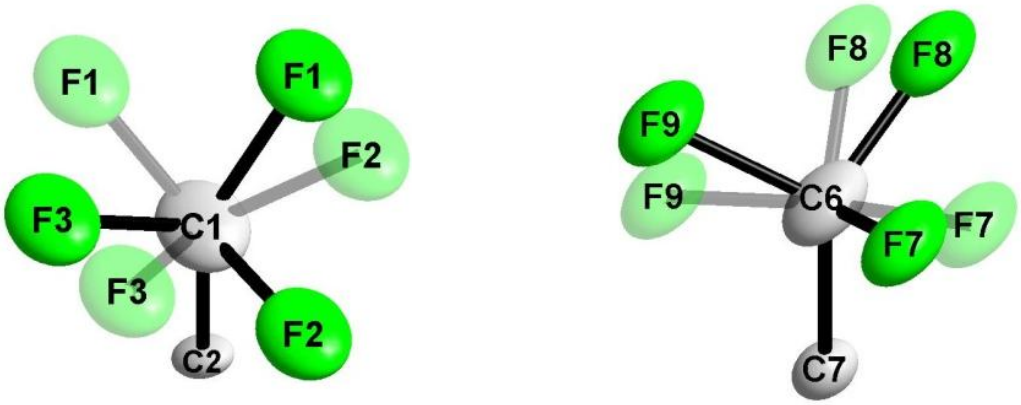

Figure 5.11: Graphical illustration of how some of the F-atoms are distorted over two positions.

The acetone solvate is disordered on a two-fold rotation axis and thus refined with 50% occupancy for each position.

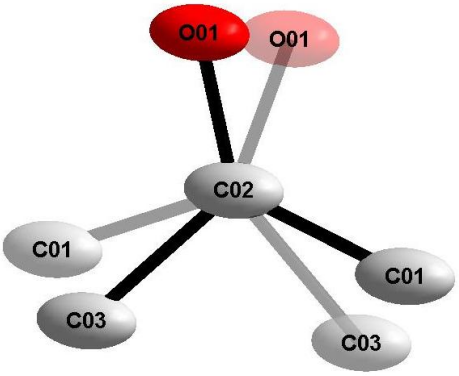

Figure 5.12: Graphic illustration of the acetone solvate which is disordered on a two-fold rotation axis (*30% probability; Hydrogen atoms omitted for clarity).*

O-H···O hydrogen bonding interactions are also observed and may add some of the geometrical strain of the $[Hf(OH)(hfaa)_3]_2 \cdot (CH_3)_2CO$ complex, as illustrated in Figure 5.13. The bond distances and angles for the hydrogen bonding are given in Table 5.7.

Table 5.7: Hydrogen-bond geometry (Å, ˚).

D-H...A	d (D-H)	d (H...A)	d (D...A)	D-H…A angle
O_7-H_7···O_{01}'(a)	0.81(6)	1.9761(8)	2.7817(11)	170.063(43)
O_7-H_7···O_{01}'(b)	0.81(6)	1.9761(8)	2.7817(11)	170.063(43)

Symmetry code: ***'(a) –1/2 + x, -1/2 - y, 1/2 + z;***
'(b) 1/2 – x , 1/2 - y, 1 - z

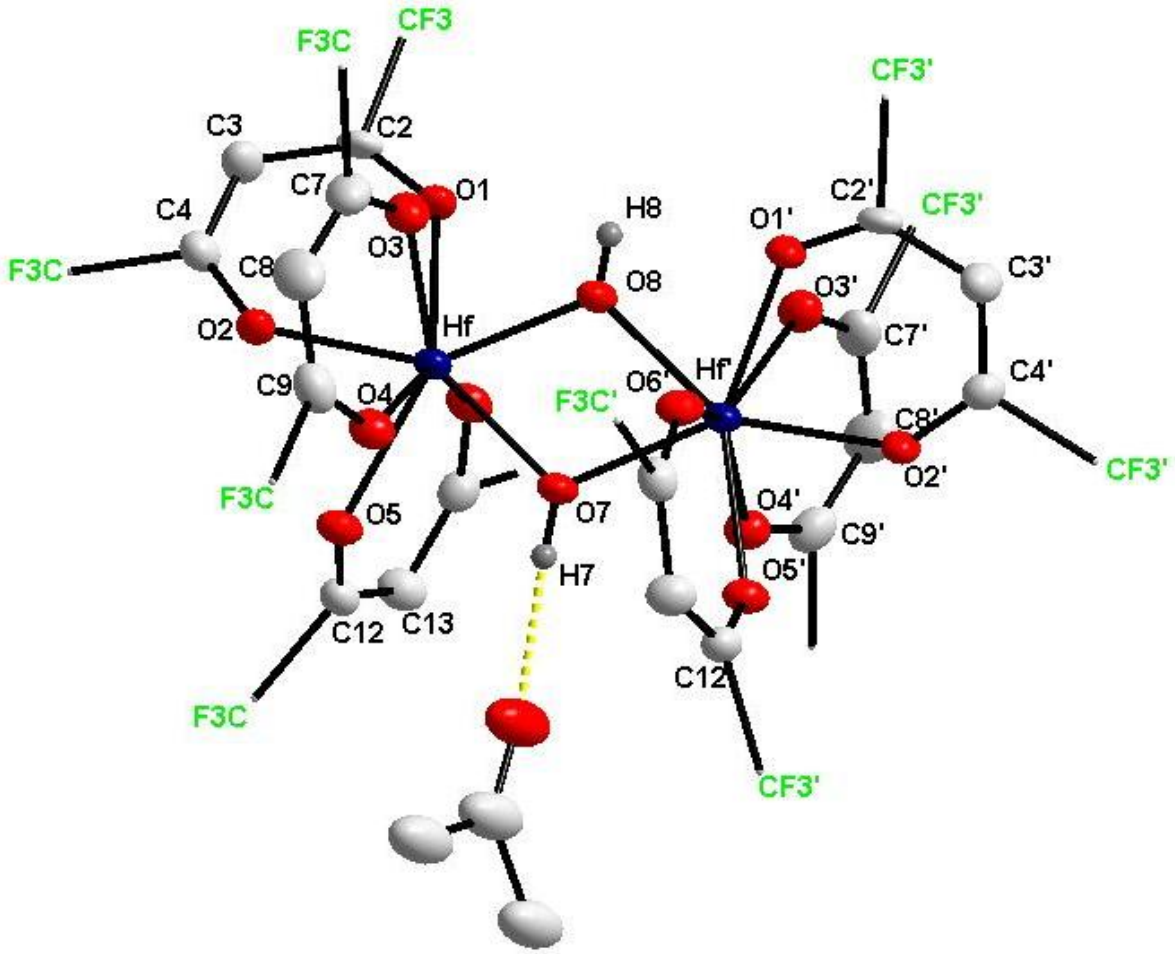

Figure 5.13: Partial structures of $[Hf(OH)(hfaa)_3]_2 \cdot 2(CH_3)_2CO$. - Hydrogen bonding between O_7-H_7···O_{01} (*only one of the interactions are indicated for clarity purposes, 30% probability; Hydrogen and fluorine atoms omitted for clarity*).

5.6 Crystal Structure of $[Hf(Ox)_4]\cdot(HCON(CH_3)_2)\cdot(H_2O)$

The title compound was prepared as reported in Section 4.2.3.3. $[Hf(Ox)_4]$ crystallized from N,N-dimetylformamide in a triclinic space group, $P\bar{1}$, with Z = 2. Selected bond distances and angles are shown in Table 5.8.

Table 5.8: Selected geometrical parameters of $[Hf(Ox)_4]$.

Selected bond lengths (Å)		**Selected bond angles (°)**	
Hf—O_1	2.0960(8)	O_1—Hf—N_1	70.912(14)
Hf—O_2	2.1145(5)	O_2—Hf—N_2	70.754(15)
Hf—O_3	2.0796(6)	O_3—Hf—N_3	71.295(14)
Hf—O_4	2.0918(8)	O_4—Hf—N_4	70.701(15)
Hf—N_1	2.4109(8)		
Hf—N_2	2.3913(7)		
Hf—N_3	2.3891(8)		
Hf—N_4	2.4052(7)		

As can be seen in Figure 5.14 (*a and b*) different side views of $[Hf(Ox)_4]$ are shown, with and without the solvate molecules and the numbering scheme respectively. The four and five-membered chelating rings have an average bite angle of only 70.92(14)°. The solvate molecule seems to have no effects on the different Hf–O and Hf–N bond distances as they are all of the same magnitude as listed in Table 5.8. Hydrogen atoms and/or solvent molecules are omitted in some molecular representations for clarity.

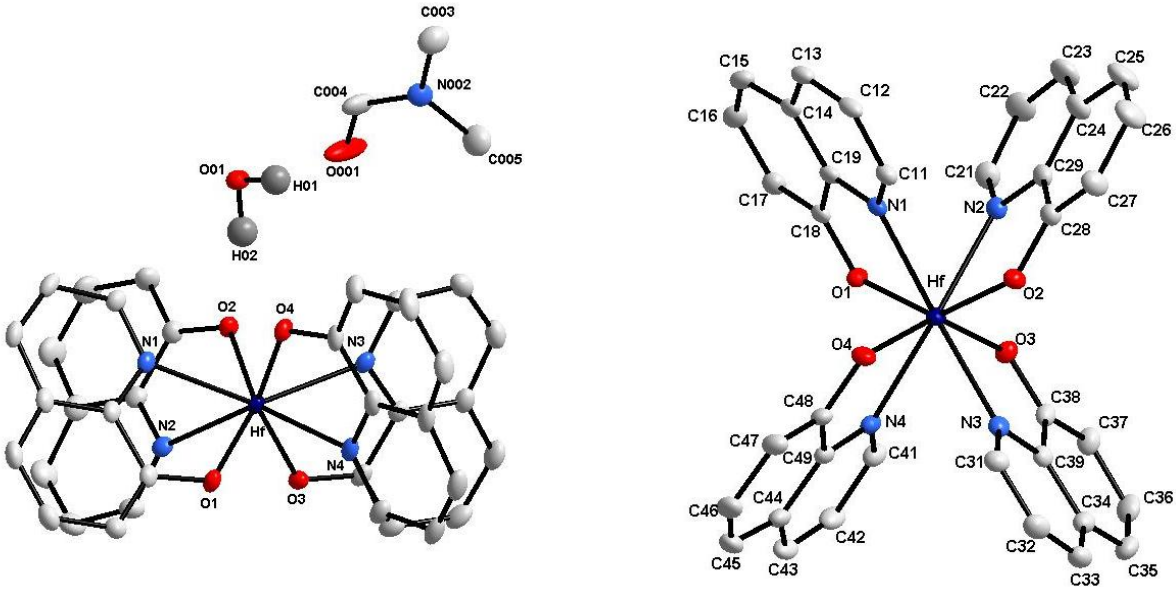

(a) ***(b)***

Figure 5.14: View of tetrakis(8-quinolinolato-κ^2-n,*o*)- hafnium(IV). The first digit indicates the ring number and the second digit indicates the position of the atom in the ring (Hydrogen atoms and/or solvent molecules are omitted in some molecular representations for clarity, 30% probability displacement ellipsoids).

An Archimedean antiprismatic coordination geometry is adopted by the hafnium metal centre when four of the bidentate ligands are coordinated to it, as shown in Figure 5.15.

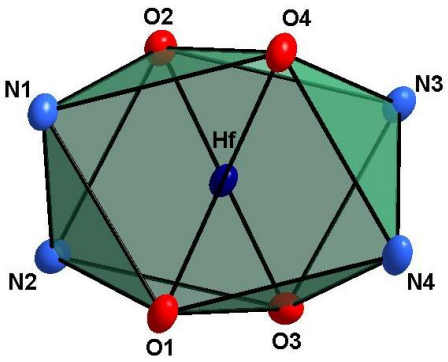

Figure 5.15: A slightly distorted Archimedean antiprism coordination polyhedron, surrounding a Hf^{IV} atom (30% probability displacement ellipsoids).

The dihedral angle between the two phenyl rings of the quinoline ligands are all less than 1°, showing little or negligible distortion due to coordination or solvent molecules within the crystal structure. The dihedral angle between the metal coordination plane and the plane formed by the quinoline ligands are also negligible, except for one quinoline ligand, ring 2, as shown in Figure 5.16. The dihedral angle between the metal coordination plane and the plane formed by this quinoline ligand is 7.313(11)°, showing a slight distortion, possibly due to the hydrogen interaction between O01-H02···O2 (1.8886(5) Å) as illustrated in Figure 5.18(b). Various packing effects such as π-π-stacking, which is clearly observed in the unit cell, are shown and reported in Figure 5.17 and Table 5.9 respectively, with an average π-π-stacking distances of 3.2207(9) Å. The molecules pack in a "head to head" fashion (equivalent quinoline substituents face another).

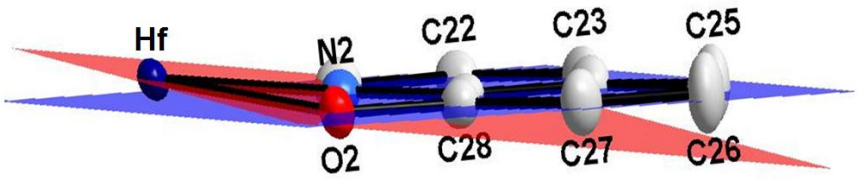

Figure 5.16: Partial structures of $[Hf(Ox)_4]$, shown as a graphic illustration of the dihedral angle between the metal coordination plane and the plane formed by the quinoline ligands (Hydrogen atoms omitted for clarity**,** 30% probability displacement ellipsoids).

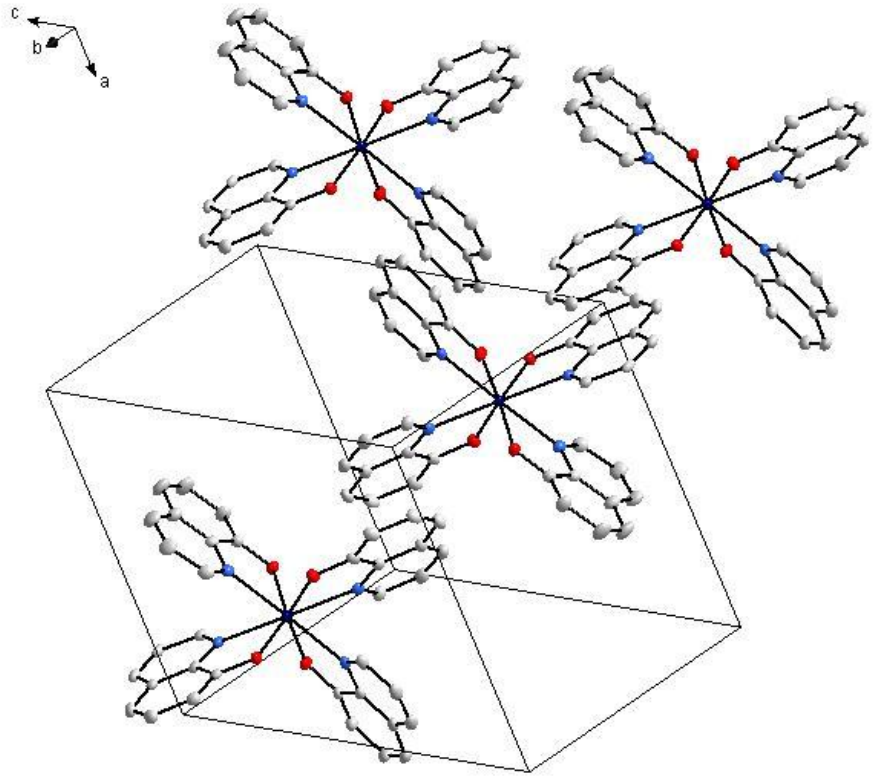

(a)

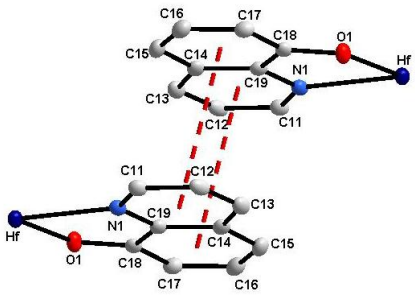

(b)

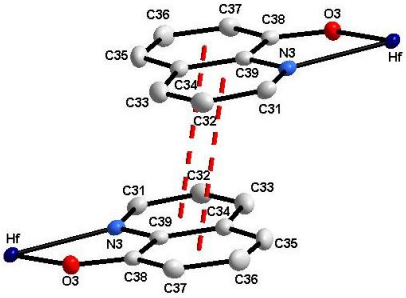

(c)

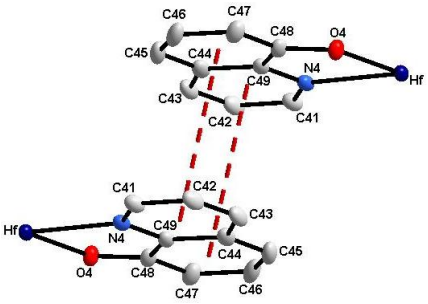

(d)

Figure 5.17: **(a)** – π-π-stacking inside the unit cell also indicating the "head to head" stacking fashion. **(b-c)** – Partial structures $[Hf(Ox)_4]$, indicating π-π-stacking between the quinoline ligands coordinated to the hafnium metal centre (Hydrogen atoms omitted for clarity**,** 30% probability displacement ellipsoids).

Table 5.9: π-π-Stacking properties of $[Hf(Ox)_4]$.

π-π-Stacking		
Fig. no.	**Interplanar distance (Å)**	**Centroid to centroid distance (Å)**
5.17(b)	3.154(12)	3.6435(13)
5.17 (c)	3.268(8)	3.5894(10)
5.17 (d)	3.240(10)	4.1531(16)

Weak O-H···O hydrogen bonding interactions are observed and may add some of the geometrical strain of the $[HF(Ox)_4]$ complex. The bond distances and angles for the hydrogen bonding are given in Table 5.10 and illustrated in Figure 5.18(a-d)

Table 5.10: Hydrogen-bond geometries (Å, °) of $[HF(Ox)_4]$.

Fig. no.	D-H...A	d (D-H)	d (H...A)	d (D...A)	D-H…A angle
5.18(a)	O_{01}-H_{02}···O_2	1.00(4)	1.89(4)	2.865(3)	165(3)
5.18 (b)	O_{01}-H_{01}···O_{001}	1.01(4)	1.78(4)	2.757(5)	160(4)
5.18 (c)	C_{004}-H_{004}···O_{01}'	0.93	2.43	3.332(6)	164(3)
5.18 (d)	C_{31}-H_{31}···O_{001}	0.93	2.43	3.418(5)	160(5)

Symmetry code: (') – x, 1 - y, - z

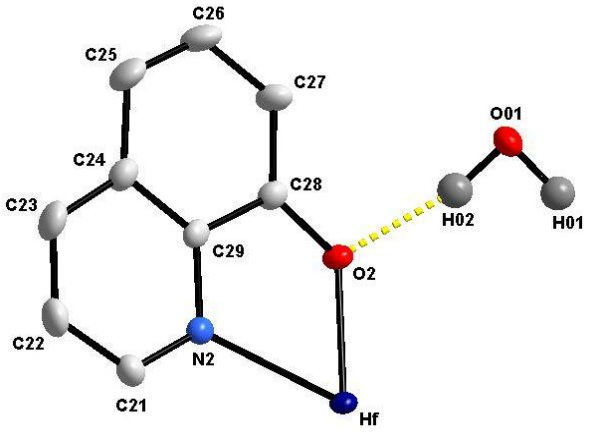

(a)

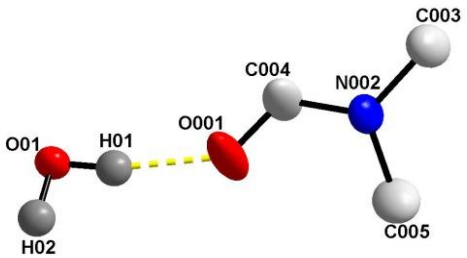

(b)

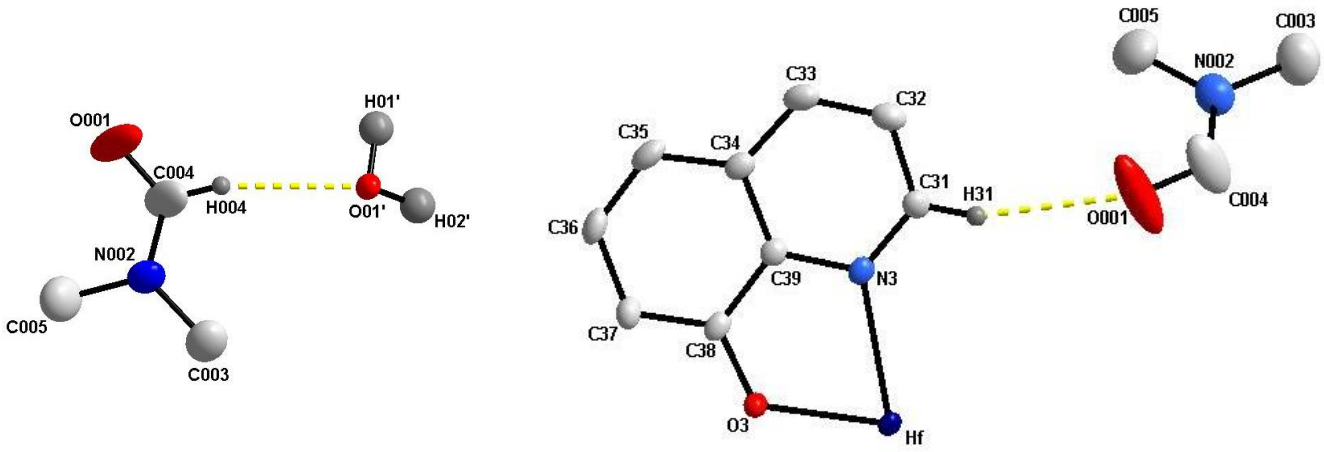

(c) ***(d)***

Figure 5.18: Partial structures of $[Hf(Ox)_4]$ indicating O-H···O hydrogen bonding interactions.

5.7 Comparison of the Crystal Structure of this Study and some Poly- and Isomorphous Crystal Structures from Literature

Tables 5.11 to 5.14 gives a short comparison between the first two structures reported here (where **(1)** and **(2)** are $[Hf(tfaa)_4]$ and $[Hf(OH)(hfaa)_3]_2$, respectively) and their polymorph structures, **(4)** and **(5)**, obtained from literature. Unit cell contents and selected inter-atomic bond distances and angles are given in these tables below.

Table 5.11: Comparative summary of crystallographic data of tetrakis(1,1,1-trifluoroacetylacetonato-κ^2-O,O') hafnium(IV) toluene solvate (crystal structure **(1)**) and tetrakis(1,1,1-trifluoroacetylacetonato-κ^2-O,O') hafnium(IV) (crystal structure **(4)**).

Complex	**(1)**	**(4)***
Crystal system	Monoclinic	Triclinic
Space group	*C2/c*	$P\bar{1}$
Z	4	2
a (Å)	22.4983(15)	8.1039(12)
b (Å)	8.0642(5)	11.4499(14)
c (Å)	22.712(2)	15.790(2)
α (°)	90	99.341(4)
β (°)	118.211(2)	103.175(4)
γ (°)	90	108.185(4)
Volume (Å^3)	3631.2(5)	1267.5(9)
Density (mg/m^3)	1.784	2.003

**** Values determined by Zherikova et al.*[8]**

Table 5.12: Comparative geometrical data of crystal structures **(1)** and **(4)**.

Complex	**(1)**	**(4)***
Angles (°)		
O_1-Hf-O_2	75.69(5)	75.6(2)
O_3-Hf-O_4	75.54(5)	75.5(3)
Bond Distances (Å)		
Hf-O_1	2.1861(13)	2.186(7)
Hf-O_2	2.1527(13)	2.169(6)
Hf-O_3	2.1933(13)	2.189(6)
Hf-O_4	2.1571(13)	2.156(7)
C-O-Hf Dihedral Angle (°)		
C_2-O_1-Hf	18.79(4)	17.49(3)
C_7-O_3-Hf	19.34(5)	18.19(4)

**** Values determined by Zherikova et al.*[8]**

Table 5.13: Comparative summary of crystallographic data of bis(μ^2-hydroxo)hexakis-(hexafluoroacetylacetonato-O,O')-di-hafnium(IV) acetone solvate (crystal structure **(2)**) and bis(μ^2-hydroxo)-hexakis(hexafluoroacetylacetonato-O,O')-di-hafnium(IV) (crystal structure **(5)**).

Complex	**(2)**	**(5)***
Crystal system	Monoclinic	Monoclinic
Space group	*C2/c*	*$P2_1/c$*
Z	4	2
a (Å)	22.129(5)	12.957(3)
b (Å)	12.410(5)	16.687(3)
c (Å)	19.501(5)	12.398(3)
α (°)	90	90
β (°)	105.197(5	108.97(3)
γ (°)	90	90
Volume ($Å^3$)	5168(3)	2535.0(9)
Density (mg/m^3)	2.171	2.137

**** Values determined by Zherikova et al.*[13]**

Table 5.14: Comparative geometrical data of crystal structures (2) and (5).

Complex	**(2)**	**(5)***
Angles (°)		
O_1—Hf—O_2	75.8(3)	75.6(4)
O_3—Hf—O_4	74.4(3)	73.9(4)
O_5—Hf—O_6	75.8(3)	75.0(3)
O_7—Hf—O_8	66.6(4)	67.8(3)
Hf—O_7—Hf'	112.5(6)	112.2(3)
Hf—O_8—Hf'	114.3(6)	112.2(3)

Complex	(2)	(5)*
Bond Distances (Å)		
Hf—Hf'	3.5130(7)	3.534(2)
Hf—O_1	2.258(8)	2.230(9)
Hf—O_2	2.146(9)	2.123(9)
Hf—O_3	2.208(9)	2.186(10)
Hf—O_4	2.150(9)	2.154(11)
Hf—O_5	2.239(9)	2.208(9)
Hf—O_6	2.136(9)	2.120(9)
Hf—O_7	2.113(7)	2.141(8)
Hf—O_8	2.091(7)	2.116(8)

**** Values determined by Zherikova et al.*[13]**

Both the compounds reported in this study $[Hf(tfaa)]_4$ and $[Hf(OH)(hfaa)_6]_2$ crystallizes in the monoclinic space group with four molecules per unit cell associated with corresponding solvate molecules. Their polymorphs crystallize in a triclinic and monoclinic space group respectively and contained only two molecules per unit cell. This explains why it occupies such large volumes per unit cell (Å^3, *see* Table 5.11 and 5.13). The small differences in density between the polymorphous complexes can be attributed to the co-crystallization of the solvate molecules. The bond distances between the hafnium centres and the coordinated oxygen atoms are all more or less the same. The Hf–O bond lengths vary from 2.091(7) Å to 2.258(8) Å, with the average Hf–O distance being 2.167(5) Å. The O–Hf–O bite angles are also the same for all these complexes, with the average bite angle being 75.28(7)°.

The triclinic polymorph of $[Hf(tfaa)_4]$, reported earlier by Zherikova *et al.* contains no solvent molecules and cannot be superimposed on $[Hf(tfaa)_4]$ (from this study), due to differences in metal coordination modes. An isomorphous zirconium complex also containing a toluene solvate has been reported by Steyn *et al.*[14] as shown in Figure 5.19.

[14] Steyn M., Roodt A. and Steyl G., *Acta Cryst*. **E64**, m827, 2008.

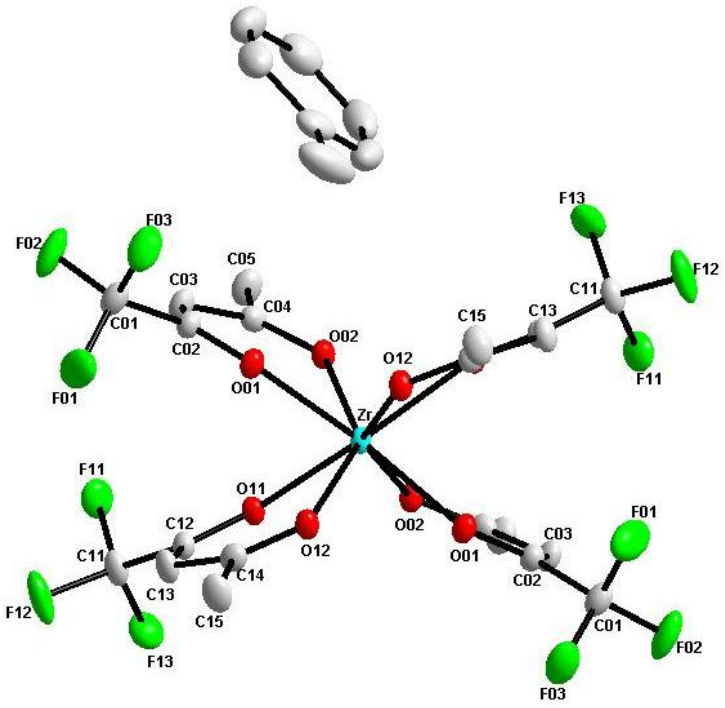

Figure 5.19: Tetrakis(1,1,1-trifluoroacetylacetonato-κ^2-O,O') zirconium(IV) toluene solvate *(30% probability; Hydrogen atoms omitted for clarity).*

An RMS overlay error of less than 1 Å (1.53×10^{-2} Å, excluding F atoms) is obtained when $[Hf(tfaa)_4]$ is superimposed on the above structure, demonstrating the strong similarities between hafnium and zirconium's coordination modes. The monoclinic polymorph of $[Hf(OH)(hfaa)_3]_2$ also reported earlier by Zherikova *et al.* also contains no solvent molecules. $[Hf(OH)(hfaa)_3]_2$.

The polymorph complex of Zherikova *et al.* does not lay on a two-fold rotation axis like $[Hf(OH)(hfaa)_3]_2$ (from this study), and therefore the two sides of the polymorph dimer (where one hafnium atom is coordinate to three hfaa ligands and two bridging oxygen atoms) have different geometries, making it impossible to superimpose the structures.

No related crystallographic data could be obtained from literature, indicating the pioneering work reported here. From literature,[11] only one report with similar type

ligands could be found (complex **(6)**) *i.e.* chloro-(μ5-cyclopentadienyl)-bis(5-chloroquinolin-8-olato-N,O)-hafnium(IV) dichloromethane solvate.[15]

Table 5.15 provides a small comparison of $[Hf(Ox)_4]$, complex **(3)**, from this study with complex **(6)**.

Table 5.15: Comparative summary of crystallographic data for crystal structures **(3)** and **(6)**.

Complex	**(3)**	**(6)**
Crystal system	Triclinic	monoclinic
Space group	$P\bar{1}$	*C2/c*
Z	2	8
a (Å)	11.360(5)	16.146(2)
b (Å)	12.245(5)	12.705(2)
c (Å)	12.504(5)	23.292(3)
α (°)	91.817(5)	90
β (°)	103.333(5)	103.38(1)
γ (°)	99.190(5)	90
Volume (Å^3)	1666.5(12)	4648.25(456)
Density (mg/m^3)	1.633	1.940

After broadening the literature search to try and quantify how many, if any, quinoline coordinated zirconium complexes do exists, only four compounds were found. Tabulated in Table 5.16 are the average Hf─O and Hf─N bond distances together with the average O─Hf─N bite angle of complex **(3)**, complex **(6)** and the four complexes obtained from literature.

[15] Demakopoulos I., Klouras N., Raptopoulou C. P. and Terzis A., *Z. Anorg. Allg. Chem.,* **621,** 1761, 1995.

Table 5.16: Comparative summary of bond distances and bite angles for crystal structures **(3)**, **(6)** and zirconium complexes containing quinoline ligands.

Complex	(3)	(6)	(Ave)* $Zr(Ox)_n$
Average bond lengths (Å)			
Hf—O	2.095(7)	2.065(5)	2.051(36)
Hf—N	2.399(8)	2.353(6)	2.395(48)
Average bond angles (°)			
O—Hf—N	70.92(15)	72.51(15)	72(2)

** Data extracted from four hits, yielding seven bond distances and seven bite angles*.

The bond distances between the hafnium and zirconium centres and the coordinated oxygen and nitrogen atoms are all more or less the same length, within experimental errors, again showing the very strong similarities in bonding modes and geometries between hafnium and zirconium. It is interesting to note that complex **(3)**, from this study, is the first eight coordinated hafnium complex reported that contain quinoline type ligands.

5.8 Conclusion

A range of new hafnium complexes containing O,O'- and N,O- bidentate ligands have been successfully synthesized and characterized by X-ray crystallography, one of which has already been published.[10] Occurrences of similar structures in literature, however, were limited, indicating a field open to study. In total, only 19 compounds have been characterized by X-ray crystallography where the acac type backbone (O,O'-bidentate) ligand is coordinated to a hafnium centre. Only one complex has been characterised by X-ray crystallography where a quinoline ligand is coordinated to hafnium.

The bent nature of the coordinated acac backbone reported earlier in this chapter (*see* Figures 5.4 and 5.9) was thought to be unique due the co-crystallization of the solvent molecules. Further research showed that the same phenomena occurs in the un-solvated $[Hf(acac)_4]$[16], $[Hf(tfaa)_4]$[8] and $[Zr(acac)_4]$[17] complexes. The dihedral angle between the metal coordination plane and the plane formed by acac backbone type ligands are listed in Table 5.17.

Table 5.17: The dihedral angle between the metal coordination plane and the plane formed by acac backbone type ligands in the un-solvated complexes.

Compound	**$[Hf(acac)_4]$**	**$[Hf(tfaa)_4]$**	**$[Zr(acac)_4]$**
Ave. dihedral angle between planes	22.42(76)	17.77(38)	21.39(23)

The bite angles and bond distances of the solvated and non-solvated molecules are also the same within experimental error. It is quite evident that the co-crystallization of the solvent molecules does not restrict or interfere with any significant physical properties of the solvated crystalline moiety. The main organometallic part of hafnium and zirconium crystal structures shows near identical dimensions, except when coordinated to hfaaH. HfaaH shows a tendency to form dimeric species when coordinated with hafnium (as reported in this study), where on the other hand it has a strong tendency to form monomers[18] when coordinated with zirconium. These differences in coordination modes will be exploited in detail in the future, as it is the first major difference observed so far between hafnium and zirconium coordination modes.

[16] Zherikova K. V., Morozova N. B.,.Kurat'eva N. V, Baidina I. A. and Igumenov I. K., *J. Struct. Chem.,* **46**, 1081, 2005.

[17] Silverton J. V., Hoard J. L., *Inorg. Chem*., **2**, 235, 1963.

[18] Zherikova K. V., Morozova N. B., Kurat'eva N. V., Baidina I. A., Stabnikov P. A. and Igumenov I. K., *J. Struct. Chem.*, **48**, 555, 2007.

6 Kinetic Study of the Halide Substitution in [$HfCl_4$] by Oxine as Entering Ligand

6.1 Introduction

This chapter contains an overview of a preliminary kinetics study of the chlorine substitution reactions of [$HfCl_4$] by OxH (8-hydroxyquinoline). A study of the available literature revealed that these reactions have not been investigated before.

By investigating the coordination of bidentate ligands with hafnium in solution, rather than merely characterising the solid state products as in Chapter 5, one might gain valuable information which can be utilized to design potentially new separation techniques for hafnium and zirconium. This kinetic study may also provide important insight on why only fully coordinated hafnium complexes, [$Hf(L,L')_4$], were isolated from solutions containing [$HfCl_4$] and different ligand ratios.

6.2 Consecutive Reactions

Complex kinetic studies sometimes involve several consecutive reactions occurring in the same time frame. The equations used to fit absorbance *vs.* time data are briefly summarized below:

If we consider a general reaction, where k_1 represents the forward reaction and k_{-1} the reverse reaction rate constants.

$$[M] + [L,L'] \underset{k_{-1}}{\overset{K_1,\, k_1}{\rightleftharpoons}} [M(L,L')] \qquad \text{. . . Eq. 6.1}$$

For a typical one-step reaction, as illustrated in Eq. 6.1, under first-order conditions with [L,L'] >> [M], the pseudo first-order rate constant for the reaction is given by Eq. 6.2:

$$k_{obs} = k_1[LL'] + k_{-1} \quad \text{. . . Eq. 6.2}$$

From this a plot of k_{obs} *vs.* [L,L'] should yield a straight line with an intercept of k_{-1} and a slope of k_1. The pseudo first-order rate constant for such a substitution reaction is obtained from fitting Absorbance *vs.* time to by Eq. 6.3.

$$A_{obs} = A_\infty-(A_\infty-A_0)e^{-kobs.t} \quad \text{. . . Eq. 6.3}$$

Similarly, in the case of two step consecutive reactions, with two pseudo first-order rate constants (k_{obs1} and k_{obs2}) and provided that [LL'] >> [M], Eq. 6.4 can be derived by:

$$A_{obs} = (A_0-B_0)e^{-kobs1.t} + (B_0-B_\infty)e^{-kobs2.t} + B_\infty \quad \text{. . . Eq. 6.4}$$

The rate constants for both steps can therefore be obtained from least-squares fits of the appropriate absorbance *vs.* time traces.

For a three step consecutive reaction, Eq. 6.5 can be derived and the three rate constants can be obtained from a least-squares fit of the absorbance *vs.* time traces

$$A_{obs} = (A_0-B_0)e^{-kobs1.t} + (B_0-C_0)e^{-kobs2.t} + (C_0-C_\infty)e^{-kobs3.t} + C_\infty \quad \text{. . . Eq. 6.5}$$

In Eq. 6.3 – 6.5, the variables are defined as follows:

$\mathbf{A_{obs}}$ = Observed absorbance as found in kinetic data.

$\mathbf{A_0}$ = Initial absorbance at the start of the experiment.

$\mathbf{B_0}$ = Calculated Initial absorbance of the 2nd product.

$\mathbf{C_0}$ = Calculated initial absorbance of the 3rd product.

$\mathbf{C_\infty}$ = Infinite 3rd/final product absorbance as found in kinetic data.

t = time (s).

$\boldsymbol{k_{obs\ x}}$ = Observed rate constant for x = 1, 2 or 3.

6.3 Experimental

Kinetic measurements were performed on a Varian Cary 50 Conc UV/Vis- (slower reactions) or Applied Photophysics Stopped-flow (fast reactions) spectrophotometers. Temperature control of the reaction solutions was maintained to within ± 0.1 ˚C by means of a circulating water bath system.

All reagents used for UV/Vis techniques were of analytical grade. If nothing else is stated, all commercially available reagents and solvents were used as received from Sigma-Aldrich without further purification.

For the kinetic study, a stock solution of 8-hydroxyquinoline (203.9 mg, 1.404 mmol) was prepared by dissolving in DMF (0.1 dm^3). The desired [OxH] concentrations were then obtained by diluting the stock solution across a series of 7 solutions with the lowest concentration solution to be no less than 1.405 x 10^{-3} M. A standard [$HfCl_4$] solution was also prepared by dissolving [$HfCl_4$] (4.6 mg, 0.014 mmol) in DMF (0.1 dm^3), yielding [$HfCl_4$] = 7.18 x 10^{-5} M.

The observed rate constants from the UV/Vis data was obtained from least squares fits of the absorbance *vs.* time traces, using the software program, Scientist[1], from Micromath.

The data obtained from the stopped-flow spectrophotometer was fitted by using the inherent software of the stopped-flow apparatus (running on an Acorn Risc work station). Rate constants determined by stopped-flow techniques are given as the average of four individual runs.

6.4 Results and Discussion

6.4.1 Preliminary observations

It was already mentioned in Chapter 2 (Scheme 2.5) that Hf(IV) hydrolyses in aqueous medium to form insoluble [HfO_2], which can only be re-dissolved in hydrofluoric acid. Preliminary experiments indicated that the solubility of both reagents and products was best obtained in N,N'-dimetylformamide (DMF). The stabilities of [$HfCl_4$] and OxH in DMF was confirmed on a UV/Vis spectrophotometer by allowing solutions of these reagents to stand for several days.

In Chapter 4, it was illustrated that [$Hf(Ox)_4$] is the only formation product isolated from solutions of [$HfCl_4$] and OxH. Even 1:1 reaction mixtures provided [$Hf(Ox)_4$] as a final product.

In mechanistic studies it is always important to try and identify intermediate species and final products. The final product in this case was [$Hf(Ox)_4$] and was confirmed by NMR, IR (*see* Chapter 4) as well as X-ray diffraction data (*see* Chapter 6). These observations point to the fact that the formation reactions between [$Hf(Ox)_4$] and OxH should include at least four separate reaction steps for every entering OxH ligand, as illustrated in Scheme 6.1.

[1] Scientist for Windows, Program for Least Squares Parameter Optimization; MicroMath Scientific Software; Utah.

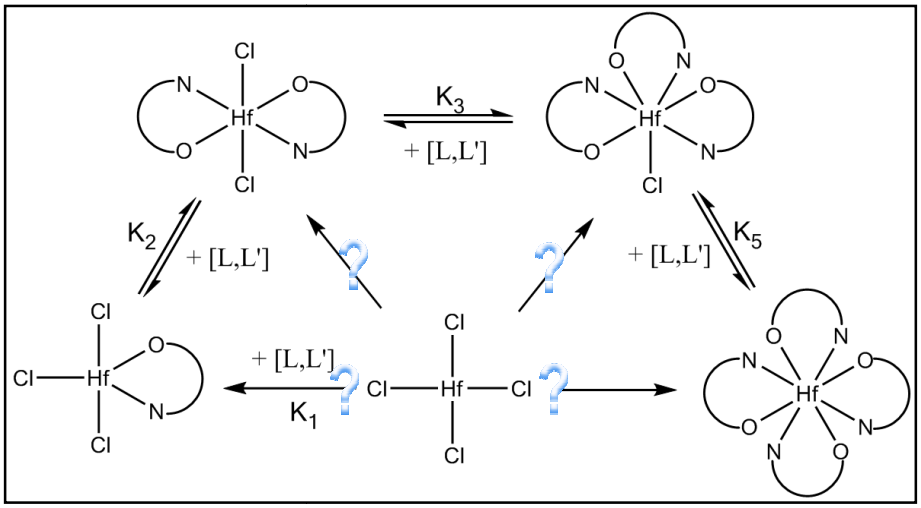

Scheme 6.1: Schematic presentation of possible reactions between [$HfCl_4$] and L,L'-bidentate ligands to form [$Hf(L,L')_4$] final products.

Figure 6.1 is a representation of a typical UV/Vis spectrum of absorbance *vs.* wavelength at 10 seconds time intervals for the reaction of [$HfCl_4$], with a minimum of a ten-fold excess of OxH, in order to ensure pseudo first-order conditions. From this graph it is obvious that there is at least one very fast reaction (shift from 1 to 2, Figure 6.1), followed by a slower reaction/s to the formation of the final product. The final UV/Vis spectrum of typical reaction mixtures used in this kinetic study is identical to that of [$Hf(Ox)_4$] (Chapter 4, Paragraph 4.2.3.3), further confirming that [$Hf(Ox)_4$] is the final product in all instances.

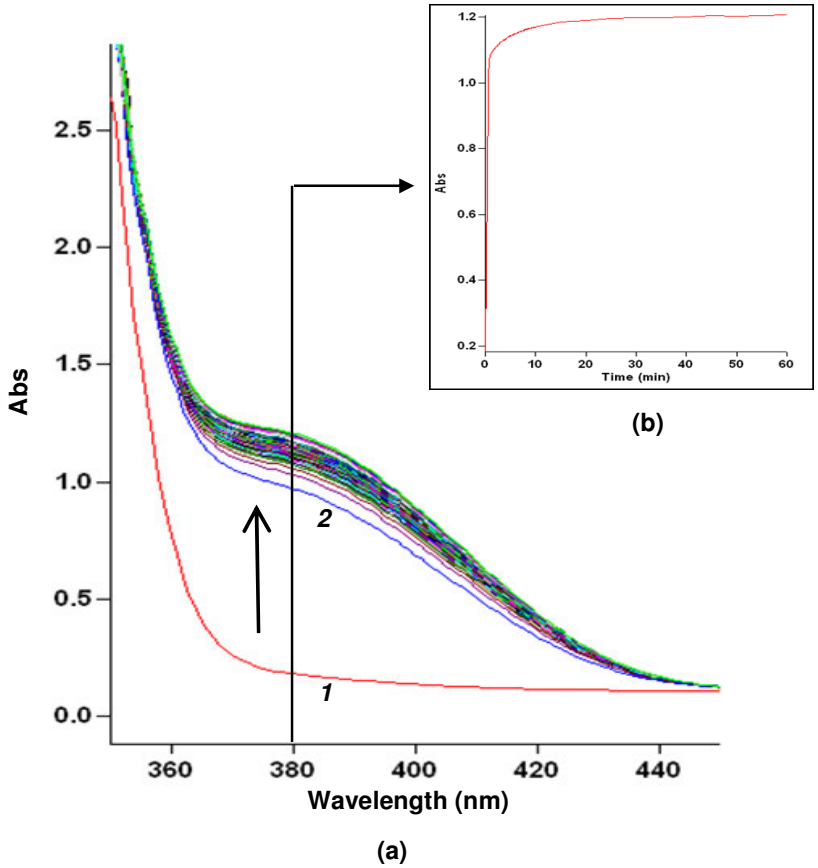

Figure 6.1: Typical UV/Vis spectra of [$HfCl_4$] (7.18 x 10^{-5} M) and [OxH] (7.02x10^{-3} M) in DMF (a) Graph of absorbance versus a range of wavelengths; (b) Graph of absorbance versus time at a specific wavelength, 380 nm.

6.4.2 Fast Stopped-flow Spectroscopy Reactions

Figure 6.1 indicates clearly that there is a large increase of absorbance in the initial few seconds of the reaction after mixing the [$HfCl_4$] and OxH solutions. These reactions are too fast to monitor on a conventional UV/Vis spectrometer. To overcome this problem a stopped-flow UV/Vis spectrophotometer, capable of studying reactions of half-lives of only a few milliseconds, was used for this portion of the reaction.

These fast reactions were studied at 380 nm by varying the ligand concentrations from 7.0 x 10^{-4} to 7.0 x 10^{-3} M to provide pseudo first-order conditions.

The best result for a fit of absorbance *vs.* time data, was obtained for a two-step pseudo first-order reaction as, indicated in Figure 6.4 (with a stopped-flow time span of 200 seconds).

The data for k_{obs1} *vs.* [OxH] was reproducible, but the data for the second reaction was not. The second reaction, although clearly present, does not go to completion in 200 seconds and accurate data points could not be obtained. Furthermore, the mechanics of the stopped-flow spectrophotometer can become somewhat unreliable after longer periods of time, due to fluctuation in applied pressure and possible backflow of reaction solutions from the trigger mechanism on the apparatus. This observation could indicate that the second reaction observed here, could possibly be detected on a normal UV/Vis spectrophotometer. The results for k_{obs1} *vs.* [L.L'] are presented in Table 6.1 and Figure 6.2.

Table 6.1: Data obtained by fast Stopped-flow spectroscopy for a two-step consecutive reaction fitted to Eq. 6.4, at 25°C in DMF with total reaction time of 200 sec and $[HfCl_4] = 7.18 \times 10^{-5}$ M.

No	[OxH] (M)	k_{obs1} (s^{-1})
1	0.00141	0.0072(3)
2	0.00281	0.023(1)
3	0.00421	0.052(3)
4	0.00492	0.075(2)
5	0.00562	0.089(4)
6	0.00702	0.1527(12)

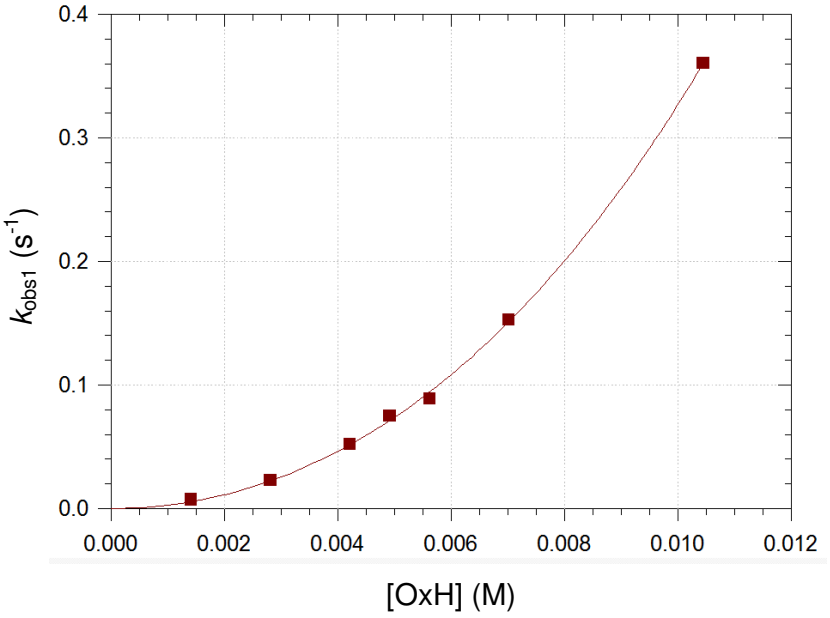

Figure 6.2: Plot of k_{obs1} versus ligand concentration in DMF at 25°C and [$HfCl_4$] = 7.18 x10^{-5} M (Data obtained from Table 6.1, columns 2 and 3, where ■ ■ ■ observed UV/Vis data; solid line calculated using Eq. 6.6)

The plot of k_{obs1} *vs.* [OxH], Figure 6.2, yielded an exponential relationship. This points towards a higher-order process that is taking place (*i.e.*, an exponential increase in reactivity with increased ligand concentration).

Preliminary fitting experiments of the data pointed towards a typical second-order reaction taking place. This could best be described by Scheme 6.2.

$$[HfCl_4] + (L,L') \overset{K_1}{\rightleftharpoons} [Hf(L,L')Cl_3]$$

$$[Hf(L,L')Cl_3] + (L,L') \xrightarrow{k_2} [Hf(L,L')_2Cl_2]$$

Scheme 6.2: The two reactions proposed for data obtained from stopped-flow spectroscopy (Chlorine ligands are omitted for clarity).

Scheme 6.2 describes the formation of a pre-equilibrium step followed by a fast second step which involves the formation of the bis-β-diketonato hafnium complex, $[Hf(Ox)_2Cl_2]$. The following rate equation can be derived (*see* Appendix C) to describe this two-step reaction.

$$k_{obs1} = \frac{k_2 K_1 [L,L']^2}{1 + K_1 [L,L']} \qquad \text{. . . Eq. 6.6}$$

A Scientist fit of Eq. 6.6 to the experimental k_{obs1} *vs.* [L,L'] data is shown in Fig. 6.2. It is however obvious that the number of k_{obs1} data points, although it clearly describes an exponential (*i.e.* 2nd order) curve, are not statistically representative to enable a very accurate least squares fit. If one uses the principle of 'visual' comparison of the experimental data points with a fit wherein acceptable visual error levels are considered,[2] reasonable values of k_2 and K_1 are obtained, *see* Table 6.2.

Eq. 6.7 can easily be obtained by simply manipulating Eq. 6.6 toward linearity within the reciprocal relationship.

$$\frac{[L,L']}{k_{obs1}} = \frac{1}{k_2 K_1 [L,L']} + \frac{1}{k_2} \qquad \text{. . . Eq. 6.7}$$

A fit of $[L]/k_{obs1}$ *vs.* $1/[L,L']$ should provide a straight line with a slope, $1/k_2K_1$ and a y-intercept, $1/k_2$. The $[L,L']/k_{obs1}$ *vs.* $1/[L,L']$ data obtained here was fitted to Eq. 6.7 and is presented in Figure 6.3. The slope, $1/k_2K_1$, and the y-intercept, $1/k_2$, of Figure 6.3 was determined as 0.00026(2) M^2s and 0.0165(33) Ms, respectively. From these values for k_2 and K_1 are obtained and this data supports the data obtained from Eq. 6.6 and are compared in Table 6.2.

[2] Roodt A., Leipoldt J. G., Helm L. and Merbach A. E., *Inorg. Chem.* **33**, 140, 1994.

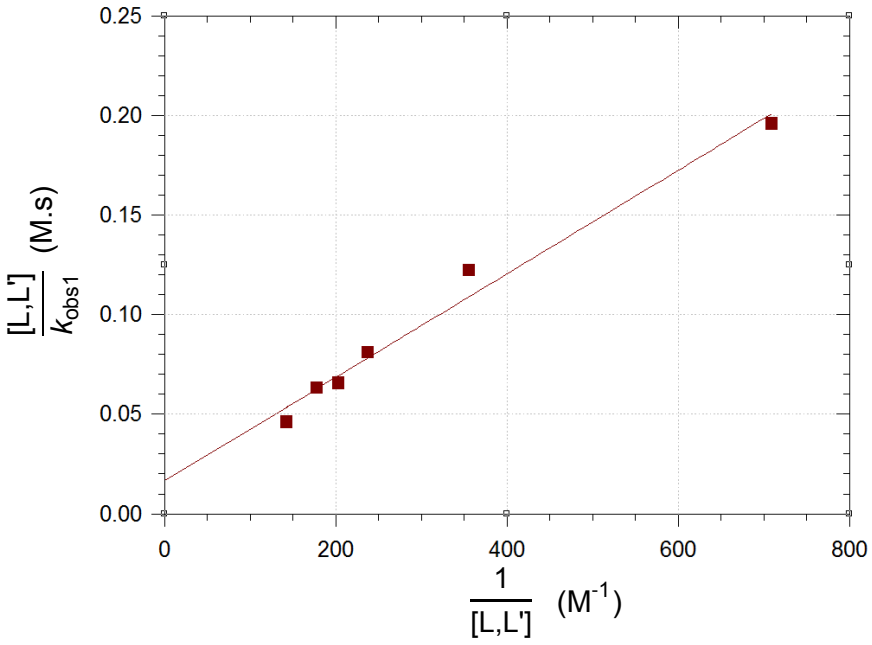

Figure 6.3: Plot of [L,L']/k_{obs1} versus 1/k_{obs1}

Table 6.2: Comparative equilibrium and rate constants obtained by Figures 6.2 and 6.3.

	K_1 (M^{-1})	k_2 ($M^{-1}s^{-1}$)
Fig. 6.2 (Eq. 6.6)	40(9)	90(15)
Fig. 6.3 (Eq. 6.7)	63(11)	60(21)

These results are discussed later on in this chapter.

6.4.3 Slow UV/Vis Spectroscopy Reactions

Figure 6.1 indicated a number of consecutive slower reactions following the fast reactions described in Section 6.4.1.

Preliminary results indicated that the best fit for absorbance *vs.* time data was obtained by fitting the data to Eq. 6.5, indicating a probable three-step process. This is best illustrated by Figure 6.4 which shows three typical plots of the same kinetic data to Eqs. 6.3, 6.4 and 6.5 for one-, two- and three step processes, respectively.

From this, it was decided to fit all the UV/Vis data to Eq 6.5. The rate constants for the three consecutive reactions (rate constants labelled k_{obs3}, k_{obs4} and k_{obs5}) are presented in Table 6.2.

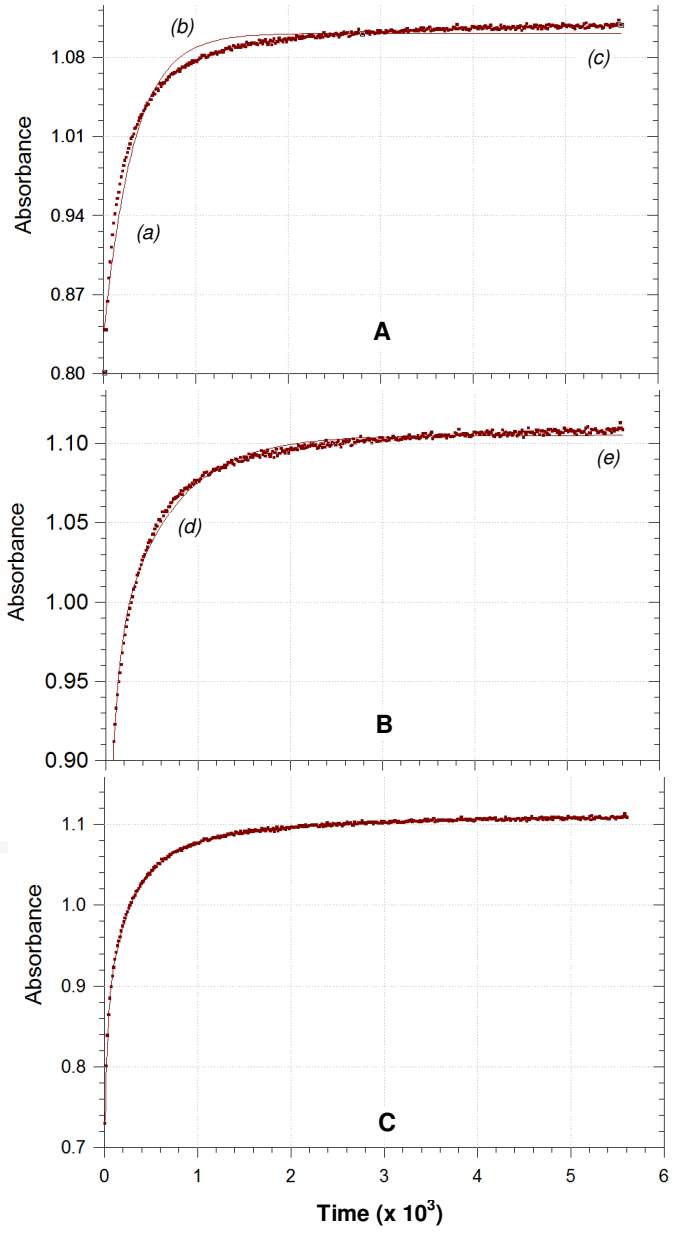

Figure 6.4: Typical UV/Vis data fitted to a (A) single step; Eq. 6.3; (B) two step; Eq. 6.4; (C) a three-step reaction; Eq. 6.5. (• • • observed UV/Vis data; solid line calculated using Eqs. 6.3, 6.4 and 6.5 for (A), (B) and (C), respectively); [OxH] = 7.02 x 10^{-4} M, [$HfCl_4$] = 7.18 x10^{-5} M, Solvent: DMF, Temp: 25.0℃, reaction time: 5600 sec.

Table 6.3: First-order rate constants for the three step consecutive reactions [From Eq. 6.5] at 25.0°C in DMF, $[HfCl_4]$ = 7.18 x10^{-5} M.

No	[OxH] (M)	k_{obs3} (s^{-1})	k_{obs4} (s^{-1})	k_{obs5} (s^{-1})
1	0.00070	0.00531(4)	0.00157(3)	0.000278(5)
2	0.00141	0.00983(8)	0.00250(4)	0.00040(1)
3	0.00281	0.0214(3)	0.00354(5)	0.00040(1)
4	0.00421	0.0287(6)	0.00383(6)	0.00050(1)
5	0.00492	0.0340(7)	0.00515(7)	0.00072(2)
6	0.00562	0.0249(8)	0.00390(7)	0.00058(2)
7	0.00632	0.04111(7)	0.00454(7)	0.00070(2)
8	0.00702	0.0357(9)	0.00403(8)	0.00081(2)

The relationships between the different pseudo first-order rate constants (k_{obs3}, k_{obs4} and k_{obs5}) and [OxH] are presented in Figure 6.5 - 6.7 and are discussed separately.

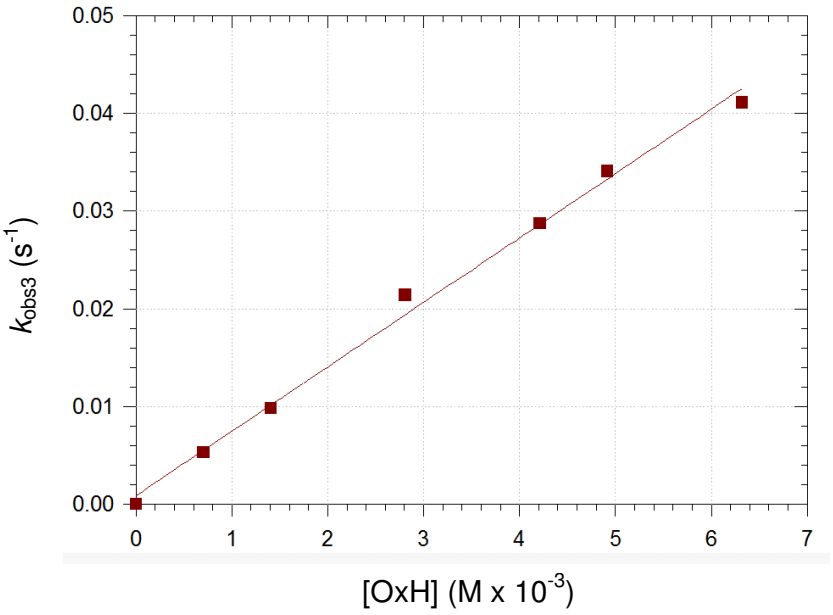

Figure 6.5: Graph of k_{obs3} versus [OxH]; $[HfCl_4]$ = 7.18 x10^{-5} M in DMF at 25.0°C for the first slow UV/Vis reaction, *see* Figure 6.4 (Data obtained from Table 6.3, columns 2 and 3, where ■ ■ ■ observed UV/Vis data; solid line calculated using Eq. 6.9).

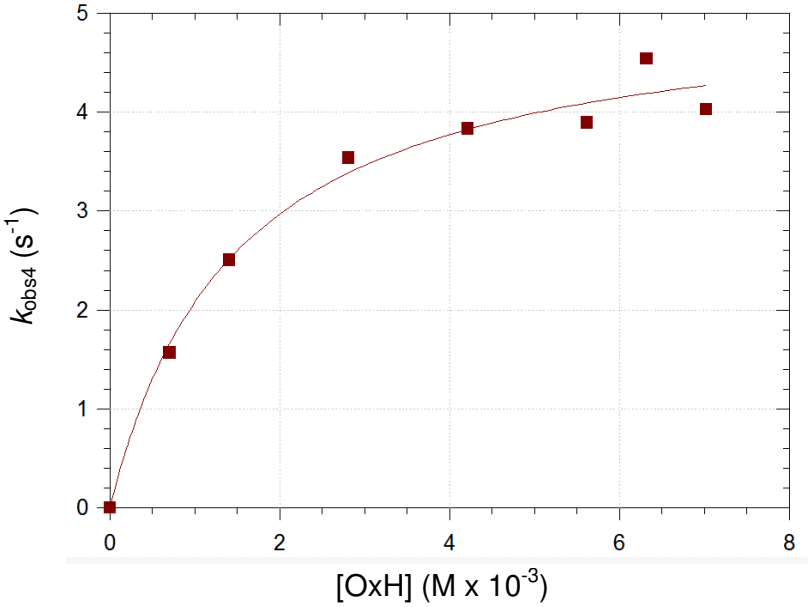

Figure 6.6: Plot of k_{obs4} versus ligand concentration in DMF at 25.0°C and $[HfCl_4]$ = 7.18 x10^{-5} M for the second slow UV/Vis reaction, *see* Figure 6.4 (Data from Table 6.3, columns 2 and 4, where ■ ■ ■ observed UV/Vis data; solid line calculated using Eq. 6.11)

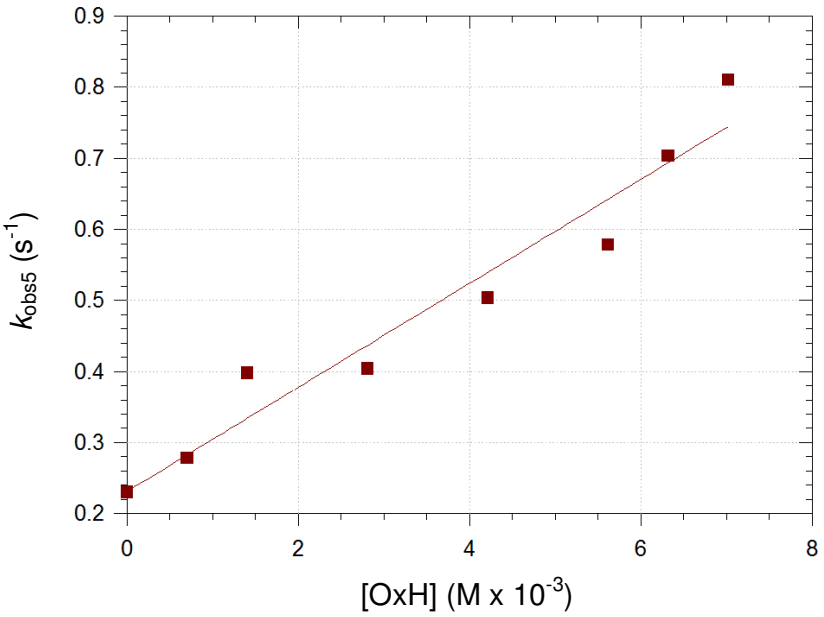

Figure 6.7: Graph of k_{obs5} versus ligand concentration in DMF at 25.0°C and [$HfCl_4$] = 7.18 x10^{-5} M for the third slow UV/Vis reaction, *see* Figure 6.4 (Data obtained from Table 6.3, columns 2 and 5, where ■ ■ ■ observed UV/Vis data; solid line calculated using Eq. 6.9)

The plots of k_{obs} *vs.* ligand concentration, [OxH], for the three slow, UV/Vis, consecutive reactions produced very interesting results. Plots of k_{obs3} *vs.* [OxH] for the **first reaction** yielded a straight line, *see* Figure 6.5. This points to a simple reversible first-order reaction that follows the usual two term rate law as presented in Eq. 6.9.

$$k_{obs3} = k_3[L,L'] + k_{-3} \qquad \textbf{. . . Eq. 6.9}$$

Another interesting aspect of this first reaction detected by UV/Vis, is that the values of the rate constants, k_{obs3}, obtained here are very similar to that obtained for the second reaction that was observed during the stopped-flow experiments. This indicates that this reaction is therefore equivalent to the second one observed on the stopped-flow apparatus.

The rate constants, k_3 and k_{-3}, were obtained from fitting the data to Eq. 6.9 and found to be 6.5(3) $M^{-1}s^{-1}$ and 1.4(1) x 10^{-3} s^{-1}, respectively. A value for the equilibrium constant, K_3 =4(3) x 10^3 M^{-1}), was also obtained from by Eq. 6.10.

$$K_3 = \frac{k_3}{k_{-3}} \qquad \text{. . . Eq. 6.10}$$

These results are discussed in more detail later on in this chapter.

The **second reaction** that was monitored by slow UV/Vis spectroscopy, gives a non-linear relationship between k_{obs4} and ligand concentration, pointing to limiting kinetics, *see* Figure 6.6. The typical rate equation which predicts the relationship between k_{obs4} and [L] as illustrated in Figure 6.6, is given by Eq. 6.11. This suggests a rapid pre-equilibrium ligand, dependent first step, followed by a slower ligand independent, second step.

$$k_{obs4} = \frac{k_3 K_4 [L,L']}{1 + K_4 [L,L']} \qquad \text{. . . Eq. 6.11}$$

The rate data was fitted to Eq 6.6 and the values of k_3 and K_4 were calculated as 5.80(7) x 10^{-3} $M^{-1}s^{-1}$ and 6(2) x 10^2 M^{-1}. These results are discussed later on.

The third reaction gave a linear relationship for plots of k_{obs5} *vs.* [OxH] (*see* Figure 6.7), indicating a simple reversible equilibrium, as for the first step discussed above, obeying $k_{obs5} = k_5[L,L'] + k_{-5}$ with constants k_5 = 0.073(9) $M^{-1}s^{-1}$, k_{-5} = 2.3(2) x 10^{-4} s^{-1} and $K_5 = k_5/k_{-5}$ = 320(50) M^{-1}. An overview of all the equilibrium and rate constants obtained for each individual substitution reaction is given in Table 6.4.

Table 6.4: Equilibrium and rate constants obtained for each individual substitution reaction.

K_1	40(9) M^{-1}
k_2	90(15) $M^{-1}s^{-1}$
k_3	6.5(3) $M^{-1}s^{-1}$
k_{-3}	1.4(1) x 10^{-3} s^{-1}
K_3	4(3) x 10^4 M^{-1}
K_4	6(2) x 10^2 M^{-1}
k_5	7.3(9) x 10^{-2} $M^{-1}s^{-1}$
k_{-5}	2.3(2) x 10^{-4} s^{-1}
K_5	320(50) M^{-1}

6.4.4 Overall Reaction Scheme

Based on the above, although preliminary, a broader picture is now emerging of the overall kinetic behaviour, and it is now possible to confirm that a minimum of five reactions are observed during the kinetic runs: two in the stopped-flow range and three for UV/Vis as indicated by Roman numerals in Scheme 6.3 and 6.4;
LL' = bidentate ligand OxH. These are illustrated below.

Fast reactions - Stopped-flow results:

$$Hf + (L,L') \underset{}{\overset{K_1}{\rightleftharpoons}} Hf(L,L') \qquad \text{... Eq. 6.12}$$

$$Hf(L,L') + (L,L') \xrightarrow{k_2} Hf(L,L')_2 \qquad \text{... Eq. 6.13}$$

Scheme 6.3: The two reactions proposed for data obtained from stopped-flow spectroscopy (halide ligand omitted for simplicity).

Slower reactions - UV/Vis Results:

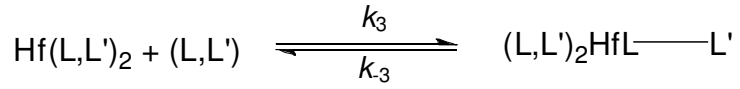

. . . Eq. 6.14

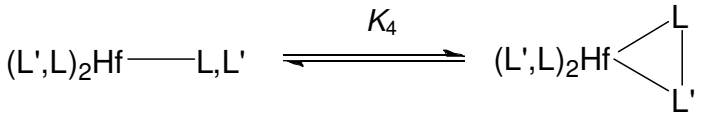

. . . Eq. 6.15

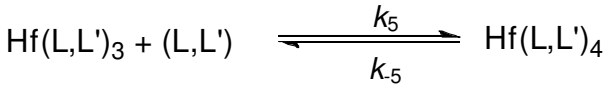

. . . Eq. 6.16

Scheme 6.4: The three proposed reactions for data obtained from UV/Vis spectroscopy (halide ligand omitted for simplicity).

6.4.5 Conclusion

The starting- and final products were well identified. Two consecutive, fast reactions (Section 6.4.1) and several slower ones were observed for the substitution reactions of the chloride ligands from [$HfCl_4$] by OxH to form [$Hf(Ox)_4$].

The **first reaction** involves a second-order reaction most likely defines the stepwise formation of [$Hf(LL)_2Cl_2$], (*see* Eq. 6.12 and 6.13 in Scheme 6.3). Eq. 6.12 is assumed where an entering bidentate ligand, OxH, coordinates to the metal centre via a rapid pre-equilibrium to form [Hf(L,L')] and Eq. 6.13 is probably similar, where a second bidentate ligand coordinates to the metal centre to yield [$Hf(L,L')_2$] (Eq. 6.13). The results from fits of the rate data obtained for this first two fast reactions to the relevant equation yielded a value of 40(15) M^{-1} and 90(15) $M^{-1}s^{-1}$, for the stability constant, K_3 and rate constant, k_2, respectively.

The **third** observable reaction [first one on slow UV/Vis] is ligand dependent, as concluded from the linear relationship obtained, by plotting k_{obs3} *vs.* [OxH]. From this it is assumed that this reaction might involve the monodentate coordination of the

first donor atom (probably the O-atom) to the metal centre, to produce the $[(L,L')_2HfL\text{-}L]$ complex, Eq. 6.14, Scheme 6.4. This means that the ligand only occupies one coordination mode and not two as in the case for a typical chelated bidentate ligand. The results from fits of the rate data, obtained for this first, slower reaction to the relevant equation, yielded the values of 6.5(3) $M^{-1}s^{-1}$ and 1.4(1) x 10^{-3} s^{-1} for the rate constants k_3 and k_{-3}, respectively and 4(3) x 10^3 M^{-1} for K_3.

The **fourth reaction** (second one on slow UV/Vis) did not yield a linear relationship, but with limiting kinetics instead, which usually means that the second reaction is ligand independent. For this reaction it is postulated that the reaction observed might be the ring closure of the five membered chelate metallocycle (Eq. 6.15, Scheme 6.4) to form $[Hf(L,L')_3]$. This action finishes the overall third ligand's entry, by allowing the bidentate ligand to occupy two coordination sites as a chelate. The value of K_4 obtained from the data in Figure 6.7 is 6(2) x 10^2 M^{-1}. This, together with the fact that the second slower reaction yielded limiting kinetics, confirms the possibility of the proposed mechanism so far.

The **fifth** and last reaction (third one on slow UV/Vis) observed, is concluded to be the formation of the $[Hf(L,L')_4]$ that was isolated and reported previously.[3] This last process (Eq. 6.16, Scheme 6.4) followed the usual two-term rate law, $k_{obs5} = k_5[LL'] + k_{-5}$ with k_5 = 7.3(9) x 10^{-2} $M^{-1}s^{-1}$ and k_{-5} = 2.3(2) x 10^{-4} s^{-1} yielding an equilibrium constant of K_5 = 320(50) M^{-1}.

A linear relationship between k_{obs5} and [OxH] is also obtained, that indicates by theory, ligand dependence for the reaction to occur. Thus, for the **fifth reaction** one bidentate ligand coordinates to the metal centre to form the final product, the eight coordinated $[Hf(L,L')_4]$ complex.

Due the high complexity of the substituting reactions observed here, a detailed discussion of the different rate constants will not be attempted. Activation parameters could also not be determined for the same reasons.

[3] Viljoen J.A., Roodt A. and Muller A.J., *Quarterly Report, Sep 2008*, AMI Project.

However, the different steps analyzed above, agree very well with the concluded observed rate constants that a more complete analysis of all the data also using different entering ligands as well as manipulating the leaving halide ligands should be done in future. In the scope of this M.Sc. thesis it is concluded that the very complex mechanism has been explored adequately and experimentally.

7 Study Evaluation

7.1 Introduction

The chemical relevance and results of this study are briefly discussed according to the pre-set aims which were established in Chapter 1. A few possibilities for future research are also briefly outlined.

7.2 Success of the Study

This study was aimed at investigating the chemical nature of hafnium in an environment of O,O'- and N,O-donating bidentate ligands such as tfaaH, hfaaH and OxH. New complexes were successfully synthesized, characterized and its solution behaviour was studied to form part of a parallel, comparative study of similar complexes of zirconium (M. Steyn, M.Sc., UFS, 2009[1]). If hafnium and zirconium show differences in its chelating behaviour, it could possibly be exploited as a novel separation technique for the two metals.

Summary of research outputs:

- Three new complexes, $[Hf(tfaa)_4]$,[2] $[Hf(OH)(hfaa)_3]_2$ and $[Hf(Ox)_4]$, have been successfully synthesized and characterized with single crystal X-ray diffraction and other spectroscopic techniques. Although different ratio's of metal:ligand were used in the synthesis, only the tetrakis complexes were isolated in all of the cases, suggesting that the crystallization energy of the tetrakis complexes

[1] Steyn M., Steyl G. and Roodt A., *M.Sc*. *Thesis*, University of the Free State, 2009.

[2] Viljoen J A., Roodt A. and Muller, A. J., *Acta Cryst*., **E64**, m838, 2008.

are the lowest in these symbiotic systems.[3] It was also found that co-crystallizing solvent molecules do not restrict or interfere with any significant physical properties of the solvated metal complexes. The solvated and non-solvated molecule's bite angles and bond distances are all the same within experimental error range (*see* Chapter 5).

Of all the crystal structures that were isolated, only one major difference in coordination geometry between the hafnium and zirconium polymorphous compounds was detected. $[Hf(OH)(hfaa)_3]_2$, from this study, forms dimeric species whereas its zirconium counterpart forms monomeric complexes when isolated in the solid state.[4] This phenomenon will also be exploited in the future as a possible separation technique between hafnium and zirconium.

- From the kinetic study it was observed that the step-wise formation reactions of $[Hf(Ox)_4]$ is ligand dependant for most of the substitution reactions. It seems that for the formation of $[Zr(Ox)_4]$, only the first few substitution reactions are ligand dependant and the rest are ligand independent. This provides scope for possible separation techniques as it seems as if the hafnium and zirconium compounds might have different coordination modes at specific times. Due to this difference in coordination geometry, it might be possible to separate the two metals via selective extraction, fractional distillation or sublimation. One main problem that was encountered in this study was the inability to isolate intermediate products in solution.

[3] Huheey J. E., Keiter E. A. and Keiter R. L., *Inorganic Chemistry, Principles of Structure and Reactivity*, 4th Ed., HarperCollins College Publishers, New York, 1993.

[4] Zherikova K. V., Morozova N. B., Kurat'eva N. V., Baidina I. A., Stabnikov P. A. and Igumenov I. K., *J. Struct. Chem.*, **48**, 3, 513, 2007.

7.3 Future Research

Further investigations which will be useful in the understanding of the coordination modes and kinetic behaviour of hafnium type complexes hopefully be addressed in a follow-up study. If these parameters are better understood, the separation of hafnium from zirconium may be achieved more economically.

Future investigations may include the following:

- A complete kinetic investigation of the formation of previously synthesized hafnium complexes.

- An expanded synthesis program that should include newly tailored O- and N-donating bi- and multi-dentate ligand families.

- An evaluation of solvent extraction methods utilizing the mentioned ligand systems.

- Kinetic solution studies and subsequent comparisons with all species previously studied.

- Specific comparative experimentation for separation of hafnium and zirconium counterparts (in conjunction with work done by Miss. M. Steyn, anticipated NECSA funded Ph.D. student at UFS – twin project on zirconium).
    - Solvent extraction
    - Sublimation
    - Selective crystallization separation

Basic reference complexes will therefore be synthesized, characterized and evaluated. Techniques include solid state infrared and X-ray crystallography, which will be used to determine different solid state coordination modes of the ligands spheres. Subsequent solvent studies will then evaluate the solution behaviour and stabilities of the different species in solution. Techniques such as multi-nuclear NMR- IR- and UV/Vis spectroscopy will also be employed to construct a thermodynamic and kinetic reaction scheme for the mixed complexes of hafnium.

Appendix A

BOHR'S THEORY[1]

In 1913 Niels Bohr proposed a model for the hydrogen atom based on a combination of classical and quantum concepts. Niels Bohr assumed that atoms exist in discrete quantum states, each with well defined energies.

Bohr's specific model of the hydrogen atom is based on the assumption that the electron moves in a planet-like orbits around the nucleus as illustrated in Figure A.1.

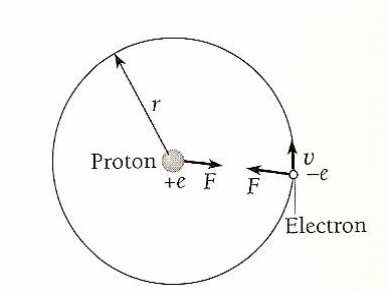

Figure A.1: Electron moving around a proton, to illustrate the force balances in the hydrogen atom.

If we look at the classical dynamics of the hydrogen atom, we assume the centripetal force

$$F_c = \frac{mv^2}{r} \qquad \text{...Eq. A.1}$$

holding the electron in an orbit *r* from the nucleus is provided by the electric force

[1] Halliday D., Resnick R., Walker J., *Fundamentals of Physics Extended*, 5th Ed., John Wiley and Sons, Inc., New York, 1997.

$$\boldsymbol{F_e = \frac{e^2}{4\pi\varepsilon_0{}^2}} \qquad \textbf{…Eq. A.2}$$

between them. The condition for a dynamically stable orbit is where

$$F_c = F_e$$

Thus can the velocity of a hydrogen electron be obtained by

$$\boldsymbol{v = \frac{e}{\sqrt{4\pi\varepsilon_0 mr}}} \qquad \textbf{…Eq. A.3}$$

The de Broglie wavelength of this electron is

$$\boldsymbol{\lambda = \frac{h}{mv}} \qquad \textbf{… Eq. A.4}$$

where h = Planck's constant = 6.626 x 10^{-34} J.s, v = velocity of the electron and m = mass of the electron.

By substituting Eq. A.3 into Eq. A4 the orbital electron wavelength is obtained

$$\boldsymbol{\lambda = \frac{h}{c}\sqrt{\frac{4\pi\varepsilon_0 r}{m}}} \qquad \textbf{…Eq. A.5}$$

By substituting 5.3 x 10^{-11}m for the radius r of the electron orbit, we find the electron wavelength to be

$$\lambda = \frac{6.626\text{x}10^{-34} J.s}{1.6\text{x}10^{-19} C}\sqrt{\frac{(4\pi)(8.85\text{x}10^{-12} C^2.N^{-1}m^2)(5.3\text{x}10^{-11} m)}{9.1\text{x}10^{-31} kg}}$$

$$= \mathbf{33x10^{-11}\ m}$$

This wavelength is exactly the same as the circumference of the electron orbit,

$$2\pi r = 33\text{x}10^{-11} m$$

Thus can an electron only circle a nucleus if its orbit contains an integral number of de Broglie wavelengths otherwise destructive interference will occur and the vibrations will die out rapidly. It's now quite easy to express the conditions for an electron to contain an integral number of de Broglie wavelengths. The circumference of a circular orbit of radius r is $2\pi r$ and so the conditions for orbit stability becomes

$$\boldsymbol{n\lambda = 2\pi r_n \quad n = 1, 2, 3, \ . \ . \ .} \qquad \textbf{...Eq. A.6}$$

Where r_n = radius of the orbit that contains n (*quantum number*) wavelengths. By substituting Eq. A.5 in the above equation the orbital radius of a Bohr atom is obtained.

$$\boldsymbol{r_n = \frac{n^2 h^2 \varepsilon_0}{\pi m e^2} \qquad n = 1, 2, 3, \ . \ . \ .} \qquad \textbf{...Eq. A.7}$$

The radius of the innermost orbit is called the Bohr radius of the hydrogen atom and is donated the symbol $\boldsymbol{a_o = r_1}$ = 5.292 x 10^{-11}m.

The other radii are given in terms of $\boldsymbol{a_o}$ by

$$\boldsymbol{r_n = n^2 a_0} \qquad \textbf{...Eq. A.8}$$

This electron theory of atomic structure made it possible to construct a model of a hafnium atom. According to this theory, the atom of the 72^{nd} element strongly resembled the atoms of elements in Group IV of the periodic table i.e., titanium and zirconium.

Appendix B

Table B.1: Fractional atomic coordinates and isotropic or equivalent isotropic displacement parameters (Å^2) for [Hf(tfaa)$_4$]. $U_{(eq)}$ is defined as one third of the trace of the orthogonalized U^{ij} tensor.

	x	*y*	*z*	U_{iso}*/U_{eq}
Hf	0.5	0.165295(14)	0.75	0.01071(4)
O1	0.51936(7)	-0.05501(17)	0.81255(6)	0.0145(3)
O2	0.49393(7)	0.25296(17)	0.83653(6)	0.0150(3)
C1	0.50749(11)	-0.2808(3)	0.87229(11)	0.0220(4)
H1A	0.508	-0.3448	0.8369	0.033
H1B	0.4696	-0.3133	0.8783	0.033
H1C	0.5485	-0.2998	0.9129	0.033
C2	0.50184(10)	-0.1008(3)	0.85482(9)	0.0156(4)
C3	0.47953(10)	0.0117(3)	0.88823(10)	0.0184(4)
H3	0.4644	-0.0284	0.9172	0.022
C4	0.48009(10)	0.1778(3)	0.87820(9)	0.0154(4)
C5	0.46372(11)	0.2975(3)	0.92078(10)	0.0207(4)
F1	0.40902(8)	0.3862(2)	0.88355(7)	0.0409(4)
F2	0.45382(8)	0.21987(18)	0.96725(7)	0.0343(3)
F3	0.51363(7)	0.40485(17)	0.95280(7)	0.0316(3)
O3	0.43603(7)	0.38624(17)	0.71276(7)	0.0146(3)
O4	0.40009(6)	0.07826(17)	0.72464(6)	0.0136(3)
C6	0.36205(11)	0.6104(3)	0.69597(12)	0.0229(4)
H6A	0.4012	0.6754	0.7049	0.034
H6B	0.3434	0.6475	0.724	0.034
H6C	0.329	0.6231	0.6499	0.034
C7	0.38151(10)	0.4318(2)	0.71005(9)	0.0158(4)
C8	0.33652(10)	0.3194(2)	0.71708(10)	0.0175(4)
H8	0.2986	0.3595	0.7188	0.021
C9	0.34868(10)	0.1536(2)	0.72125(9)	0.0148(4)
C10	0.29459(10)	0.0341(3)	0.71829(11)	0.0197(4)
F4	0.31970(6)	-0.07336(16)	0.76889(6)	0.0261(3)
F5	0.24293(7)	0.11096(17)	0.72015(8)	0.0338(3)
F6	0.26890(6)	-0.05534(17)	0.66195(6)	0.0274(3)
C11	0.65622(14)	0.3966(4)	0.96674(17)	0.0550(9)
H11A	0.6943	0.427	0.9608	0.082
H11B	0.6541	0.4676	0.9996	0.082
H11C	0.6156	0.4084	0.9251	0.082
C12	0.66358(11)	0.2194(3)	0.98981(12)	0.0313(5)
C13	0.66964(12)	0.1760(3)	1.05128(12)	0.0336(6)
H13	0.6681	0.258	1.0793	0.04
C14	0.67800(13)	0.0117(4)	1.07158(12)	0.0376(6)
H14	0.682	-0.0156	1.1131	0.045
C15	0.68046(13)	-0.1112(4)	1.03081(14)	0.0384(6)
H15	0.6867	-0.2213	1.0446	0.046
C16	0.67360(12)	-0.0688(4)	0.96942(14)	0.0406(7)
H16	0.6747	-0.1509	0.9412	0.049
C17	0.66513(12)	0.0941(4)	0.94935(12)	0.0372(6)
H17	0.6603	0.1204	0.9075	0.045

Table B.2: Atomic displacement parameters ($Å^2$) of [Hf(tfaa)$_4$].

	U^{11}	U^{22}	U^{33}	U^{12}	U^{13}	U^{23}
Hf	0.01298(6)	0.00766(6)	0.01517(6)	0	0.00966(4)	0
O1	0.0157(6)	0.0118(7)	0.0192(6)	0.0027(5)	0.0108(5)	0.0011(5)
O2	0.0207(7)	0.0117(7)	0.0170(6)	0.0003(5)	0.0126(6)	-0.0013(6)
C1	0.0315(12)	0.0136(10)	0.0271(11)	0.0039(8)	0.0190(9)	0.0000(9)
C2	0.0145(9)	0.0143(10)	0.0175(9)	0.0020(8)	0.0071(7)	-0.0012(8)
C3	0.0239(10)	0.0171(10)	0.0195(9)	0.0026(8)	0.0148(8)	-0.0018(8)
C4	0.0160(9)	0.0166(10)	0.0161(8)	-0.0013(8)	0.0097(7)	-0.0014(8)
C5	0.0300(11)	0.0179(11)	0.0211(10)	0.0009(8)	0.0179(9)	0.0006(8)
F1	0.0431(9)	0.0495(10)	0.0335(8)	-0.0008(7)	0.0209(7)	0.0248(8)
F2	0.0647(10)	0.0234(7)	0.0379(8)	-0.0026(6)	0.0433(8)	-0.0053(7)
F3	0.0485(9)	0.0217(7)	0.0361(7)	-0.0127(6)	0.0294(7)	-0.0106(6)
O3	0.0160(7)	0.0110(7)	0.0210(7)	0.0026(5)	0.0122(6)	0.0019(5)
O4	0.0136(6)	0.0109(7)	0.0194(7)	0.0003(5)	0.0104(5)	0.0020(5)
C6	0.0229(11)	0.0131(10)	0.0375(12)	0.0040(9)	0.0183(10)	0.0034(8)
C7	0.0187(9)	0.0124(10)	0.0183(9)	0.0008(7)	0.0104(8)	0.0012(8)
C8	0.0164(9)	0.0131(10)	0.0288(10)	0.0005(8)	0.0155(8)	0.0017(8)
C9	0.0147(9)	0.0147(10)	0.0186(9)	0.0002(8)	0.0109(7)	0.0005(8)
C10	0.0185(10)	0.0143(10)	0.0312(11)	0.0002(8)	0.0158(9)	0.0008(8)
F4	0.0291(7)	0.0205(7)	0.0348(7)	0.0060(6)	0.0201(6)	-0.0030(5)
F5	0.0273(7)	0.0185(7)	0.0731(10)	-0.0005(7)	0.0382(7)	0.0012(6)
F6	0.0228(6)	0.0246(7)	0.0335(7)	-0.0067(6)	0.0122(6)	-0.0089(5)
C11	0.0259(14)	0.0496(19)	0.067(2)	0.0194(16)	0.0033(13)	-0.0055(13)
C12	0.0156(10)	0.0374(14)	0.0306(12)	0.0040(11)	0.0024(9)	-0.0050(10)
C13	0.0294(12)	0.0384(15)	0.0324(12)	-0.0126(11)	0.0141(10)	-0.0058(11)
C14	0.0352(13)	0.0514(18)	0.0272(12)	0.0039(12)	0.0154(10)	-0.0092(13)
C15	0.0270(13)	0.0302(14)	0.0523(16)	-0.0008(12)	0.0141(12)	-0.0051(11)
C16	0.0235(12)	0.0549(19)	0.0425(15)	-0.0250(14)	0.0150(11)	-0.0074(12)
C17	0.0229(12)	0.065(2)	0.0222(11)	-0.0013(12)	0.0094(10)	-0.0077(12)

Table B.3: Geometric parameters (Å, °) for [Hf(tfaa)$_4$].

Hf—O2	2.1527 (13)	C8—C7—C6	119.06 (18)
Hf—O2i	2.1527 (13)	O4i—Hf—O1	72.52 (5)
Hf—O4	2.1571 (13)	C9—C8—C7	120.28 (18)
C7—C8	1.423 (3)	O1i—Hf—O1	71.28 (7)
Hf—O4i	2.1571 (13)	C9—C8—H8	119.9
C8—C9	1.359 (3)	O2—Hf—O3i	72.21 (5)
Hf—O1i	2.1861 (13)	C7—C8—H8	119.9
Hf—O1	2.1861 (13)	O2i—Hf—O3i	76.82 (5)
C9—C10	1.529 (3)	O4—C9—C8	128.26 (18)
Hf—O3i	2.1933 (14)	O4—Hf—O3i	141.11 (5)
C10—F4	1.333 (2)	O4—C9—C10	112.50 (17)
Hf—O3	2.1933 (13)	O4i—Hf—O3i	75.54 (5)
C10—F5	1.335 (2)	C8—C9—C10	119.16 (17)
O1—C2	1.253 (2)	O1i—Hf—O3i	143.48 (5)
C10—F6	1.339 (2)	F4—C10—F5	107.15 (16)

O2—C4	1.280 (2)	O1—Hf—O3i	121.11 (5)
C11—C12	1.504 (4)	F4—C10—F6	106.83 (17)
C1—C2	1.494 (3)	O2—Hf—O3	76.82 (5)
C6—H6B	0.96	F5—C10—F6	106.94 (17)
C6—H6C	0.96	O2i—Hf—O3	72.21 (5)
C8—H8	0.93	F4—C10—C9	111.58 (16)
C11—H11A	0.96	O4—Hf—O3	75.54 (5)
C1—H1A	0.96	F5—C10—C9	113.11 (17)
C1—H1B	0.96	O4i—Hf—O3	141.11 (5)
C1—H1C	0.96	F6—C10—C9	110.90 (16)
C11—H11B	0.96	O1i—Hf—O3	121.11 (5)
C11—H11C	0.96	C12—C11—H11A	109.5
C2—C3	1.418 (3)	O1—Hf—O3	143.48 (5)
C12—C13	1.382 (4)	C12—C11—H11B	109.5
C12—C17	1.377 (4)	O3i—Hf—O3	71.35 (7)
C3—C4	1.359 (3)	H11A—C11—H11B	109.5
C13—C14	1.386 (4)	C2—O1—Hf	134.34 (13)
C13—H13	0.93	C12—C11—H11C	109.5
C3—H3	0.93	C4—O2—Hf	131.45 (13)
C4—C5	1.530 (3)	H11A—C11—H11C	109.5
C14—C15	1.375 (4)	C2—C1—H1A	109.5
C5—F1	1.325 (3)	C2—C1—H1B	109.5
C14—H14	0.93	H11B—C11—H11C	109.5
C5—F3	1.329 (3)	C17—C12—C13	117.8 (3)
C15—C16	1.372 (4)	H1A—C1—H1B	109.5
C5—F2	1.333 (2)	C17—C12—C11	119.9 (3)
C15—H15	0.93	C2—C1—H1C	109.5
O3—C7	1.254 (2)	C13—C12—C11	122.3 (3)
C16—C17	1.374 (4)	H1A—C1—H1C	109.5
O4—C9	1.276 (2)	C12—C13—C14	120.7 (2)
C16—H16	0.93	H1B—C1—H1C	109.5
C6—C7	1.496 (3)	C12—C13—H13	119.6
C17—H17	0.93	O1—C2—C3	122.69 (19)
C6—H6A	0.96	C14—C13—H13	119.6
O2—Hf—O2i	141.66 (7)	O1—C2—C1	118.14 (18)
F3—C5—C4	111.30 (17)	C15—C14—C13	120.5 (2)
O2—Hf—O4	80.96 (5)	C3—C2—C1	119.12 (18)
F2—C5—C4	112.58 (17)	C15—C14—H14	119.8
O2i—Hf—O4	111.77 (5)	C4—C3—C2	120.47 (18)
C7—O3—Hf	134.87 (13)	C13—C14—H14	119.8
O2—Hf—O4i	111.77 (5)	C4—C3—H3	119.8
C9—O4—Hf	131.43 (13)	C16—C15—C14	118.9 (3)
O2i—Hf—O4i	80.96 (5)	C2—C3—H3	119.8
C7—C6—H6A	109.5	O2—C4—C3	127.96 (18)
O4—Hf—O4i	142.02 (7)	C14—C15—H15	120.5
C7—C6—H6B	109.5	O2—C4—C5	112.58 (17)
O2—Hf—O1i	141.35 (5)	C15—C16—C17	120.5 (3)
H6A—C6—H6B	109.5	C16—C15—H15	120.5
O2i—Hf—O1i	75.69 (5)	C3—C4—C5	119.46 (17)
C7—C6—H6C	109.5	C15—C16—H16	119.8
O4—Hf—O1i	72.52 (5)	F1—C5—F3	106.71 (18)
H6A—C6—H6C	109.5	C17—C16—H16	119.8
O4i—Hf—O1i	76.79 (5)	F1—C5—F2	107.83 (17)

H6B—C6—H6C	109.5	C16—C17—C12	121.6 (2)
O2—Hf—O1	75.69 (5)	F3—C5—F2	106.67 (17)
O3—C7—C8	122.62 (18)	C16—C17—H17	119.2
O2i—Hf—O1	141.35 (5)	F1—C5—C4	111.44 (17)
O3—C7—C6	118.27 (18)	C12—C17—H17	119.2
O4—Hf—O1	76.79 (5)		

Symmetry codes: (i) −*x*+1, *y*, −*z*+3/2.

Table B.4: Fractional atomic coordinates and isotropic or equivalent isotropic displacement parameters (Å^2) of $[Hf_2(OH)_2(hfaa)_6]$. $U_{(eq)}$ is defined as one third of the trace of the orthogonalized U^{ij} tensor.

	x	*y*	*z*	U_{iso}*/U_{eq}
Hf	0.41961(2)	0.22771(4)	0.20705(3)	0.02117(19)
C1	0.3711(11)	-0.0845(16)	0.0809(13)	0.072(3)
C2	0.3592(6)	0.0258(10)	0.1080(7)	0.027(3)
C3	0.2981(6)	0.0644(11)	0.0885(7)	0.033(3)
H1	0.2669	0.0245	0.0578	0.039
C4	0.2839(6)	0.1603(10)	0.1140(7)	0.027(3)
C5	0.2168(6)	0.2039(12)	0.0939(9)	0.038(3)
C6	0.3335(8)	-0.0077(17)	0.3312(12)	0.064(3)
C7	0.3517(6)	0.1041(12)	0.3104(8)	0.036(3)
C8	0.3329(7)	0.1939(14)	0.3365(8)	0.042(4)
H2	0.3033	0.1876	0.3625	0.051
C9	0.3543(6)	0.2932(12)	0.3274(7)	0.032(3)
C10	0.3407(7)	0.3948(14)	0.3659(8)	0.044(4)
C11	0.3635(6)	0.5603(10)	0.1099(7)	0.030(3)
C12	0.3980(6)	0.4503(10)	0.1193(7)	0.026(3)
C13	0.4325(6)	0.4228(11)	0.0713(7)	0.030(3)
H3	0.4416	0.4746	0.041	0.036
C14	0.4526(6)	0.3192(11)	0.0693(7)	0.027(3)
C15	0.4830(7)	0.2825(12)	0.0116(7)	0.035(3)
O1	0.4055(4)	0.0693(7)	0.1481(5)	0.0286(19)
O2	0.3212(4)	0.2241(7)	0.1555(5)	0.0256(19)
O3	0.3870(4)	0.1031(8)	0.2698(5)	0.032(2)
O4	0.3911(4)	0.3135(8)	0.2892(4)	0.0270(18)
O5	0.3885(4)	0.3933(7)	0.1676(4)	0.0266(18)
O6	0.4472(4)	0.2417(7)	0.1103(5)	0.0283(19)
O7	0.5	0.3224(10)	0.25	0.025(2)
O8	0.5	0.1363(10)	0.25	0.027(3)
F1A	0.3226(18)	-0.142(3)	0.0495(19)	0.072(3)
F2A	0.3985(15)	-0.061(2)	0.0202(17)	0.072(3)
F3A	0.4208(18)	-0.134(3)	0.1157(19)	0.072(3)

F1B	0.3628(9)	-0.1582(14)	0.1312(10)	0.072(3)
F2B	0.3347(10)	-0.1112(15)	0.0203(12)	0.072(3)
F3B	0.4280(10)	-0.1047(15)	0.0807(12)	0.072(3)
F4	0.1769(4)	0.1340(8)	0.0531(6)	0.061(3)
F5	0.1964(4)	0.2225(8)	0.1501(6)	0.049(2)
F6	0.2137(5)	0.2953(8)	0.0573(5)	0.054(3)
F7A	0.3759(9)	-0.0493(17)	0.3801(12)	0.064(3)
F8A	0.3263(9)	-0.0788(15)	0.2726(10)	0.064(3)
F9A	0.2781(9)	-0.0119(15)	0.3432(13)	0.064(3)
F7B	0.3876(18)	-0.065(3)	0.360(2)	0.064(3)
F8B	0.3021(18)	-0.059(3)	0.276(2)	0.064(3)
F9B	0.2995(17)	-0.001(3)	0.379(3)	0.064(3)
F10	0.3100(5)	0.4661(8)	0.3203(5)	0.055(3)
F11	0.3060(7)	0.3715(11)	0.4103(7)	0.088(4)
F12	0.3927(5)	0.4404(9)	0.4033(5)	0.066(3)
F13	0.3084(4)	0.5496(7)	0.0617(5)	0.045(2)
F14	0.3532(4)	0.5951(7)	0.1687(4)	0.046(2)
F15	0.3962(5)	0.6343(8)	0.0856(6)	0.062(3)
F16	0.4473(4)	0.2112(8)	-0.0304(5)	0.047(2)
F17	0.5388(4)	0.2379(8)	0.0390(5)	0.048(2)
F18	0.4919(5)	0.3644(8)	-0.0295(5)	0.054(2)
H8	0.5	0.08(2)	0.25	0.064
H7	0.5	0.388(5)	0.25	0.064
C02	0.5	0.639(2)	0.25	0.060(5)
O01	0.5046(16)	0.5448(16)	0.2347(13)	0.060(5)
C01	0.4629(16)	0.684(3)	0.2975(17)	0.060(5)
H01A	0.4332	0.7353	0.2718	0.09
H01B	0.4907	0.718	0.3377	0.09
H01C	0.4411	0.6261	0.3136	0.09
C03	0.5346(18)	0.726(3)	0.217(2)	0.060(5)
H03A	0.5738	0.6972	0.2126	0.09
H03B	0.5421	0.7886	0.2465	0.09
H03C	0.5092	0.745	0.1704	0.09

Table B.5: Atomic displacement parameters (Å^2) of $[Hf_2(OH)_2(hfaa)_6]$.

	U^{11}	U^{22}	U^{33}	U^{12}	U^{13}	U^{23}
Hf	0.0229(3)	0.0143(3)	0.0265(3)	-0.0010(2)	0.0068(2)	0.00091(18)
C1	0.085(6)	0.038(5)	0.088(8)	-0.027(5)	0.013(5)	0.018(4)
C2	0.033(6)	0.011(6)	0.037(7)	-0.002(5)	0.010(5)	0.001(5)
C3	0.029(6)	0.026(7)	0.038(7)	-0.006(6)	-0.002(5)	0.000(5)
C4	0.027(6)	0.023(7)	0.028(6)	0.001(5)	0.003(5)	0.004(5)
C5	0.026(7)	0.025(8)	0.055(9)	-0.009(7)	-0.002(6)	0.001(5)
C6	0.047(5)	0.056(5)	0.091(7)	0.031(5)	0.023(4)	-0.006(4)
C7	0.031(7)	0.031(8)	0.045(8)	0.011(6)	0.009(6)	-0.003(6)
C8	0.042(8)	0.042(9)	0.049(9)	0.010(7)	0.023(7)	0.003(7)
C9	0.031(7)	0.036(8)	0.028(7)	0.002(6)	0.006(5)	0.009(6)
C10	0.051(9)	0.048(10)	0.037(8)	0.005(7)	0.020(7)	0.016(8)
C11	0.034(7)	0.015(6)	0.037(7)	-0.001(5)	0.003(6)	0.003(5)
C12	0.025(6)	0.020(6)	0.030(6)	0.000(5)	0.003(5)	0.002(5)
C13	0.038(7)	0.026(7)	0.025(6)	0.001(5)	0.008(5)	0.002(5)
C14	0.026(6)	0.029(7)	0.025(6)	-0.002(5)	0.004(5)	-0.004(5)
C15	0.036(7)	0.043(9)	0.026(7)	-0.006(6)	0.010(6)	-0.002(6)
O1	0.026(4)	0.017(4)	0.042(5)	-0.007(4)	0.008(4)	0.000(3)
O2	0.024(4)	0.018(5)	0.033(5)	-0.006(4)	0.005(4)	0.000(3)
O3	0.030(5)	0.026(5)	0.041(5)	0.006(4)	0.011(4)	0.001(4)
O4	0.032(4)	0.024(5)	0.027(4)	0.002(4)	0.010(4)	0.002(4)
O5	0.033(5)	0.017(4)	0.028(4)	0.000(4)	0.007(4)	0.001(4)
O6	0.035(5)	0.021(5)	0.030(5)	-0.003(4)	0.009(4)	0.003(4)
O7	0.027(6)	0.013(6)	0.032(6)	0	0.005(5)	0
O8	0.026(6)	0.015(6)	0.036(7)	0	0.001(5)	0
F1A	0.085(6)	0.038(5)	0.088(8)	-0.027(5)	0.013(5)	0.018(4)
F2A	0.085(6)	0.038(5)	0.088(8)	-0.027(5)	0.013(5)	0.018(4)
F3A	0.085(6)	0.038(5)	0.088(8)	-0.027(5)	0.013(5)	0.018(4)
F1B	0.085(6)	0.038(5)	0.088(8)	-0.027(5)	0.013(5)	0.018(4)
F2B	0.085(6)	0.038(5)	0.088(8)	-0.027(5)	0.013(5)	0.018(4)
F3B	0.085(6)	0.038(5)	0.088(8)	-0.027(5)	0.013(5)	0.018(4)
F4	0.036(5)	0.042(6)	0.090(8)	-0.025(5)	-0.012(5)	0.009(4)
F5	0.029(4)	0.049(6)	0.070(7)	-0.006(5)	0.015(4)	0.006(4)
F6	0.055(6)	0.040(6)	0.062(6)	0.011(5)	0.005(5)	0.022(4)
F7A	0.047(5)	0.056(5)	0.091(7)	0.031(5)	0.023(4)	-0.006(4)
F8A	0.047(5)	0.056(5)	0.091(7)	0.031(5)	0.023(4)	-0.006(4)
F9A	0.047(5)	0.056(5)	0.091(7)	0.031(5)	0.023(4)	-0.006(4)
F7B	0.047(5)	0.056(5)	0.091(7)	0.031(5)	0.023(4)	-0.006(4)
F8B	0.047(5)	0.056(5)	0.091(7)	0.031(5)	0.023(4)	-0.006(4)
F9B	0.047(5)	0.056(5)	0.091(7)	0.031(5)	0.023(4)	-0.006(4)
F10	0.066(6)	0.052(6)	0.043(5)	-0.003(4)	0.008(4)	0.034(5)
F11	0.131(11)	0.073(8)	0.093(9)	-0.001(7)	0.088(8)	0.014(8)
F12	0.067(7)	0.071(8)	0.049(6)	-0.029(5)	-0.003(5)	0.019(6)

F13	0.044(5)	0.040(5)	0.043(5)	-0.002(4)	-0.005(4)	0.015(4)
F14	0.062(6)	0.032(5)	0.040(5)	-0.004(4)	0.006(4)	0.018(4)
F15	0.060(6)	0.028(5)	0.107(8)	0.019(5)	0.039(6)	0.006(4)
F16	0.052(5)	0.056(6)	0.033(5)	-0.025(4)	0.010(4)	-0.014(4)
F17	0.038(5)	0.066(6)	0.043(5)	-0.015(4)	0.014(4)	0.010(4)
F18	0.073(6)	0.054(6)	0.044(5)	-0.001(5)	0.034(5)	-0.008(5)
C02	0.068(9)	0.033(7)	0.060(11)	0	-0.018(8)	0
O01	0.068(9)	0.033(7)	0.060(11)	0	-0.018(8)	0
C01	0.068(9)	0.033(7)	0.060(11)	0	-0.018(8)	0
C03	0.068(9)	0.033(7)	0.060(11)	0	-0.018(8)	0

Table B.6: Geometric parameters (Å, °) for $[Hf_2(OH)_2(hfaa)_6]$.

Hf—O8	2.091 (7)	O2—Hf—O5	71.1 (3)
C6—F8A	1.42 (3)	F7B—C6—C7	108 (2)
Hf—O7	2.113 (7)	O4—Hf—O5	71.2 (3)
C6—C7	1.53 (2)	F8A—C6—C7	109.4 (16)
Hf—O6	2.136 (9)	O3—Hf—O5	135.9 (3)
C7—O3	1.249 (16)	O3—C7—C8	124.0 (13)
Hf—O2	2.146 (9)	O8—Hf—O1	73.8 (3)
C7—C8	1.34 (2)	O3—C7—C6	114.3 (15)
Hf—O4	2.150 (9)	O7—Hf—O1	132.5 (3)
C8—C9	1.35 (2)	C8—C7—C6	121.7 (14)
Hf—O3	2.208 (9)	O6—Hf—O1	69.8 (3)
C9—O4	1.264 (16)	C7—C8—C9	123.7 (14)
Hf—O5	2.239 (9)	O2—Hf—O1	75.8 (3)
C9—C10	1.54 (2)	O4—C9—C8	124.3 (13)
Hf—O1	2.258 (8)	O4—Hf—O1	141.4 (3)
C10—F10	1.311 (18)	O4—C9—C10	111.4 (13)
C1—F3B	1.29 (3)	O3—Hf—O1	69.6 (3)
C10—F12	1.318 (19)	C8—C9—C10	124.2 (13)
C1—F2B	1.29 (3)	O5—Hf—O1	129.4 (3)
C10—F11	1.329 (17)	F10—C10—F12	107.9 (15)
C1—F3A	1.29 (4)	F3B—C1—F2B	109 (2)
C11—F14	1.302 (15)	F10—C10—F11	107.8 (13)
C1—F1A	1.30 (4)	F3B—C1—F3A	37.4 (18)
C11—F15	1.330 (16)	F12—C10—F11	107.7 (14)
C1—F1B	1.39 (3)	F2B—C1—F3A	127 (2)
C11—F13	1.336 (15)	F10—C10—C9	110.7 (12)
C1—F2A	1.49 (4)	F3B—C1—F1A	125 (2)
C11—C12	1.551 (17)	F12—C10—C9	111.5 (12)
C1—C2	1.52 (2)	F2B—C1—F1A	35.6 (18)
C12—O5	1.239 (15)	F11—C10—C9	111.1 (14)
C2—O1	1.239 (15)	F3A—C1—F1A	118 (3)
C12—C13	1.395 (17)	F14—C11—F15	108.8 (11)
C2—C3	1.389 (17)	F3B—C1—F1B	101 (2)
C13—C14	1.365 (19)	F14—C11—F13	108.3 (11)
C3—C4	1.358 (18)	F2B—C1—F1B	108 (2)

C14—O6	1.277 (16)	F15—C11—F13	107.4 (11)
C4—O2	1.270 (15)	F3A—C1—F1B	64 (2)
C14—C15	1.523 (18)	F14—C11—C12	112.5 (11)
C4—C5	1.531 (18)	F1A—C1—F1B	74 (2)
C15—F16	1.318 (16)	F15—C11—C12	110.7 (11)
C5—F5	1.310 (19)	F3B—C1—F2A	55.5 (18)
C15—F17	1.332 (17)	F13—C11—C12	109.0 (10)
C5—F6	1.331 (18)	F2B—C1—F2A	66.9 (19)
C15—F18	1.341 (17)	O5—C12—C13	127.0 (12)
C5—F4	1.341 (16)	F3A—C1—F2A	92 (3)
O7—Hf^{i}	2.113 (7)	O5—C12—C11	114.6 (11)
C6—F7A	1.26 (3)	F1A—C1—F2A	101 (3)
O8—Hf^{i}	2.091 (7)	C13—C12—C11	118.3 (12)
C6—F8B	1.28 (5)	F1B—C1—F2A	147.6 (19)
C02—O01	1.22 (3)	C14—C13—C12	119.3 (12)
C6—F9A	1.31 (2)	F3B—C1—C2	115.9 (19)
C02—C01	1.49 (3)	O6—C14—C13	127.3 (12)
C6—F9B	1.35 (4)	F2B—C1—C2	115.4 (18)
C02—C03	1.56 (3)	O6—C14—C15	111.8 (12)
C6—F7B	1.38 (4)	F3A—C1—C2	117 (2)
O8—Hf—O7	66.6 (4)	C13—C14—C15	120.9 (12)
F7A—C6—F9A	113.2 (18)	F1A—C1—C2	118 (2)
O8—Hf—O6	89.3 (2)	F16—C15—F17	108.2 (12)
F8B—C6—F9A	79 (2)	F1B—C1—C2	106.4 (17)
O7—Hf—O6	84.2 (3)	F16—C15—F18	107.2 (12)
F7A—C6—F9B	87 (2)	F2A—C1—C2	104.1 (19)
O8—Hf—O2	145.9 (4)	F17—C15—F18	106.7 (12)
F8B—C6—F9B	109 (2)	O1—C2—C3	127.4 (12)
O7—Hf—O2	147.4 (3)	F16—C15—C14	110.6 (11)
F9A—C6—F9B	32.7 (16)	O1—C2—C1	115.0 (13)
O6—Hf—O2	94.4 (4)	F17—C15—C14	111.7 (11)
F7A—C6—F7B	24 (2)	C3—C2—C1	117.5 (14)
O8—Hf—O4	110.8 (3)	F18—C15—C14	112.2 (12)
F8B—C6—F7B	108 (3)	C4—C3—C2	120.3 (12)
O7—Hf—O4	79.1 (3)	C2—O1—Hf	133.0 (8)
F9A—C6—F7B	132 (2)	O2—C4—C3	127.2 (12)
O6—Hf—O4	145.5 (3)	C4—O2—Hf	136.2 (8)
F9B—C6—F7B	110 (3)	O2—C4—C5	111.6 (11)
O2—Hf—O4	84.2 (3)	C7—O3—Hf	133.9 (9)
F7A—C6—F8A	105 (2)	C3—C4—C5	121.2 (12)
O8—Hf—O3	76.4 (3)	C9—O4—Hf	134.4 (9)
F8B—C6—F8A	25.5 (17)	F5—C5—F6	108.5 (12)
O7—Hf—O3	122.2 (3)	C12—O5—Hf	133.4 (8)
F9A—C6—F8A	102.0 (18)	F5—C5—F4	107.0 (13)
O6—Hf—O3	139.2 (3)	C14—O6—Hf	135.3 (9)
F9B—C6—F8A	129 (2)	F6—C5—F4	107.4 (13)
O2—Hf—O3	78.8 (3)	Hf—O7—Hf^{i}	112.5 (6)
F7B—C6—F8A	85 (2)	F5—C5—C4	111.8 (12)
O4—Hf—O3	74.4 (3)	Hf^{i}—O8—Hf	114.3 (6)
F7A—C6—C7	112.2 (17)	F6—C5—C4	110.4 (12)
O8—Hf—O5	142.0 (4)	O01—C02—C01	127 (2)
F8B—C6—C7	111 (2)	F4—C5—C4	111.5 (11)
O7—Hf—O5	77.1 (3)	O01—C02—C03	118.5 (19)

F9A—C6—C7	114.1 (17)	F7A—C6—F8B	124 (3)
O6—Hf—O5	75.8 (3)	C01—C02—C03	114 (3)
F9B—C6—C7	111 (2)		

Symmetry codes: (i) −*x*+1, *y*, −*z*+1/2

Table B.7: Fractional atomic coordinates and isotropic or equivalent isotropic displacement parameters (Å^2) for [Hf(Ox)$_4$]. $U_{(eq)}$ is defined as one third of the trace of the orthogonalized U^{ij} tensor.

	x	*y*	*z*	U_{iso}*/U_{eq}
Hf1	0.279296(10)	0.175184(9)	0.304673(8)	0.01334(4)
O3	0.42709(17)	0.17339(15)	0.43809(15)	0.0165(4)
N2	0.4355(2)	0.11053(19)	0.23297(18)	0.0166(5)
N4	0.1772(2)	0.14072(18)	0.45181(18)	0.0167(5)
N1	0.1973(2)	0.10354(18)	0.11572(17)	0.0150(4)
O1	0.22623(17)	0.00278(15)	0.30000(14)	0.0167(4)
O4	0.10611(17)	0.22173(16)	0.26120(15)	0.0183(4)
O2	0.35700(17)	0.30047(15)	0.21652(15)	0.0168(4)
N3	0.3101(2)	0.34199(18)	0.41944(18)	0.0164(5)
C22	0.4339(3)	0.4311(2)	0.5966(2)	0.0194(6)
C9	0.1703(2)	-0.0094(2)	0.1058(2)	0.0156(5)
C2	0.1362(2)	0.1030(2)	-0.0806(2)	0.0190(6)
H2	0.127	0.1437	-0.1427	0.023
C4	0.1252(2)	-0.0713(2)	0.0029(2)	0.0174(5)
C28	0.2161(3)	0.0956(2)	0.5456(2)	0.0206(6)
H28	0.2926	0.0736	0.56	0.025
C18	0.4814(2)	0.1817(2)	0.1647(2)	0.0170(5)
C27	0.4008(2)	0.3433(2)	0.5136(2)	0.0165(5)
C32	-0.1291(3)	0.1914(3)	0.4739(3)	0.0270(7)
H32	-0.1824	0.1827	0.5206	0.032
C36	0.0651(3)	0.1725(2)	0.4312(2)	0.0178(5)
C13	0.5653(3)	0.1558(3)	0.1042(2)	0.0236(6)
C23	0.5283(3)	0.4231(3)	0.6904(2)	0.0248(6)
H23	0.5513	0.4794	0.7467	0.03
C12	0.6015(3)	0.0514(3)	0.1181(3)	0.0295(7)
H12	0.6549	0.0295	0.0786	0.035
C29	0.1450(3)	0.0799(2)	0.6241(2)	0.0244(6)
H29	0.1748	0.0484	0.6894	0.029
C30	0.0329(3)	0.1109(2)	0.6045(2)	0.0258(7)
H30	-0.0142	0.1004	0.6562	0.031
C1	0.1792(2)	0.1576(2)	0.0254(2)	0.0168(5)
H1	0.1956	0.2347	0.0319	0.02
C15	0.5602(3)	0.3317(3)	0.0250(3)	0.0316(7)
H15	0.5861	0.3827	-0.0219	0.038
C7	0.1634(2)	-0.1762(2)	0.2017(2)	0.0185(5)
H7	0.1761	-0.2127	0.2664	0.022
C31	-0.0125(3)	0.1594(2)	0.5050(2)	0.0218(6)
C26	0.4622(3)	0.2505(2)	0.5219(2)	0.0174(5)
C10	0.4753(3)	0.0155(2)	0.2457(2)	0.0218(6)

H10	0.447	-0.0319	0.2945	0.026
C3	0.1082(2)	-0.0100(2)	-0.0917(2)	0.0200(6)
H3	0.0779	-0.0466	-0.1613	0.024
C24	0.5858(3)	0.3330(3)	0.6985(2)	0.0243(6)
H24	0.647	0.3285	0.7611	0.029
C33	-0.1629(3)	0.2353(3)	0.3746(3)	0.0279(7)
H33	-0.2396	0.2565	0.3547	0.033
C11	0.5586(3)	-0.0176(3)	0.1891(3)	0.0274(7)
H11	0.5842	-0.0857	0.2	0.033
C34	-0.0845(3)	0.2494(3)	0.3008(2)	0.0243(6)
H34	-0.1099	0.2808	0.2344	0.029
C20	0.2814(3)	0.5200(2)	0.4831(2)	0.0236(6)
H20	0.2394	0.5793	0.4702	0.028
C35	0.0284(3)	0.2172(2)	0.3266(2)	0.0186(6)
C17	0.4362(2)	0.2839(2)	0.1560(2)	0.0181(5)
C5	0.0986(3)	-0.1884(2)	0.0019(2)	0.0224(6)
H5	0.0675	-0.2309	-0.0645	0.027
C25	0.5549(3)	0.2463(2)	0.6142(2)	0.0209(6)
H25	0.597	0.1867	0.6209	0.025
C19	0.2531(3)	0.4285(2)	0.4055(2)	0.0191(6)
H19	0.1917	0.4287	0.3418	0.023
C6	0.1189(3)	-0.2386(2)	0.0991(2)	0.0226(6)
H6	0.103	-0.3156	0.0977	0.027
C8	0.1883(2)	-0.0618(2)	0.2071(2)	0.0153(5)
C16	0.4761(3)	0.3576(2)	0.0858(2)	0.0238(6)
H16	0.4477	0.4247	0.0782	0.029
C14	0.6040(3)	0.2345(3)	0.0332(3)	0.0325(7)
H14	0.6592	0.2197	-0.0076	0.039
C21	0.3708(3)	0.5215(2)	0.5774(2)	0.0239(6)
H21	0.3899	0.582	0.6289	0.029
N002	-0.1265(3)	0.5625(2)	0.2283(2)	0.0347(6)
O99	0.0360(3)	0.4985(4)	0.1928(3)	0.0963(16)
C003	-0.2444(4)	0.5958(4)	0.1883(4)	0.0519(10)
H00A	-0.2623	0.5955	0.1094	0.078
H00B	-0.2423	0.6691	0.2191	0.078
H00C	-0.3069	0.5448	0.2098	0.078
C004	-0.0657(4)	0.5254(4)	0.1614(4)	0.0597(13)
H004	-0.1014	0.5191	0.0862	0.072
C005	-0.0741(4)	0.5701(4)	0.3460(4)	0.0543(11)
H00D	0.0117	0.6009	0.3609	0.081
H00E	-0.084	0.4974	0.3729	0.081
H00F	-0.1153	0.6169	0.3823	0.081
O01	0.2194(2)	0.4528(2)	0.0962(2)	0.0362(6)
H01	0.152(3)	0.453(4)	0.138(3)	0.057(13)
H02	0.260(4)	0.402(3)	0.148(3)	0.061(13)

Table B.8: Atomic displacement parameters (Å^2) of [Hf(Ox)$_4$]

	U^{11}	U^{22}	U^{33}	U^{12}	U^{13}	U^{23}
Hf1	0.01495 (6)	0.01537 (6)	0.00977 (6)	0.00116 (4)	0.00401 (4)	0.00116 (4)
O3	0.0188 (10)	0.0145 (9)	0.0149 (9)	0.0030 (7)	0.0013 (8)	0.0012 (7)
N2	0.0144 (11)	0.0198 (11)	0.0149 (11)	0.0026 (9)	0.0023 (9)	0.0020 (9)
N4	0.0211 (12)	0.0148 (11)	0.0132 (11)	−0.0023 (9)	0.0057 (9)	−0.0019 (8)
N1	0.0118 (11)	0.0209 (11)	0.0129 (10)	0.0026 (9)	0.0045 (9)	0.0007 (9)
O1	0.0196 (10)	0.0177 (9)	0.0118 (9)	−0.0007 (8)	0.0047 (7)	−0.0003 (7)
O4	0.0190 (10)	0.0244 (10)	0.0129 (9)	0.0049 (8)	0.0059 (8)	0.0012 (7)
O2	0.0193 (10)	0.0171 (9)	0.0156 (9)	0.0026 (8)	0.0075 (8)	0.0022 (7)
N3	0.0181 (11)	0.0181 (11)	0.0130 (11)	0.0002 (9)	0.0055 (9)	0.0028 (8)
C22	0.0216 (14)	0.0198 (14)	0.0165 (13)	−0.0014 (11)	0.0074 (11)	0.0001 (10)
C9	0.0117 (12)	0.0214 (13)	0.0155 (13)	0.0047 (10)	0.0056 (10)	−0.0004 (10)
C2	0.0138 (13)	0.0333 (16)	0.0116 (12)	0.0064 (11)	0.0044 (10)	0.0030 (11)
C4	0.0120 (13)	0.0236 (14)	0.0181 (13)	0.0031 (11)	0.0068 (10)	−0.0030 (11)
C28	0.0268 (15)	0.0182 (13)	0.0148 (13)	−0.0023 (11)	0.0053 (11)	0.0010 (10)
C18	0.0117 (13)	0.0224 (14)	0.0157 (13)	0.0014 (11)	0.0017 (10)	0.0013 (10)
C27	0.0174 (13)	0.0165 (13)	0.0159 (13)	−0.0004 (10)	0.0065 (11)	0.0032 (10)
C32	0.0235 (16)	0.0315 (16)	0.0278 (16)	−0.0012 (13)	0.0152 (13)	−0.0082 (13)
C36	0.0204 (14)	0.0158 (13)	0.0167 (13)	−0.0026 (11)	0.0079 (11)	−0.0044 (10)
C13	0.0177 (14)	0.0299 (16)	0.0255 (15)	0.0053 (12)	0.0085 (12)	0.0032 (12)
C23	0.0261 (16)	0.0267 (15)	0.0175 (14)	−0.0048 (12)	0.0042 (12)	−0.0049 (11)
C12	0.0209 (16)	0.0362 (18)	0.0368 (18)	0.0118 (13)	0.0131 (14)	0.0028 (14)
C29	0.0355 (17)	0.0222 (14)	0.0143 (13)	−0.0044 (13)	0.0099 (12)	0.0013 (11)
C30	0.0343 (17)	0.0233 (15)	0.0202 (14)	−0.0067 (13)	0.0161 (13)	−0.0021 (11)
C1	0.0142 (13)	0.0216 (14)	0.0159 (13)	0.0036 (11)	0.0059 (10)	0.0025 (10)
C15	0.0353 (18)	0.0341 (18)	0.0325 (17)	0.0056 (14)	0.0216 (15)	0.0122 (14)
C7	0.0171 (14)	0.0191 (13)	0.0206 (14)	0.0056 (11)	0.0056 (11)	0.0020 (11)
C31	0.0264 (15)	0.0199 (14)	0.0182 (14)	−0.0044 (12)	0.0102 (12)	−0.0062 (11)
C26	0.0185 (14)	0.0185 (13)	0.0136 (12)	−0.0029 (11)	0.0041 (10)	0.0027 (10)
C10	0.0197 (14)	0.0223 (14)	0.0237 (15)	0.0061 (12)	0.0036 (12)	0.0055 (11)
C3	0.0150 (13)	0.0315 (16)	0.0141 (13)	0.0043 (12)	0.0051 (11)	−0.0034 (11)
C24	0.0214 (15)	0.0299 (16)	0.0166 (14)	−0.0015 (12)	−0.0020 (11)	0.0032 (12)
C33	0.0197 (15)	0.0353 (17)	0.0292 (16)	0.0042 (13)	0.0091 (13)	−0.0109 (13)
C11	0.0238 (16)	0.0290 (16)	0.0327 (17)	0.0145 (13)	0.0061 (13)	0.0054 (13)
C34	0.0219 (15)	0.0308 (16)	0.0199 (14)	0.0051 (12)	0.0054 (12)	−0.0058 (12)
C20	0.0275 (16)	0.0185 (14)	0.0276 (15)	0.0047 (12)	0.0120 (13)	0.0024 (11)
C35	0.0192 (14)	0.0210 (14)	0.0149 (13)	0.0000 (11)	0.0059 (11)	−0.0056 (10)
C17	0.0166 (13)	0.0195 (13)	0.0182 (13)	0.0013 (11)	0.0055 (11)	0.0006 (10)
C5	0.0194 (14)	0.0269 (15)	0.0209 (14)	0.0049 (12)	0.0058 (12)	−0.0081 (11)
C25	0.0207 (14)	0.0205 (14)	0.0192 (14)	0.0012 (11)	0.0009 (11)	0.0056 (11)
C19	0.0224 (14)	0.0204 (14)	0.0165 (13)	0.0048 (11)	0.0074 (11)	0.0036 (10)
C6	0.0210 (15)	0.0204 (14)	0.0273 (15)	0.0046 (12)	0.0077 (12)	−0.0043 (12)
C8	0.0105 (12)	0.0210 (13)	0.0153 (12)	0.0030 (10)	0.0052 (10)	−0.0009 (10)
C16	0.0285 (16)	0.0205 (14)	0.0257 (15)	0.0037 (12)	0.0125 (13)	0.0065 (11)
C14	0.0298 (17)	0.0411 (19)	0.0354 (18)	0.0099 (15)	0.0222 (15)	0.0086 (15)
C21	0.0254 (16)	0.0221 (14)	0.0256 (15)	0.0002 (12)	0.0121 (13)	−0.0042 (12)
N002	0.0284 (15)	0.0357 (16)	0.0429 (17)	0.0020 (12)	0.0159 (13)	0.0101 (13)

O99	0.085 (3)	0.168 (4)	0.086 (3)	0.094 (3)	0.060 (2)	0.089 (3)
C003	0.039 (2)	0.064 (3)	0.054 (3)	0.006 (2)	0.0149 (19)	0.014 (2)
C004	0.064 (3)	0.084 (3)	0.053 (3)	0.040 (3)	0.035 (2)	0.045 (2)
C005	0.046 (2)	0.053 (3)	0.055 (3)	−0.001 (2)	0.003 (2)	−0.008 (2)
O01	0.0388 (14)	0.0413 (14)	0.0328 (13)	0.0168 (11)	0.0091 (11)	0.0106 (11)

Table B.9: Geometric parameters (Å, °) of $[Hf(Ox)_4]$.

Hf1—O3	2.0796 (19)	C12—C13—C14	125.3 (3)
C18—C13	1.413 (4)	O2—Hf1—N2	70.75 (8)
Hf1—O4	2.092 (2)	C18—C13—C14	118.2 (3)
C18—C17	1.424 (4)	N3—Hf1—N2	124.52 (8)
Hf1—O1	2.096 (2)	C24—C23—C22	120.1 (3)
C27—C26	1.420 (4)	O3—Hf1—N4	78.49 (8)
Hf1—O2	2.1145 (19)	C11—C12—C13	120.2 (3)
C32—C33	1.366 (5)	O4—Hf1—N4	70.70 (8)
Hf1—N3	2.389 (2)	C30—C29—C28	119.9 (3)
C32—C31	1.413 (4)	O1—Hf1—N4	73.72 (7)
Hf1—N2	2.391 (2)	C29—C30—C31	120.1 (3)
C36—C31	1.413 (4)	O2—Hf1—N4	144.28 (7)
Hf1—N4	2.405 (2)	N1—C1—C2	122.5 (3)
C36—C35	1.431 (4)	N3—Hf1—N4	70.60 (8)
Hf1—N1	2.411 (2)	C14—C15—C16	121.9 (3)
C13—C12	1.408 (4)	N2—Hf1—N4	139.28 (8)
O3—C26	1.332 (3)	C8—C7—C6	120.8 (3)
C13—C14	1.417 (4)	O3—Hf1—N1	141.74 (7)
N2—C10	1.315 (4)	C36—C31—C32	118.6 (3)
C23—C24	1.364 (4)	O4—Hf1—N1	75.46 (7)
N2—C18	1.366 (3)	C36—C31—C30	116.2 (3)
C12—C11	1.363 (4)	O1—Hf1—N1	70.91 (7)
N4—C28	1.326 (3)	C32—C31—C30	125.1 (3)
C29—C30	1.358 (5)	O2—Hf1—N1	77.35 (8)
N4—C36	1.361 (4)	O3—C26—C25	124.2 (3)
C30—C31	1.418 (4)	N3—Hf1—N1	140.80 (8)
N1—C1	1.319 (3)	O3—C26—C27	117.1 (2)
C15—C14	1.360 (5)	N2—Hf1—N1	69.91 (8)
N1—C9	1.363 (3)	C25—C26—C27	118.7 (3)
C15—C16	1.417 (4)	N4—Hf1—N1	125.15 (8)
O1—C8	1.327 (3)	N2—C10—C11	123.0 (3)
C7—C8	1.381 (4)	C26—O3—Hf1	123.71 (17)
O4—C35	1.331 (3)	C2—C3—C4	119.8 (2)
C7—C6	1.414 (4)	C10—N2—C18	118.1 (2)
O2—C17	1.336 (3)	C23—C24—C25	121.8 (3)
C26—C25	1.379 (4)	C10—N2—Hf1	128.68 (19)
N3—C19	1.324 (4)	C32—C33—C34	122.0 (3)
C10—C11	1.405 (4)	C18—N2—Hf1	113.03 (17)
N3—C27	1.371 (4)	C12—C11—C10	119.1 (3)
C24—C25	1.414 (4)	C28—N4—C36	118.8 (2)
C22—C21	1.410 (4)	C35—C34—C33	120.6 (3)
C33—C34	1.419 (4)	C28—N4—Hf1	128.40 (19)

C22—C23	1.412 (4)	C21—C20—C19	119.8 (3)
C22—C27	1.413 (4)	C36—N4—Hf1	112.81 (17)
C20—C21	1.365 (4)	O4—C35—C34	125.3 (3)
C9—C4	1.415 (4)	C1—N1—C9	118.5 (2)
C20—C19	1.403 (4)	O4—C35—C36	116.9 (2)
C9—C8	1.425 (4)	C1—N1—Hf1	129.27 (18)
C17—C16	1.376 (4)	C34—C35—C36	117.8 (3)
C2—C3	1.365 (4)	C9—N1—Hf1	112.21 (16)
C5—C6	1.369 (4)	O2—C17—C16	124.9 (3)
C2—C1	1.408 (4)	C8—O1—Hf1	123.31 (16)
N002—C004	1.313 (5)	O2—C17—C18	117.1 (2)
C4—C3	1.413 (4)	C35—O4—Hf1	124.28 (17)
N002—C003	1.445 (5)	C16—C17—C18	118.0 (3)
C4—C5	1.416 (4)	C17—O2—Hf1	122.97 (16)
N002—C005	1.449 (5)	C6—C5—C4	119.7 (3)
C28—C29	1.408 (4)	C19—N3—C27	117.9 (2)
O99—C004	1.232 (5)	C26—C25—C24	119.8 (3)
O3—Hf1—O4	142.38 (7)	C19—N3—Hf1	129.97 (19)
N4—C28—C29	121.9 (3)	N3—C19—C20	122.6 (3)
O3—Hf1—O1	91.75 (7)	C27—N3—Hf1	112.11 (17)
N2—C18—C13	123.0 (3)	C5—C6—C7	121.6 (3)
O4—Hf1—O1	99.60 (8)	C21—C22—C23	125.2 (3)
N2—C18—C17	115.3 (2)	O1—C8—C7	124.5 (2)
O3—Hf1—O2	100.40 (8)	C21—C22—C27	116.6 (3)
C13—C18—C17	121.7 (3)	O1—C8—C9	117.8 (2)
O4—Hf1—O2	92.65 (8)	C23—C22—C27	118.2 (3)
N3—C27—C22	123.2 (2)	C7—C8—C9	117.7 (2)
N3—C27—C26	115.4 (2)	N1—C9—C4	123.0 (2)
O3—Hf1—N3	71.29 (8)	C17—C16—C15	120.4 (3)
C22—C27—C26	121.4 (3)	N1—C9—C8	115.3 (2)
O4—Hf1—N3	78.35 (8)	C15—C14—C13	119.8 (3)
C33—C32—C31	119.4 (3)	C4—C9—C8	121.8 (2)
O1—Hf1—N3	142.80 (7)	C20—C21—C22	119.8 (3)
N4—C36—C31	123.1 (3)	C3—C2—C1	119.6 (3)
O2—Hf1—N3	75.26 (8)	C004—N002—C003	122.1 (4)
N4—C36—C35	115.3 (2)	C3—C4—C9	116.6 (2)
O3—Hf1—N2	73.34 (8)	C004—N002—C005	119.1 (3)
C31—C36—C35	121.6 (3)	C3—C4—C5	125.0 (3)
O4—Hf1—N2	144.02 (7)	C003—N002—C005	118.8 (3)
C12—C13—C18	116.5 (3)	C9—C4—C5	118.4 (3)
O1—Hf1—N2	78.33 (8)	O99—C004—N002	123.7 (4)

Appendix C

Derivation of Eq. 6.6

Consider the following reactions:

$$[A] + [L] \underset{}{\overset{K_1}{\rightleftharpoons}} [AL] \qquad \text{. . . Eq. C1}$$

$$[AL] + [L] \xrightarrow{k_2} [AL_2] \qquad \text{. . . Eq. C2}$$

The rate of Eq. C2 can be expressed as

$$k^2_{obs} = k_2[AL][L] \qquad \text{. . . Eq. C3}$$

where [AL] = concentration of reactant AL

[L] = concentration of reactant L

The equilibrium constant, K_1, of Eq. C1 can be expressed as

$$K_1 = \frac{[AL]}{[A][L]} \qquad \text{. . . Eq. C4}$$

where [A] = concentration of reactant A

[L] = concentration of reactant L

[AL] = concentration of product AL

Eq. C4 can be easily manipulated to produce Eq. C5

$$[A] = \frac{[AL]}{K_1[L]} \qquad \text{. . . Eq. C5}$$

The total concentration of reactant A in Eq. C1 and C2 is given by Eq. C6

$$[AL]_t = [AL] + [A] \qquad \text{. . . Eq. C6}$$

If Eq. C5 is substituted into Eq. C6, Eq. C7 is obtained

$$[AL]_t = [AL] + \frac{[AL]}{K_1[L]} \quad \text{. . . Eq. C7}$$

By rearranging Eq. C7 the following equation is obtained

$$[AL] = \frac{[AL]_t K_1[L]}{1+K_1[L]} \quad \text{. . . Eq. C8}$$

Under pseudo-second order conditions where [L] >> [A], Eq. C8 simplifies to

$$[AL] = \frac{K_1[L]}{1+K_1[L]} \quad \text{. . . Eq. C9}$$

If Eq. C8 is substituted into Eq. C3 the rate equation becomes

$$k^2_{obs} = \frac{k_2 K_1[L]^2}{1+K_1[L]} \quad \text{. . . Eq. C10}$$

Derivation of Eq. 6.11

Consider the following reactions:

$$[A] + [L] \underset{}{\overset{K_1}{\rightleftharpoons}} [AL] \quad \text{. . . Eq. C10}$$

$$[AL] \xrightarrow{k_2} [AL_2] \quad \text{. . . Eq. C11}$$

The rate of Eq. C11 can be expressed as

$$k_{obs} = k_2[AL] \quad \text{. . . Eq. C12}$$

where [AL] = concentration of reactant AL

The equilibrium constant, K_1, of Eq. C10 can expressed as

$$K_1 = \frac{[AL]}{[A][L]} \quad \text{. . . Eq. C13}$$

where [A] = concentration of reactant A

[L] = concentration of reactant L

[AL] = concentration of product AL

Eq. C13 can be easily manipulated to produce Eq. C14

$$[A] = \frac{[AL]}{K_1[L]} \quad \text{. . . Eq. C14}$$

The total concentration of reactant A in Eq. C10 and C11 is given by Eq. C15

$$[AL]_t = [AL] + [A] \quad \text{. . . Eq. C15}$$

If Eq. C14 is substituted into Eq. C15, Eq. C16 is obtained

$$[AL]_t = [AL] + \frac{[AL]}{K_1[L]} \quad \text{. . . Eq. C16}$$

By rearranging Eq. C16 the following equation is obtained

$$[AL] = \frac{[AL]_t K_1[L]}{1+K_1[L]} \quad \text{. . . Eq. C17}$$

Under pseudo-second order conditions where [L] >> [A], Eq. C17 simplifies to

$$[AL] = \frac{K_1[L]}{1+K_1[L]} \quad \text{. . . Eq. C18}$$

If Eq. C18 is substituted into Eq. C12 the rate equation becomes

$$k^2_{obs} = \frac{k_2 K_1[L]}{1+K_1[L]} \quad \text{. . . Eq. C19}$$